

Aus dem Institut für Schlaganfall- und Demenzforschung (ISD)
der Ludwig-Maximilians-Universität München
Vorstand: Prof. Dr. Martin Dichgans

PHENOTYPIC SWITCHING
OF CONTRACILE CELLS
IN HTRA1-RELATED
CEREBRAL SMALL VESSEL DISEASE

Dissertation
zum Erwerb des Doktorgrades der Medizin
an der Medizinischen Fakultät der
Ludwig–Maximilians–Universität zu München

vorgelegt von
Sophie von Brauchitsch
aus Bonn

München, 2023

Mit Genehmigung der Medizinischen Fakultät
der Universität München

1. Berichterstatter: Prof. Dr. med. Martin Dichgans
2. Berichterstatter: PD Dr. Nicole Angela Terpolilli
Mitberichterstatter: Prof. Dr. Ali Ertürk

Mitbetreuung durch die promovierte Mitarbeiterin: Dr. Nathalie Beaufort

Dekan: Prof. Dr. med. Thomas Gudermann
Tag der mündlichen Prüfung: 26.01.2023

Meinen Eltern

TABLE OF CONTENTS

1	Summary	8
2	Zusammenfassung	10
3	List of Figures	12
4	List of Tables	13
5	List of Abbreviations/Acronyms.....	14
6	Introduction.....	18
6.1	Cerebral Small Vessel Disease	18
6.1.1	General features.....	18
6.1.2	Etiology.....	19
6.1.3	Clinical features.....	21
6.1.4	Neuroimaging	22
6.1.5	Histopathology	23
6.2	HTRA1-Related Cerebral Small Vessel Disease.....	24
6.2.1	HTRA1 mutations are linked to familial cerebral SVD.....	24
6.2.2	Neuroimaging, clinical and histopathological features in HTRA1-related cerebral SVD	25
6.2.3	HTRA1-related pathological mechanisms	27
6.3	Phenotypic Switching of Vascular Smooth Muscle Cells	31
6.3.1	Vascular smooth muscle cells.....	31
6.3.2	Regulation of the phenotype of VSMCs.....	33
6.4	Aim of the Thesis	35
7	Materials and Methods.....	36

7.1	Mouse Tissue.....	36
7.1.1	Mouse strain.....	36
7.1.2	Collection and lysis of mouse tissues	36
7.2	Cell Culture and Treatment	36
7.2.1	Cells.....	36
7.2.2	Cell culture.....	37
7.2.3	Cell treatment.....	39
7.2.4	Collection of cell extracts	40
7.3	Genomic DNA Analysis.....	42
7.3.1	DNA amplification	42
7.3.2	DNA electrophoresis.....	42
7.3.3	DNA sequencing.....	42
7.4	mRNA Analysis.....	43
7.4.1	RNA isolation	43
7.4.2	cDNA synthesis.....	43
7.4.3	Analysis of splicing variants.....	43
7.4.4	Quantitative real-time PCR.....	44
7.5	Protein Analysis.....	46
7.5.1	Determination of total protein concentration.....	46
7.5.2	Sodium dodecyl sulfate polyacrylamide gel electrophoresis (SDS-PAGE)	46
7.5.3	Immunoblot	46
7.6	Cloning of a $\Delta 5$ HTRA1 Expression Vector	48
7.6.1	Preparation of the insert.....	48
7.6.2	Preparation of the vector	49
7.6.3	DNA ligation.....	49
7.6.4	Bacterial transformation and amplification	49
7.6.5	DNA mini- and midipreps.....	50
7.7	Protease Activity Assays	50

7.7.1	Processing of LTBP-1	50
7.8	Statistics.....	50
8	Results.....	51
8.1	Consequences of HtrA1 Deficiency on Contractile Cell Differentiation	51
8.1.1	Consequences of HtrA1 deficiency on the contractile differentiation of mouse embryonic fibroblasts.....	51
8.1.2	Consequences of HtrA1 deficiency on calponin protein levels in mouse brain	55
8.2	Analysis of Human Skin Fibroblasts Carrying the Intronic <i>HTRA1</i> Mutation	
	c.1005+1G>T	57
8.2.1	Consequences of the intronic <i>HTRA1</i> mutation c.1005+1G>T on mRNA splicing	57
8.2.2	Consequences of the c.1005+1G>T mutation on HTRA1 protein and protease function in overexpressing HEK-293T cells	59
8.2.3	Consequences of the c.1005+1G>T mutation on HTRA1 mRNA levels, protein levels and protease function in human skin fibroblasts	63
8.2.4	Consequences of the c.1005+1G>T mutation on TGF- β signaling and contractile cell differentiation in human skin fibroblasts.....	68
9	Discussion	71
9.1	Consequences of the Pathogenic HTRA1 Mutation c.1005+1G>T on Molecular and Cellular Determinants of HTRA1 Function	71
9.2	Consequences of HTRA1 Loss of Function on the Contractile Cell Phenotype.....	73
10	Copyright Declaration.....	75
11	References.....	76
12	Acknowledgements.....	86
13	Affidavit.....	87

14 Curriculum Vitae	88
15 Publications.....	89

1 SUMMARY

Loss-of-function mutations in the gene encoding the high-temperature requirement A1 (*HTRA1*) protease cause familial cerebral small vessel disease (SVD), ischemic stroke and dementia. Bi-allelic mutations are linked to the severe and early onset disorder CARASIL (cerebral autosomal-recessive arteriopathy with subcortical infarcts and leukoencephalopathy), while monoallelic mutations result in a milder and less penetrant SVD. Our laboratory previously established that HTRA1 loss of function causes an accumulation of matrisomal HTRA1 substrates and a reduction in transforming growth factor beta (TGF- β) signaling in mouse and/or human cells and tissues. However, the consequences of HTRA1 loss of function on the phenotype of brain vascular cells remain elusive. Since TGF- β signaling is a key regulator of cell differentiation, including that of vascular smooth muscle cells, I sought to examine the impact of HTRA1 loss of function on contractile cell differentiation using embryonic fibroblasts and brain tissues from *htra1*^{-/-} mice, as well as skin fibroblasts from individuals from an SVD pedigree who carried an intronic *HTRA1* mutation.

I evidenced that three established markers of contractile differentiation (α -smooth muscle actin, calponin and smooth muscle protein 22-a) display reduced mRNA and/or protein levels in embryonic fibroblasts from *htra1*^{-/-} mice compared to control mice. Conversely, markers of synthetic or phagocytic differentiation (fibronectin and galectin 3, respectively) and the key transcriptional regulators of cell differentiation Krüppel like factor 4 and 5 remained unchanged. I further confirmed a reduction in calponin at protein level in brain extracts from *htra1*^{-/-} mice. As a complementary model for HTRA1 loss of function, I investigated human skin fibroblasts from individuals carrying the *HTRA1* mutation c.1005+1G>T. First, I uncovered that this intronic variant causes skipping of exon 5, which encodes the catalytic residue Ser328. Accordingly, I demonstrated that the corresponding mutant protein ($\Delta 5$ HTRA1) is devoid of enzymatic activity in transfected cells as well as in skin fibroblasts from a homozygous mutation carrier. Second, I established that both recombinant and endogenous $\Delta 5$ HTRA1 display reduced intracellular stability and aberrant secretion, suggesting that this mutant protein is detected and degraded by the protein quality control systems. I further observed that, in sharp contrast to mouse *htra1*^{-/-} fibroblasts, human *HTRA1* c.1005+1G>T fibroblasts exhibit hyperphosphorylation of Smad2 (mothers against decapentaplegic homolog 2), a marker of TGF- β signaling activity and elevated contractile marker protein abundance. These discrepancies might reflect the fact that $\Delta 5$ HTRA1 hijacks the cell quality control systems.

Together, my work sheds new light on HTRA1-related SVD. Specifically, my data *(i)* suggest that HTRA1 deficiency interferes with the differentiation of contractile cells and *(ii)* provide evidence that an atypical intronic mutation interferes with the protein stability and enzymatic function of HTRA1.

2 ZUSAMMENFASSUNG

Mutationen im Gen, das für die High-Temperature Requirement A1 (HTRA1) kodiert und welche zu einem Funktionsverlust führen, verursachen familiäre zerebrale Mikroangiopathien, ischämische Schlaganfälle und Demenz. Bi-allelische Mutationen werden mit der schweren und früh einsetzenden zerebralen autosomal-rezessiven Arteriopathie mit subkortikalen Infarkten und Leukoenzephalopathie (CARASIL) in Verbindung gebracht. Mono-allelische Mutationen hingegen führen zu einer milderen und weniger penetranten Mikroangiopathie. Unser Labor konnte in vorangegangenen Studien zeigen, dass der Funktionsverlust von HTRA1 mit einer Ansammlung von matrisomalen HTRA1-Substraten und eine Reduktion der Signalübertragung des Transforming Growth Factor beta (TGF- β) in Zellen und Geweben von Mäusen und/oder Menschen einhergeht. Die Folgen des Funktionsverlustes von HTRA1 auf den Phänotyp von Hirngefäßzellen sind bisher jedoch nicht bekannt. Die TGF- β -Signalübertragung spielt eine essenzielle Rolle in der Regulierung der Zelldifferenzierung (einschließlich der Differenzierung von glatten Gefäßmuskelzellen). Daher war mein Ziel, die Auswirkungen des HTRA1-Funktionsverlusts auf die Differenzierung kontraktiler Zellen zu untersuchen. Hierfür verwendete ich embryonale Fibroblasten und Hirngewebe von *htra1*^{-/-} Mäusen sowie Hautfibroblasten eines CARASIL Patienten mit einer bi-allelischen intronischen *HTRA1* Mutation und dessen heterozygoten Eltern.

Ich konnte nachweisen, dass die mRNA- und/oder Proteinspiegel drei etablierter Marker für die kontraktile Differenzierung (α -Smooth Muscle Actin, Calponin und Smooth Muscle Protein 22-a) in embryonalen Fibroblasten von *htra1*^{-/-} Mäusen im Vergleich zu Kontrollmäusen verringert sind. Im Gegensatz dazu blieben die Marker der synthetischen oder phagozytischen Differenzierung (Fibronectin bzw. Galectin 3) und die wichtigen Transkriptionsregulatoren der Zelldifferenzierung (Krüppel like factor 4 und 5) unverändert. Darüber hinaus konnte ich vorhergehende Befunde einer Verringerung des Calponin-Proteinspiegels in Gehirnextrakten von *htra1*^{-/-} Mäusen replizieren. Als ergänzendes Modell für den Funktionsverlust von HTRA1, untersuchte ich Hautfibroblasten von einer Person mit einer homozygoten und den beiden Eltern, mit einer heterozygoten HTRA1-Mutation c.1005+1G>T. Zunächst beobachtete ich, dass diese intronische Variante zum Überspringen des Exons 5 beim Spleißen führt, welches das katalytische Serin beinhaltet. Dementsprechend konnte ich zeigen, dass das mutierte Protein ($\Delta 5$ HTRA1) sowohl in transfizierten Zellen, als auch in Hautfibroblasten eines homozygoten Mutationsträgers, im Gegensatz zum physiologischem HTRA1 keine enzymatische Aktivität aufweist. Zweitens habe

ich festgestellt, dass sowohl rekombinantes als auch endogenes $\Delta 5$ HTRA1 eine verringerte intrazelluläre Stabilität und eine untypische Sekretion aufweisen. Dies deutet darauf hin, dass das mutierte Protein von den Systemen der Proteinqualitätskontrolle erkannt und abgebaut wird. Zudem habe ich beobachtet, dass humane HTRA1 c.1005+1G>T-Fibroblasten im Gegensatz zu *htra1*^{-/-}-Fibroblasten der Maus eine Hyperphosphorylierung von Smad2 (Mothers against decapentaplegic homolog 2), einem Marker für TGF- β -Signalaktivität, und eine erhöhte Menge an kontraktilen Markerproteinen aufweisen. Diese Diskrepanzen könnten darauf hindeuten, dass $\Delta 5$ HTRA1 die Qualitätskontrollsysteme der Zellen stört.

Insgesamt wirft meine Arbeit ein neues Licht auf HTRA1-bezogene zerebrale Mikroangiopathien. Insbesondere deuten meine Daten (i) darauf hin, dass ein HTRA1-Mangel die Differenzierung kontraktiler Zellen beeinträchtigt, und (ii) liefern sie Beweise dafür, dass eine atypische intronische Mutation die Proteinstabilität und enzymatische Funktion von HTRA1 beeinträchtigt.

3 LIST OF FIGURES

- Figure 6.1: Factors determining the clinical presentation and progression of SVD
- Figure 6.2: MRI characteristics in cerebral SVD
- Figure 6.3: Brain vessel architecture
- Figure 6.4: Neuroimaging and clinical findings in CARASIL
- Figure 6.5: Histology of cerebral vessels in CADASIL and CARASIL
- Figure 6.6: Exon and domain organization of HTRA1
- Figure 6.7: HTRA1 mutations identified in CARASIL and CADASIL 2 cases
- Figure 6.8: HTRA1 associates with the ECM and facilitates TGF- β signaling
- Figure 6.9: Phenotypic switching of VSMC
- Figure 6.10: Schematic of the TGF- β signaling pathway
- Figure 8.1: Calponin, SM22, and α -SMA protein levels in mouse embryonic fibroblasts
- Figure 8.2: Calponin and SM22 mRNA levels in mouse embryonic fibroblasts
- Figure 8.3: Fibronectin and galectin 3 protein levels in mouse embryonic fibroblasts
- Figure 8.4: *Klf4* and *Klf5* mRNA levels in mouse embryonic fibroblasts
- Figure 8.5: Calponin protein levels in mouse brain extracts
- Figure 8.6: *HTRA1* genotyping in human skin fibroblasts
- Figure 8.7: *HTRA1* splicing analysis in human skin fibroblasts
- Figure 8.8: Intra- and extracellular protein levels of $\Delta 5$ HTRA1 in overexpressing HEK-293T cells
- Figure 8.9: Stability of $\Delta 5$ HTRA1 in overexpressing HEK-293T cells
- Figure 8.10: Protease activity of $\Delta 5$ HTRA1 in overexpressing HEK-293T cells
- Figure 8.11: *HTRA1* mRNA levels in human skin fibroblasts
- Figure 8.12: Intracellular HTRA1 protein levels in human skin fibroblasts
- Figure 8.13: HTRA1 protein stability in human skin fibroblasts
- Figure 8.14: HTRA1 secretion in human skin fibroblasts
- Figure 8.15: Protease activity of $\Delta 5$ HTRA1 in human skin fibroblasts
- Figure 8.16: TGF- β signaling activity in human skin fibroblasts
- Figure 8.17: Calponin, SM22, and α -SMA protein levels in human skin fibroblasts

4 LIST OF TABLES

Table 6.1	Familial cerebral small vessel diseases
Table 7.1:	Volume or quantity of reagents used for cell culture and treatment
Table 7.2:	Buffer composition
Table 7.3:	List of RT-qPCR primers
Table 7.4:	List of primary and secondary antibodies
Table 11.1:	License numbers and copyright holders for Figures 1.1–1.5

5 LIST OF ABBREVIATIONS/ACRONYMS

α -SMA	α -smooth muscle actin
Ab	antibody
BCA	bicinchoninic acid
bp	base pairs
BSA	bovine serum albumin
C	Celsius
CAA	cerebral amyloid angiopathy
CADASIL	cerebral autosomal-dominant arteriopathy with subcortical infarcts and leukoencephalopathy
CARASAL	cathepsin A-related arteriopathy with strokes and leukoencephalopathy
CARASIL	cerebral autosomal-recessive arteriopathy with subcortical infarcts and leukoencephalopathy
cDNA	complementary DNA
CHX	cycloheximide
COL	collagen
co-SMAD	common-mediator SMAD
CP	process capability
CRISPR/Cas	clustered regularly interspaced short palindromic repeats/CRISPR-associated
Ctrl	control
CTGF	connective tissue growth factor
dH ₂ O	distilled water
DMEM	Dulbecco's modified Eagle's medium
DMSO	dimethyl sulfoxide
DNA	deoxyribonucleic acid
DNase	deoxyribonuclease
dNTP	deoxynucleoside triphosphate
DTT	dithiothreitol
ECM	extracellular matrix
<i>E. coli</i>	<i>Escherichia coli</i>

EDTA	ethylenediaminetetraacetic acid
FCS	fetal calf serum
FLAIR	fluid-attenuated inversion recovery
GAPDH	glyceraldehyde 3-phosphate dehydrogenase
GC	guanine cytosine
HEK	human embryonic kidney
Het	heterozygous
Hom	homozygous
HRP	horseradish peroxidase
HTRA1	high-temperature requirement A1
iPSC	induced pluripotent stem cell
ISD	Institute of Stroke and Dementia Research
kDa	kilodalton
kg	kilogram
Klf	Krüppel-like factor
LAP	latency-associated peptide
LB	Luria broth
LTBP	latent TGF- β binding protein
M	molar
MAC	membrane attack complex
MEF	mouse embryonic fibroblasts
mg	milligram
mL	milliliter
mM	millimolar
mm	millimeter
MRI	magnetic resonance imaging
mRNA	messenger RNA
μ g	microgram
μ L	microliter
μ M	micromolar
μ m	micrometer

n	number
ng	nanogram
nM	nanomolar
nm	nanometer
PAI	plasminogen activator inhibitor
PBS	phosphate-buffered saline
PCR	polymerase chain reaction
PVDF	polyvinylidene fluoride
qPCR	quantitative real-time polymerase chain reaction
RIPA	radioimmunoprecipitation assay
RNA	ribonucleic acid
RNase	ribonuclease
R-SMAD	receptor-regulated SMAD
RT	reverse transcriptase
RT	room temperature
TGF- β	transforming growth factor- β
RT-qPCR	reverse transcription-quantitative real-time PCR
s	second(s)
SBE	SMAD-binding element
SDS	sodium dodecyl sulfate
SDS-PAGE	SDS-polyacrylamide gel electrophoresis
SEM	standard error of the mean
SM22	smooth muscle protein 22-a/transgelin
Smad	mothers against decapentaplegic homolog
SMC	smooth muscle cells
SM-MHC	smooth muscle myosin heavy chain / myosin-11x
SNP	single nucleotide polymorphism
SVD	small vessel disease
TAE	Tris-acetate-EDTA
TBS-T	Tris-buffered saline-Tween
TEMED	tetramethylethylenediamine

TGF- β	transforming growth factor- β
TGFBR	TGF- β receptor
Tris	tris(hydroxymethyl)aminomethane
UV	ultraviolet
V	Volt
VSMC	vascular smooth muscle cells
WMH	white matter hyperintensities
wt	wild type

6 INTRODUCTION

6.1 CEREBRAL SMALL VESSEL DISEASE

6.1.1 General features

Cerebral small vessel disease (SVD) is one of the most common age-related conditions (Haffner, Malik et al. 2016) and is the most common cause of vascular dementia (often accompanying Alzheimer's disease). Furthermore approximately 25% of all ischemic strokes and most hemorrhagic strokes are due to cerebral SVD (Bos, Wolters et al. 2018). Cerebral SVD can be divided into cerebral amyloid angiopathy (CAA) and non-amyloid SVD. The following introduction will focus on non-amyloid SVD.

Cerebral SVD is a disorder of the brain that involves the small perforating arterioles reaching from either the large basal cerebral arteries or the subarachnoid circulation into the white matter of the brain, as well as the capillaries and venules (Pantoni 2010). This vascular disorder causes lesions such as white matter hyperintensities, subcortical infarcts and intracerebral hemorrhages (Wardlaw, Smith et al. 2013b) that can be identified by neuroimaging or neuropathological findings (Wardlaw, Smith et al. 2013a). Subcortical infarcts and intracerebral hemorrhages usually present with stroke symptoms (Wardlaw, Smith et al. 2013b). In contrast, lacunes, microbleeds, perivascular spaces and microinfarcts may be asymptomatic, but at a high enough number and depending on their location (Wardlaw, Smith et al. 2013b, van Veluw, Shih et al. 2017), they can cause cognitive impairment/dementia, depression, mobility difficulties and increased risk of stroke (Debette, Schilling et al. 2019).

6.1.2 Etiology

Most cerebral SVDs are sporadic. Established risk factors include age and arterial hypertension (the two predominant risk factors) as well as hypercholesterolemia and diabetes mellitus (Khan, Porteous et al. 2007, Thompson and Hakim 2009, Hilal, Mok et al. 2017). In addition, recent genome-wide analyses in patients with sporadic SVD have highlighted an important contribution of genetics to the disease, with a heritability in the range of 15%–30% (Malik and Dichgans 2018). In particular, it was found that common variants in genes involved in Mendelian SVDs, including *COL4A1/2* and *HTRA1*, confer risk of sporadic SVD or stroke (Mishra, Chauhan et al. 2019).

In addition to the sporadic forms, an increasing number of monogenic cerebral SVDs have been reported [selected disorders are presented in Table 6.1 (Dichgans, Pulit et al. 2019, Rutten-Jacobs and Rost 2020)]. Mendelian SVDs are very rare but provide useful experimental models to identify the fundamental SVD mechanisms. These diseases include cerebral autosomal-dominant arteriopathy with subcortical infarcts and leukoencephalopathy (CADASIL), the most common familial SVD, and cerebral autosomal-recessive arteriopathy with subcortical infarcts and leukoencephalopathy (CARASIL)/CADASIL 2, on which I will focus in my dissertation.

Table 6.1 Familial cerebral SVD		CADASIL (cerebral autosomal dominant arteriopathy with subcortical infarcts and leukoencephalopathy)	CARASIL (cathepsin A-related arteriopathy with strokes and leukoencephalopathy)	COL4A1/2-related angiopathies	CARASIL (cerebral autosomal recessive arteriopathy with subcortical infarcts and leukoencephalopathy)	CADASIL 2* (cerebral autosomal dominant arteriopathy with subcortical infarcts and leuko- encephalopathy 2)
Causative gene(s)	<i>NOTCH3</i>	<i>CTSA</i>	<i>COL4A1/2</i>	<i>HTRA1</i>	<i>HTRA1</i>	
Inheritance pattern	Autosomal dominant	Autosomal dominant	Autosomal dominant	Autosomal recessive	Autosomal dominant	
Protein	Transmembrane receptor NOTCH3	Lysosomal protease cathepsin A	Basement membrane collagen IV $\alpha 1$ and $\alpha 2$	Secreted protease HTRA1	Secreted protease HTRA1	
Vascular pathology	Intimal thickening, fibro-hyaline material deposition in media, degeneration of SMC	Intimal thickening, fibro-hyaline material deposition in media, degeneration of SMC	Intimal thickening, fibro-hyaline material deposition in media, degeneration of SMC	Intimal thickening, fibro-hyaline material deposition in media, degeneration of SMC	Intimal thickening, fibro-hyaline material deposition in media, degeneration of SMC	
Clinical features	Cognitive impairment/dementia, stroke, mood disturbance/depression, migraine with aura	Cognitive impairment/dementia, stroke, treatment-resistant hypertension, dry eyes/mouth, muscle cramps	Stroke, infantile hemiparesis, nephropathy Axenfeld-Rieger anomaly, porencephalopathy	Early-onset cognitive impairment/dementia, stroke, alopecia, spondylosis	Late-onset cognitive impairment/dementia, stroke	
Neuro-radiological findings (MRI)	WMH, subcortical infarcts, brain atrophy	WMH, subcortical ischemic and hemorrhagic strokes	WMH, intracerebral hemorrhagic strokes	WMH, subcortical infarcts, microbleeds	WMH, subcortical infarcts, microbleeds	
Reference	Chabriat et al. 2009 Rutten et al. 2014	Bugiani et al. 2016	Kuo et al. 2012 Joutel et al. 2016 Verdura et al. 2016	Hara et al. 2009 Oka et al. 2004 Beaufort et al. 2014	Verdura et al. 2015	
SMC: smooth muscle cells; WMH: white matter hyperintensities. *proposed nomenclature based on the inheritance pattern of the disease						

6.1.3 Clinical features

Clinical diagnosis of cerebral SVD can be made either in the setting of acute small vessel stroke or by an insidious onset of different symptoms including cognitive impairment and dementia, late-life depression, incontinence and gait dysfunction, among others (van der Flier, van Straaten et al. 2005, Herrmann, Le Masurier et al. 2008, Inzitari, Pracucci et al. 2009, Pantoni 2010, de Laat, Tuladhar et al. 2011, Mok and Kim 2015) as well as executive and motor slowing (Craggs, Yamamoto et al. 2014). The symptoms in small vessel strokes are often less pronounced than in non-SVD strokes and are determined by lesion type, extent, and anatomical location (Duering, Gesierich et al. 2014, Ter Telgte, van Leijssen et al. 2018). However, SVD patients presenting with clinical strokes are faced with a higher rate of complications in acute treatment and a poorer post-stroke outcome compared to non-SVD stroke cases (Etherton, Wu et al. 2017). The manifestation and progression of the disease is influenced by various factors, such as comorbidities, accompanying secondary neurodegeneration and resilience factors (Figure 6.1).

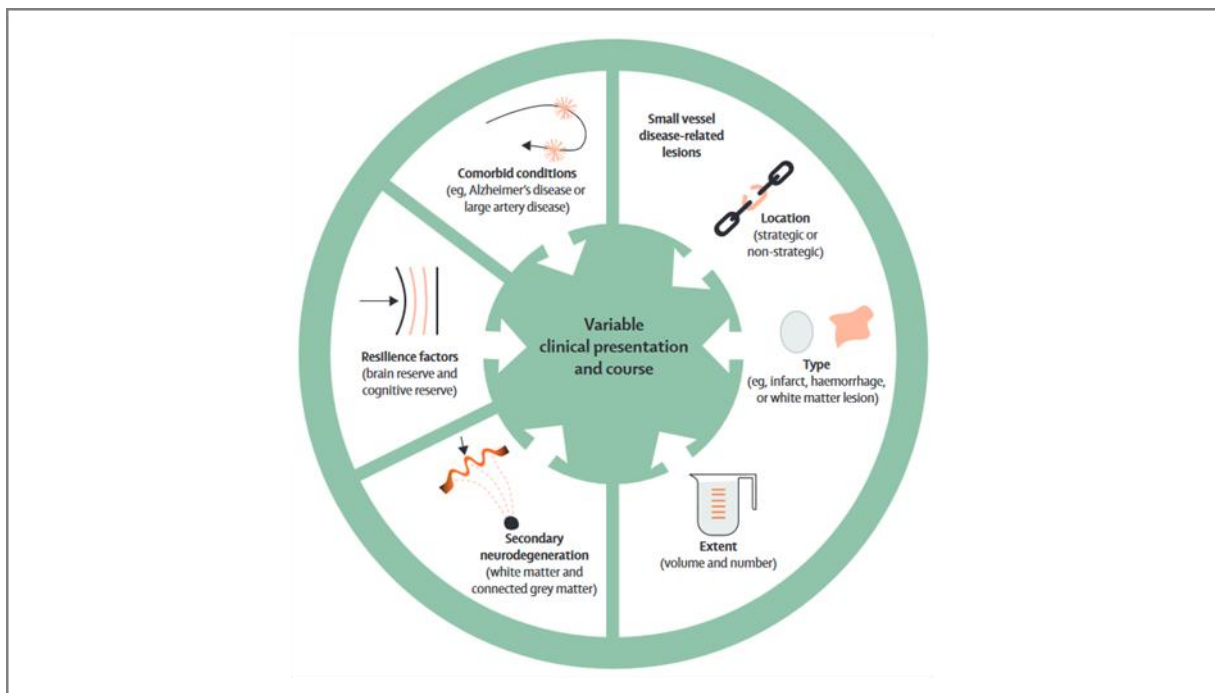


Figure 6.1: Factors determining the clinical presentation and progression of small vessel disease. The clinical presentation of small vessel disease is highly variable and influenced by the extent, type and location of the lesions, as well as comorbidities, resilience factors and the extent of secondary neurodegeneration (Wardlaw, Smith et al. 2019).

6.1.4 Neuroimaging

Lesions observed in magnetic resonance imaging (MRI) are used as a diagnostic biomarker for the disease. Common lesions (depicted in Figure 6.2) include (i) recent subcortical or cortical microinfarcts, (ii) lacunes [lesions < 20 mm in diameter, in the white and deep grey matter that are fluid-filled and gliotic (Rincon and Wright 2014)], and (iii) white matter hyperintensities (WMHs; T2-weighted hyperintensity that is punctate, patchy or confluent) that provide a surrogate marker for both demyelination and increased interstitial fluid. Further lesions include (iv) enlarged perivascular spaces (dilated spaces with cerebrospinal fluid around perforating venules and arterioles), (v) cerebral microbleeds, and (vi) cerebral atrophy (Wardlaw, Smith et al. 2013a, Wardlaw, Smith et al. 2013b, Hilal, Mok et al. 2017, Munoz Maniega, Chappell et al. 2017, Wardlaw, Smith et al. 2019).

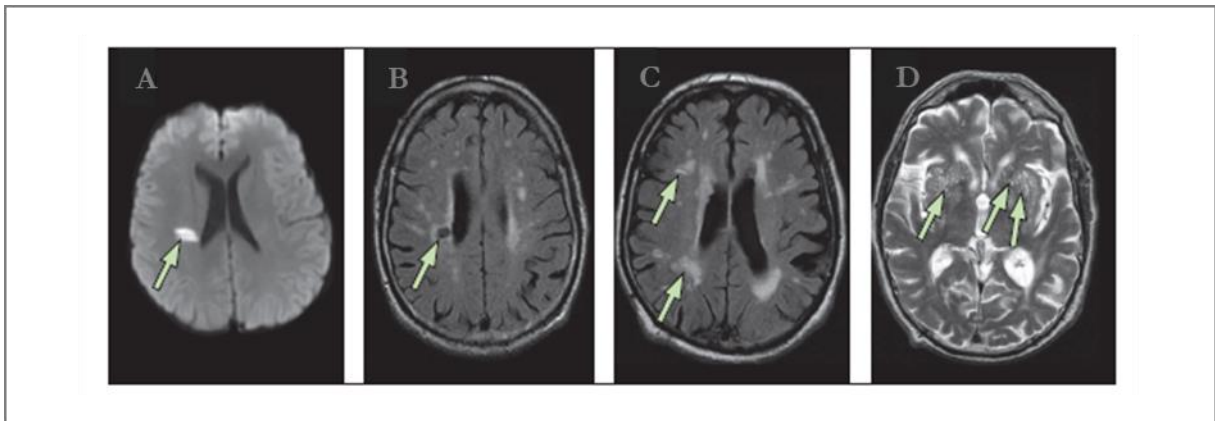


Figure 6.2: Magnetic resonance imaging characteristics in cerebral small vessel disease. A. Acute small deep (lacunar) infarct (arrow) in a diffusion-weighted image. B. Lacune in white matter (arrow) on a fluid-attenuated inversion recovery (FLAIR) image. C. White matter hyperintensities (arrows) on a FLAIR image. D. Perivascular spaces in white and deep grey matter (arrows) on a T2-weighted image (modified after Wardlaw, Smith et al. 2013a).

6.1.5 Histopathology

Cerebral SVD mostly affects small penetrating vessels below 1 mm in diameter within white matter and deeper grey matter such as the basal ganglia, thalamus and brainstem (Pantoni 2010). Depending on the vascular segment (Figure 6.3), vessels consist of endothelial cells, pericytes or vascular smooth muscle cells (SMCs) and astrocytes (Iadecola 2017).

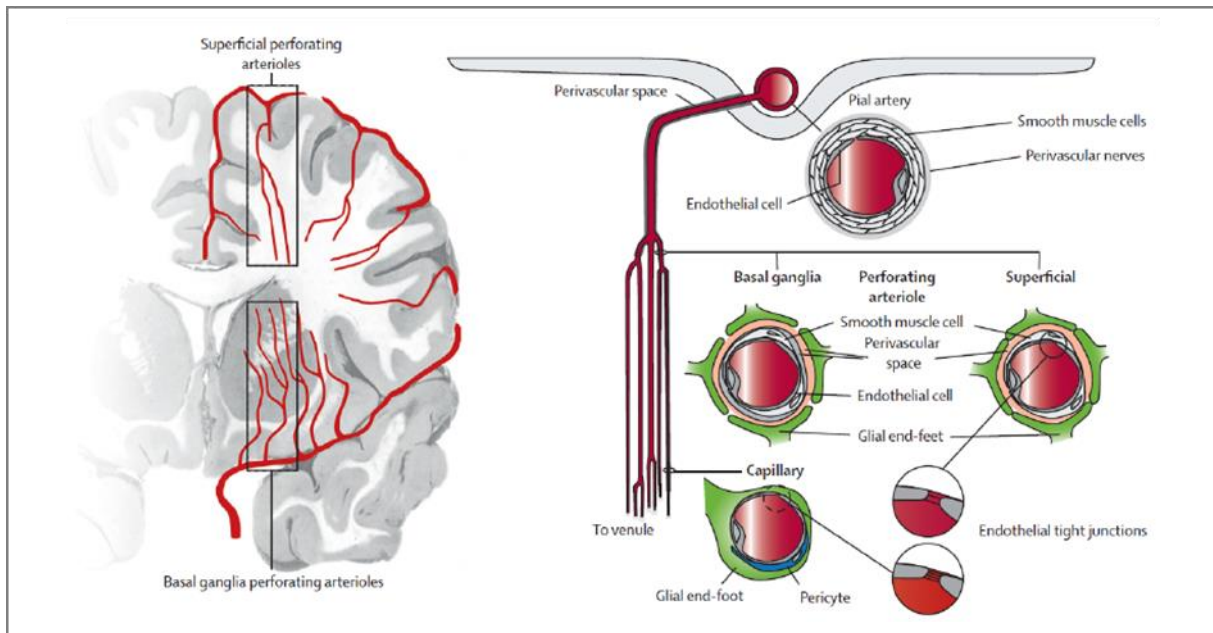


Figure 6.3: Brain vessel architecture. The vessel architecture varies in the different vascular segments. Pericytes cover capillaries, while smooth muscle cells are dominant in arterioles and arteries (Wardlaw, Smith et al. 2013a; originated from Antonia Weingart, Institute for Stroke and Dementia Research, University of Munich, Germany).

Typical histopathological findings in SVD include thickening of the tunica intima (the endothelial cell layer), fibrinoid necrosis, hyalinization of the tunica media with accumulation of extracellular matrix (ECM) and degeneration of SMCs (Wardlaw, Smith et al. 2013a). This remodeling of the vessel wall affects vessel elasticity, diameter, and reactivity as well as the blood–brain barrier (Pantoni 2010, Wardlaw, Smith et al. 2013a, Craggs, Yamamoto et al. 2014, Vinters, Zarow et al. 2018).

Loss of the SMC marker α -smooth muscle actin (α -SMA) in the tunica media is commonly referred to as “SMC loss” (Craggs, Yamamoto et al. 2014) but might in fact reflect SMC phenotypic switching (as described in Section 6.3).

6.2 HTRA1-RELATED CEREBRAL SMALL VESSEL DISEASE

6.2.1 HTRA1 mutations are linked to familial cerebral SVD

CARASIL is a very rare autosomal recessive familial cerebral SVD that was first reported by Maeda et al. as type of Binswanger disease without hypertension (Maeda, Nakayama et al. 1976, Hara, Shiga et al. 2009). It is caused by homozygous or compound heterozygous mutations in the high-temperature requirement serine peptidase A1 (*HTRA1*) gene (Hara, Shiga et al. 2009). More recently, monoallelic *HTRA1* mutations were identified as a significant cause of dominant cerebral SVD (Verdura, Herve et al. 2015, Nozaki, Kato et al. 2016). Indeed, analysis of independent cohorts indicated that up to 5% of patients suffering familial SVD of unknown etiology display heterozygous *HTRA1* mutations. The corresponding disease is referred to as CADASIL 2 (Bianchi, Di Palma et al. 2014, Verdura, Herve et al. 2015, Nozaki, Kato et al. 2016, Lee, Chung et al. 2018).

6.2.2 Neuroimaging, clinical and histopathological features in HTRA1-related cerebral SVD

CARASIL presents in 25–40-year-old normotensive patients as a cerebral SVD that includes WMH and multiple lacunar infarcts predominantly in the thalamus and basal ganglia on MRI. In the T2-weighted MRI, hyperintensities are detected in periventricular and deep white matter and rarely in the capsula externa and the anterior temporal white matter (Yanagawa, Ito et al. 2002, Fukutake 2011, Nozaki, Nishizawa et al. 2014, Nozaki, Kato et al. 2016). Fifty percent of the patients experience recurrent ischemic (mostly lacunar) strokes leading to gait disturbance, mood changes (irritability and apathy), cognitive impairment, hyperreflexia, urinary incontinence, and pseudobulbar palsy (Maeda, Nakayama et al. 1976, Fukutake and Hirayama 1995, Fukutake 2011, Tikka, Baumann et al. 2014). Further symptoms include spondylosis deformans with disc herniation and early-onset alopecia (Figure 6.4).

CADASIL 2 is less penetrant than CARASIL. Compared to individuals with CARASIL, heterozygous mutation carriers suffer later onset (i.e., at the age of 50–60 years) and milder symptoms, excluding extra-neurological ones (Bianchi, Di Palma et al. 2014, Verdura, Herve et al. 2015, Nozaki, Kato et al. 2016, Lee, Chung et al. 2018).

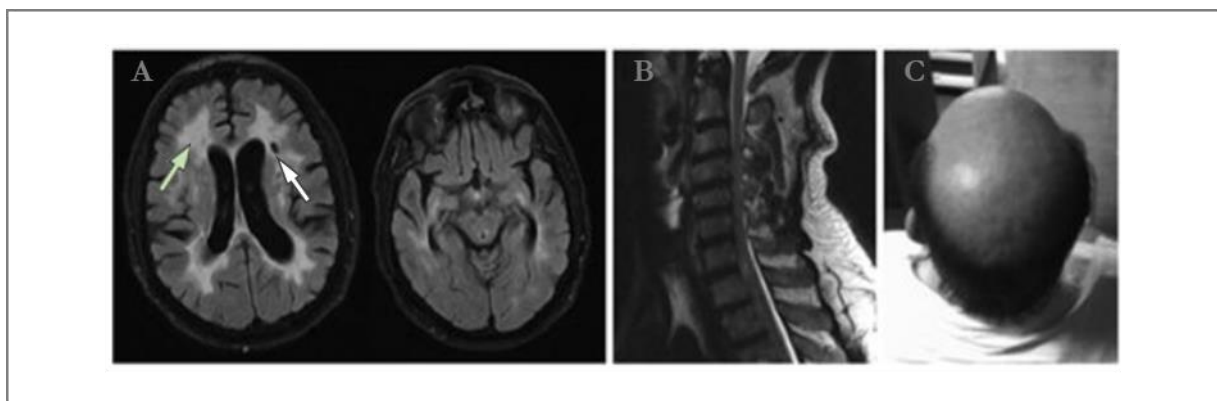


Figure 6.4: Neuroimaging and clinical findings in CARASIL. A. Diffuse white matter hyperintensities involving periventricular and deep white matter (yellow arrow). Multiple lacunar infarcts in brainstem and both hemispheres (white arrow; T2-weighted fluid-attenuated inversion recovery MRI). B. Multilevel degenerative changes and stenosis of the cervical canal (T2-weighted MRI). C. Alopecia. (Taken from Menezes Cordeiro, Nzwalo et al. 2015)

Histologically, CARASIL (and similarly CADASIL 2) manifests in small penetrating cerebral arteries, mainly in the basal ganglia and the white matter (Fukutake 2011, Tikka, Baumann et al. 2014, Ito, Nozaki et al. 2018). Cerebral vessels show extensive arteriosclerosis in the absence of amyloid deposits or basophilic granular material, which are observed in CAA and CADASIL, respectively. As depicted in Figure 6.5, the intima displays fibrous thickening with accumulation of ECM components (Maeda, Nakayama et al. 1976, Yanagawa, Ito et al. 2002, Arima, Yanagawa et al. 2003, Oide, Nakayama et al. 2008, Nozaki, Nishizawa et al. 2014, Tikka, Baumann et al. 2014). The lamina elastica is split. The media is thinned and displays reduced levels of α -SMA, an SMC differentiation marker. This observation led to the conclusion that SMC loss occurs, but, as assessed in this dissertation, it could also reflect – at least in part – a change in cell phenotype (see Section 6.3).

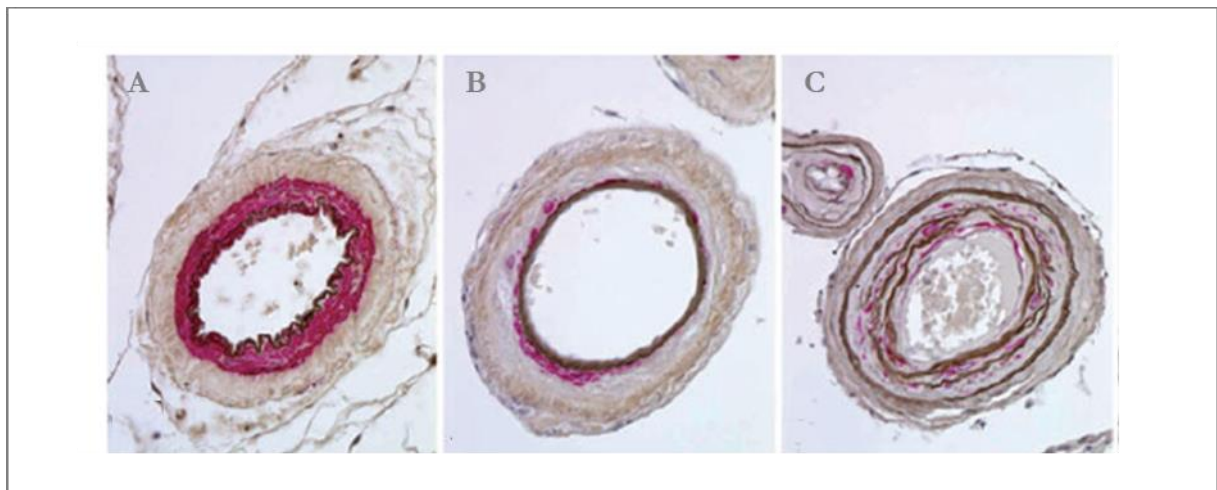


Figure 6.5: Histology of cerebral vessels in CADASIL and CARASIL. Small cerebral arteries, diameter 200 μ m. Black: Weigert staining (lamina elastica); red: α -actin immunostaining (smooth muscle cells). A. nonarteriosclerotic control. B. CADASIL. C. CARASIL (note the splitting of the lamina elastica). (Modified from Oide, Nakayama et al. 2008)

6.2.3 HTRA1-related pathological mechanisms

6.2.3.1 Pathogenic HTRA1 mutations are loss-of-function mutations

HTRA1 is a secreted protease that consists of nine exons and three functional domains (Figure 6.6). The protease domain harbors a typical serine protease catalytic triad at residues His220, Asp250, and Ser 328 (Truebestein, Tennstaedt et al. 2011, Hansen and Hilgenfeld 2013). In addition to its protease domain, HTRA1 displays amino- and carboxyterminal extensions involved in protein/protein interactions (i.e., a Mac domain and a PDZ domain) whose functions are not clearly established.

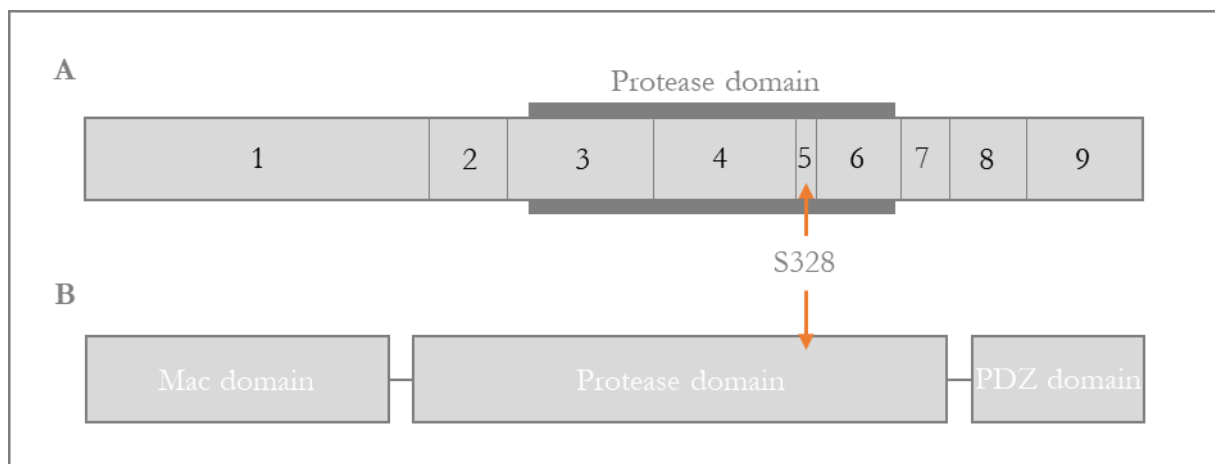


Figure 6.6: Exon and domain organization of HTRA1. A. HTRA1 exons. B. HTRA1 functional domains.

As depicted in Figure 6.7, most pathogenic HTRA1 mutations are missense mutations within the protease domain. They were shown to reduce or fully abrogate HTRA1 protease activity, indicating that lack of processing of one or more HTRA1 substrates is a key pathological mechanism in HTRA1-related SVD (Hara, Shiga et al. 2009, Nishimoto, Shibata et al. 2011, Shiga, Nozaki et al. 2011). Other mutations include frameshift or nonsense mutations that result in truncated forms missing one or more catalytic residues. In addition, few mutations targeting the Mac or PDZ domains have been identified. In the latter cases, the mechanism underlying HTRA1 loss of function remains to be determined, as these mutations leave HTRA1 enzymatically active *in vitro*.

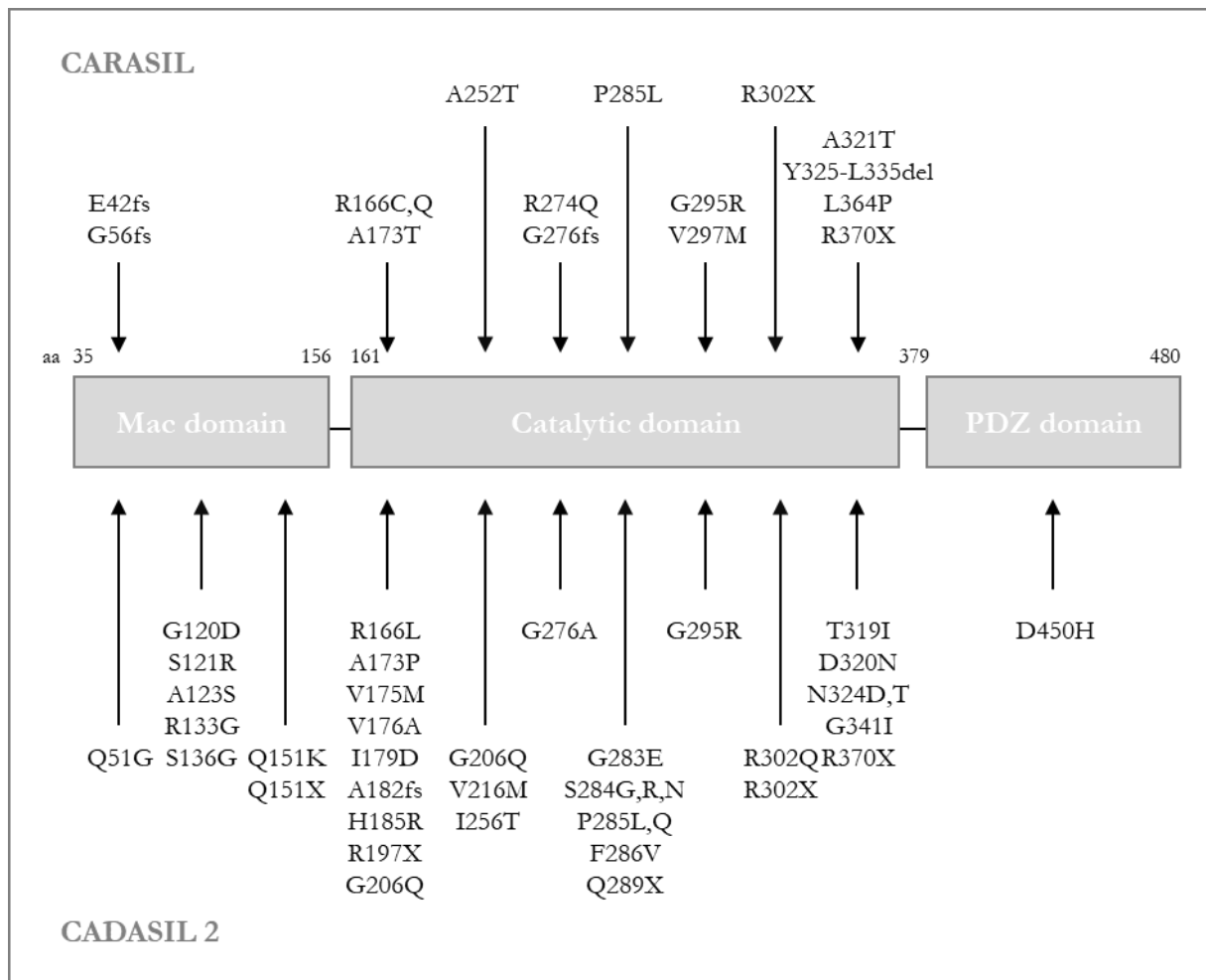


Figure 6.7: HTRA1 mutations identified in CARASIL and CADASIL 2 cases. Schematic representation showing the distribution of CARASIL and CADASIL 2 mutations in HtrA1. Mutations consist of missense, nonsense, frameshift, and splice site mutations.

Importantly, the exact mechanisms underlying the pathogenicity of monoallelic HTRA1 mutations are debated. HTRA1 haploinsufficiency might be sufficient to cause late-onset SVD. Alternatively, a subset of mutations has been proposed to display dominant-negative effects. Indeed, the corresponding mutant proteins were found to impair the activity of wildtype (wt) HTRA1 (Nozaki, Kato et al. 2016, Lee, Chung et al. 2018, Uemura, Nozaki et al. 2019). However, evidence for this is restricted to in vitro assays with methodological limitations. Moreover, the fact that pathogenic mutations identified in heterozygous patients (*i*) partially overlap with those observed in CARASIL cases and (*ii*) include early frameshift mutations suggest that HTRA1 haploinsufficiency causes the disease.

6.2.3.2 HTRA1 processes extracellular matrix proteins and regulates transforming growth factor beta signaling

HTRA1 is a highly conserved and ubiquitously expressed enzyme that is involved in a large number of processes, including protein degradation, signaling, cell differentiation and cell survival (Clausen et al. 2011b), in both physiological and pathological conditions.

After secretion, HTRA1 is deposited in the ECM (Beaufort, Scharrer et al. 2014). Here, HTRA1 processes a panel of ECM and ECM-related proteins, including fibronectin, vitronectin and fibromodulin (Murwantoko, Yano et al. 2004, Grau, Richards et al. 2006), and therefore plays a key role in ECM homeostasis. Accordingly, my host laboratory recently demonstrated that a multitude of ECM proteins, including several HTRA1 substrates, are highly enriched in the cerebral vasculature of *htra1*^{-/-} mice (Zellner, Scharrer et al. 2018). Notably, alterations in the cerebrovascular matrisome (the ensemble of proteins constituting the ECM as well as the proteins associated with the ECM) are not restricted to CARASIL, but have also been reported in, for example, COL4A1/2-related SVD and CADASIL, and have been proposed as a convergent pathomechanism in SVD (Haffner, Malik et al. 2016, Joutel, Haddad et al. 2016).

HTRA1 targets several proteins involved in cell signaling pathways. In particular, interactions between HTRA1 and transforming growth factor beta (TGF- β) signaling pathway components have received attention (see detailed description of the TGF- β signaling pathway in paragraph 6.3.2.2). It has been proposed that HTRA1 inhibits TGF- β signaling via the proteolytic degradation of TGF- β and TGF- β receptors (Oka, Tsujimoto et al. 2004, Shiga, Nozaki et al. 2011, Graham, Chabon et al. 2013). In contrast, my host laboratory demonstrated that HTRA1 cleaves latent TGF- β binding protein 1 (LTBP1), resulting in the release of LTBP1/TGF- β complexes from the ECM, which ultimately facilitates TGF- β signaling (Figure 6.8) (Beaufort, Scharrer et al. 2014). Accordingly, HTRA1 loss of function was linked to a marked reduction in TGF- β signaling levels in skin fibroblasts from a CARASIL patient as well as in embryonic fibroblasts and brain tissue from *htra1*^{-/-} mice (Beaufort, Scharrer et al. 2014). Beyond CARASIL, abnormal levels of TGF- β signaling-related proteins have been described in other cerebral vascular disorders, including CADASIL, Alzheimer's disease and incontinentia pigmenti. This suggests that TGF- β signaling alterations might be a common denominator in SVD (Muller, Courtois et al. 2017).

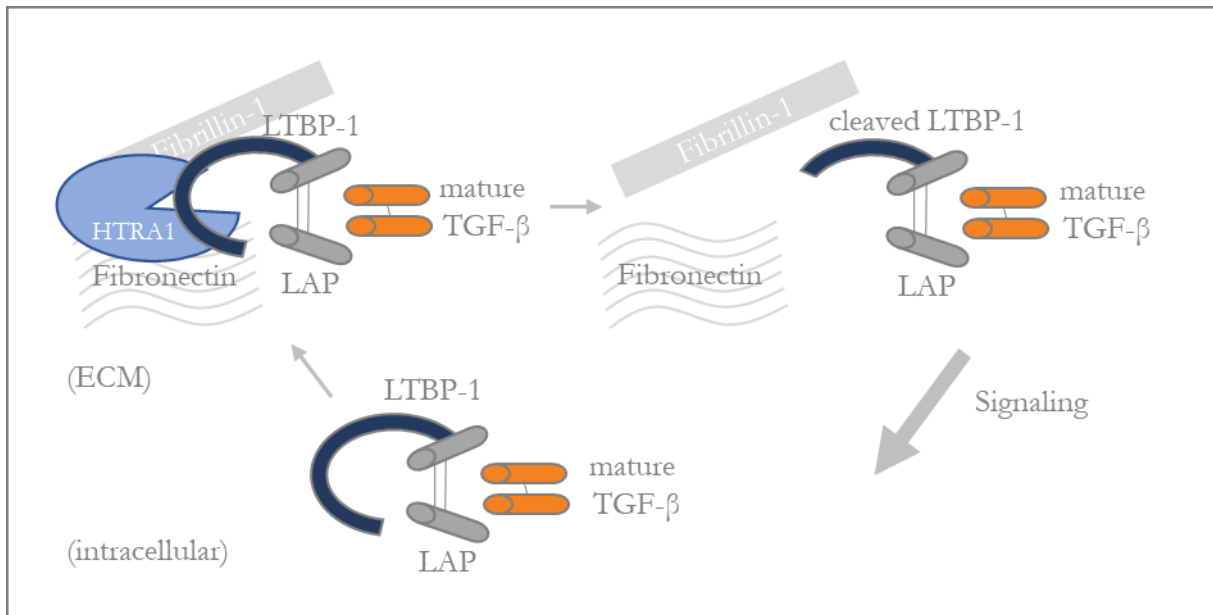


Figure 6.8: HTRA1 associates with the ECM and facilitates TGF- β signaling. After secretion, TGF- β in complex with LTBP-1 is sequestered in the ECM in an inactive form. HTRA1-dependent cleavage of LTBP-1 liberates LTBP-1/TGF- β complexes from the ECM and promotes TGF- β signaling (Beaufort, Scharrer et al. 2014). ECM: extracellular matrix; LAP: latency-associated peptide; LTBP-1: latent TGF- β binding protein; TGF- β : transforming growth factor beta.

6.3 PHENOTYPIC SWITCHING OF VASCULAR SMOOTH MUSCLE CELLS

6.3.1 Vascular smooth muscle cells

6.3.1.1 Location and function

Vascular SMCs (VSMCs) are located in the tunica media of venules, veins, arterioles and arteries. They are highly contractile mononuclear cells and are distinguished from SMCs of the digestive, respiratory, and urogenital tracts by their abundant expression of vimentin (intermediate filament) and low levels of desmins (Gabbiani, Schmid et al. 1981).

Through contraction and relaxation of the cell and consecutive adjustments to the diameter of the vessel, VSMCs regulate the blood flow and therefore the pressure within the vessel (Owens, Kumar et al. 2004, Gomez and Owens 2012).

During vascular development, VSMCs play a key role through their ability to proliferate, migrate and produce ECM proteins like collagens (Owens, Kumar et al. 2004). Furthermore, together with pericytes, they determine the mechanical properties of mature vessels through the secretion of ECM components, including elastin and collagens (Wolinsky and Glagov 1964, Li, Brooke et al. 1998, Wagenseil and Mecham 2009). VSMCs also play a major role in vessel remodeling in physiological conditions like pregnancy and exercise and after vascular injury (Owens, Kumar et al. 2004). In these situations, they increase proliferation and migration and synthesize ECM components, as will be described below.

6.3.1.2 Phenotypic characteristics

Depending on their environment, VSMCs can adopt a variety of phenotypes via the modulation of their proteome, morphology, and proliferation/migration characteristics. This phenotypic switching, which is to some extent reversible, occurs physiologically, but also during several vascular diseases, such as atherosclerosis (Chamley-Campbell, Campbell et al. 1979, Rensen, Doevendans et al. 2007, Majesky, Dong et al. 2011) (Figure 6.9). Among the spectrum of possible phenotypes, my experimental work examined three well-defined phenotypic states:

The contractile phenotype. Contractile VSMCs are highly specialized or differentiated and proliferate and migrate at low rates (Hao, Gabbiani et al. 2003). While they express a unique pattern of contractile markers and intracellular signaling molecules needed for the contractile function like

calponin, smooth muscle protein 22-a (SM22), and α -SMA (Iyemere, Proudfoot et al. 2006), they produce low levels of ECM proteins (Owens, Kumar et al. 2004).

The synthetic (or migroproliferative) phenotype. Synthetic VSMCs exhibit a high rate of proliferation and increased migration (Hao, Gabbiani et al. 2003). The synthetic phenotype is mostly defined by a reduction in contractile markers with an increased production of ECM (Owens, Kumar et al. 2004).

The phagocytic phenotype. Phagocytic VSMCs are macrophage-like cells found in atherosclerotic lesions. While contractile markers are reduced, the expression of galectin 3 (also known as MAC-2) is enhanced (Rong, Shapiro et al. 2003, Feil, Fehrenbacher et al. 2014). Galectin 3 is usually expressed in macrophages and is involved in inflammation and fibrosis (Papaspyridonos, McNeill et al. 2008). It interacts with cell surface receptors (integrins) as well as ECM proteins like collagen, elastin and fibronectin (Ochieng, Furtak et al. 2002).

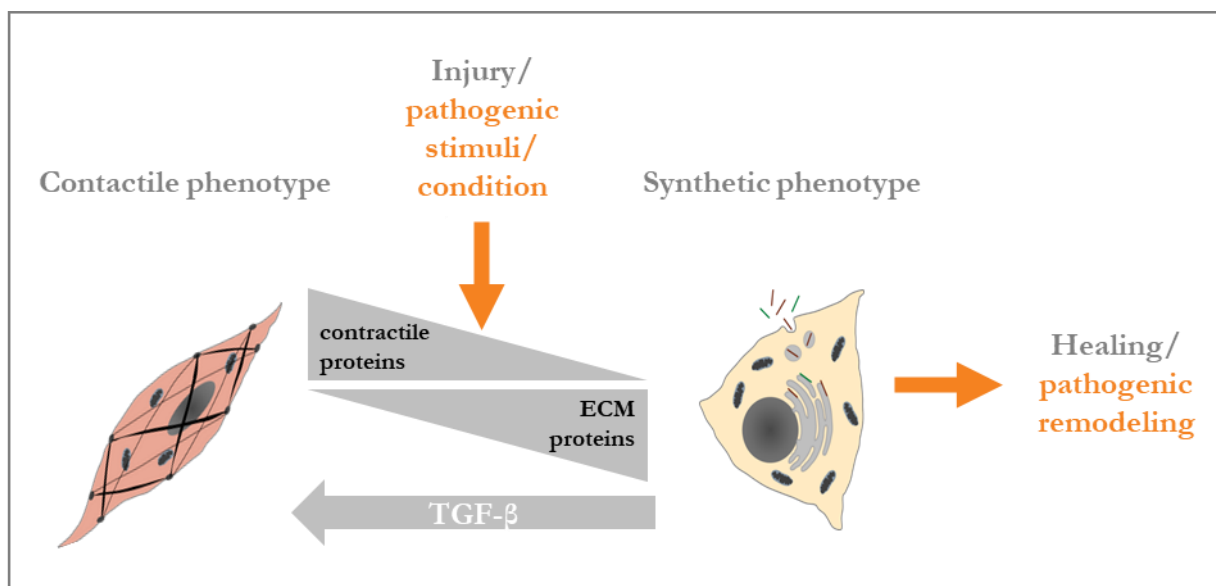


Figure 6.9: Phenotypic switching of vascular smooth muscle cells. In response to a vascular injury, vascular smooth muscle cells (VSMCs) switch from a contractile to a synthetic phenotype. This reversible phenotypic modulation, which contributes to healing, also occurs in various pathological conditions. Several growth factors, including transforming growth factor beta (TGF- β), promote VSMC switching from the synthetic to the contractile phenotype.

6.3.2 Regulation of the phenotype of VSMCs

6.3.2.1 External regulators of the VSMC phenotype

The phenotype of VSMCs is highly dependent on their interaction with the environment. Several factors that regulate their phenotype have been identified:

Mechanical forces, including shear stress and cyclic strain.

Vessel injury by, for example, mechanical trauma, toxins, reactive oxygen species and chemicals, as well as inflammatory mediators, lipids and lipid products.

Interactions with other cells or ECM. These interactions involve several adhesion receptors, especially integrins.

Humoral factors, including a variety of growth factors and their downstream signaling: TGF- β , platelet-derived growth factor (Deguchi, Namba et al. 1999), angiotensin II, Wnt/Notch and retinoic acid (Li, Brooke et al. 1998, Owens, Kumar et al. 2004, Rensen, Doevendans et al. 2007, Wang, Jacquet et al. 2015).

6.3.2.2 Transcriptional regulation of the VSMC phenotype by TGF- β signaling

When released from the ECM, TGF- β binds the TGF- β receptor 2 (TGFBR2) on the surface of its target cells (Lopez-Casillas, Wrana et al. 1993) (Figure 6.10). Subsequently, the activated TGFBR2 recruits TGF- β receptor 1 (TGFBR1) to form a heterotetrameric receptor complex. Upon phosphorylation, this receptor complex phosphorylates the receptor regulated (R)-Smads (mothers against decapentaplegic homolog), such as Smad 2/3 (Derynck and Zhang 2003, Massague, Seoane et al. 2005). These intracellular mediators recruit the co-Smad Smad4 and the Smad complex translocates into the nucleus (Feng and Derynck 1997, Chen, Kitchen et al. 2002, Massague 2012). In the nucleus, Smads interact with Smad-binding element (SBE) and GC-rich sequences located in the promoters of their target genes and promote their transcription. Among many other targets, connective tissue growth factor (CTGF) and plasminogen activator inhibitor-1 (PAI-1) are frequently used as surrogate markers of TGF- β signaling (Dennler, Itoh et al. 1998, Schmierer and Hill 2007, Massague 2012). Furthermore, several TGF- β target genes are associated with the contractile phenotype of VSMCs, including the genes encoding calponin, SM22, and α -SMA (Guo and Chen 2012, Miano 2015).

In addition to the Smads, various other transcriptional regulators of the VSMC phenotype have been reported. These regulators can act as Smad co-factors or as Smad antagonists, an example of which is Krüppel-like factor 4 (KLF4; Figure 6.10) (Liu, Sinha et al. 2003, Guo and Chen 2012, Salmon, Gomez et al. 2012).

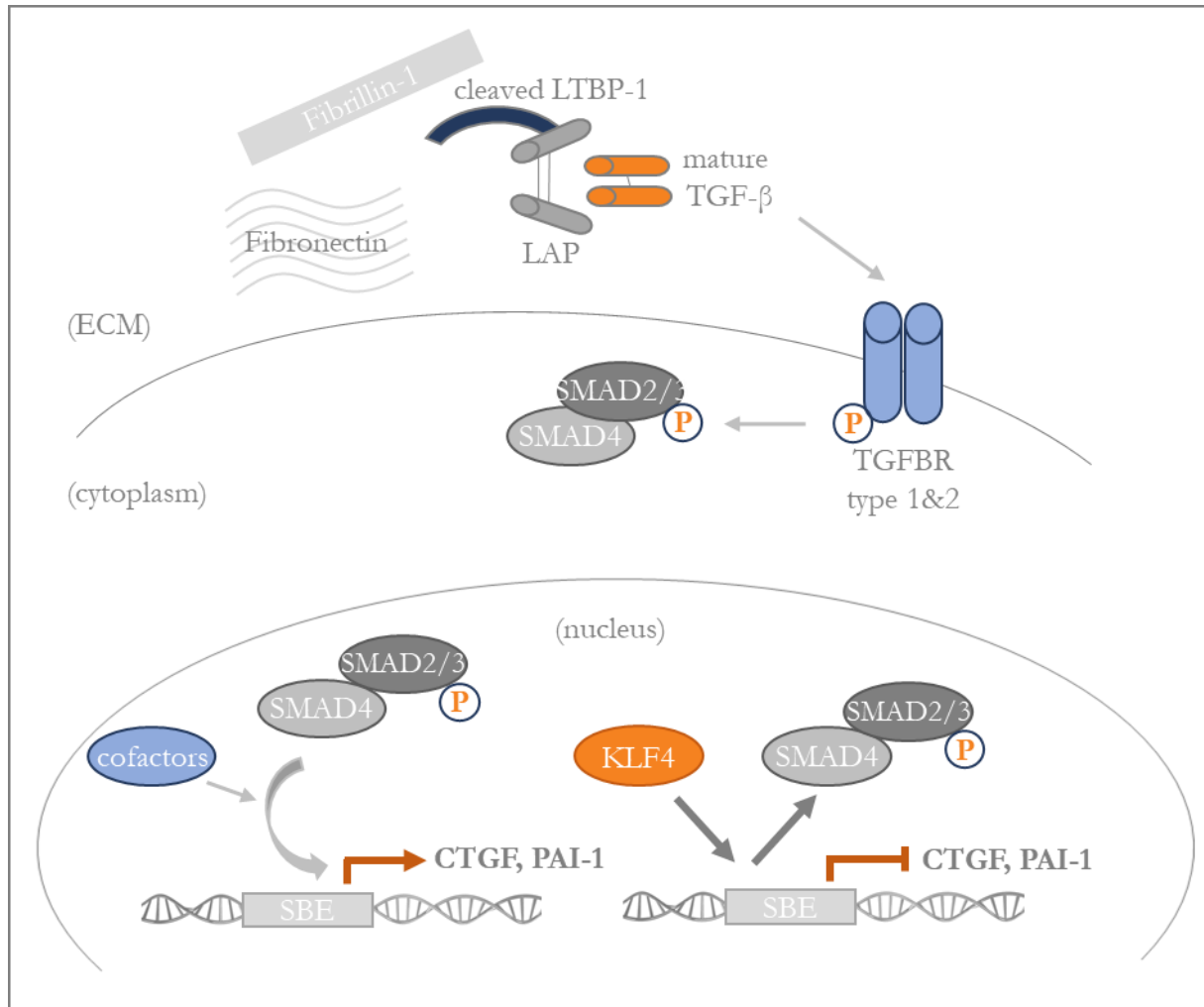


Figure 6.10: Schematic of the TGF- β signaling pathway. Mature TGF- β activates cell surface receptor kinases, resulting in the phosphorylation and nuclear translocation of the Smads and the transcriptional activation of TGF- β target genes. Smad binding to the promotor of target genes can be facilitated by co-factors or antagonized by repressors such as KLF4. CTGF: connective tissue growth factor; ECM: extracellular matrix; LAP: latency associated peptide; LTBP-1: latent TGF- β binding protein 1; KLF4: Krüppel-like factor 4; PAI-1: plasminogen activator inhibitor-1; SBE: Smad binding element; Smad: mothers against decapentaplegic homolog; TGF- β : transforming growth factor beta; TGFBR: TGF- β receptor.

6.4 AIM OF THE THESIS

Loss-of-function mutations in HTRA1 are linked to familial cerebral SVD, but the underlying pathological mechanisms are poorly understood and treatment options are lacking.

My laboratory provided evidence that HTRA1 loss of function impairs TGF- β signaling (Beaufort, Scharrer et al. 2014, Scharrer 2015, Landinger 2021), which is a key regulator of VSMC contractile differentiation. Accordingly, previous analyses suggested that skin fibroblasts derived from HTRA1 mutation carriers and brain tissue from *htra1*^{-/-} mice exhibit reduced contractile cell differentiation markers (Landinger 2021).

To complement these findings, the first aim of my work was to assess the **impact of HTRA1 loss of function on contractile cell differentiation** using embryonic fibroblasts and brain tissue from *htra1*^{-/-} mice, as well as skin fibroblasts from a CARASIL proband and their two asymptomatic parents.

In this context, I used human skin fibroblasts carrying the intronic mutation c.1005+1G>T. Hence, as a second aim, I intended to evaluate the **consequences of this atypical mutation on multiple determinants of HTRA1 function**, including gene expression and mRNA splicing, as well as protein stability and enzymatic activity.

7 MATERIALS AND METHODS

7.1 MOUSE TISSUE

7.1.1 Mouse strain

Htra1^{-/-} mice (strain HtrA1 Gt(OST394864)Lex) were generated by gene trapping in collaboration with Taconic (Hudson) (Beaufort, Scharrer et al. 2014) and were backcrossed onto a C57BL6J background. Animals are viable, fertile, and display no obvious phenotype. C57BL6J mice were used as *htra1*^{+/+} controls. Animal experiments were performed in compliance with the German Animal Welfare Law and the Government of Upper Bavaria.

7.1.2 Collection and lysis of mouse tissues

Mouse brains were harvested from phosphate-buffered saline (PBS)-perfused animals and lysed in radioimmunoprecipitation assay (RIPA) buffer using the TissueLyser system (Qiagen) prior to my stay at the Institute for Stroke and Dementia Research (ISD). Samples were stored at -80°C.

7.2 CELL CULTURE AND TREATMENT

7.2.1 Cells

7.2.1.1 Mouse embryonic fibroblasts

Fibroblasts were derived from 12.5 days pc *htra1*^{+/+} or *htra1*^{-/-} embryos according to standard procedures and were immortalized via serial replating. Cells were kindly provided by Eva Scharrer (Scharrer 2015).

7.2.1.2 Human skin fibroblasts

Fibroblasts were derived from skin biopsies according to standard procedures. Cultures from healthy controls and *HTRA1* mutation carriers were kindly provided by Dr. Matthis Synofzik (Hertie Institute, University of Tübingen). The use of human fibroblasts at the ISD is approved by the ethical review board of the Ludwig-Maximilians University (Project N° 570-16).

7.2.1.3 HEK-293T cells

HEK-293T cells were isolated from human embryonic kidneys and transformed to stably express the SV40 large T antigen (American Type Culture Collection). HEK-293T cells are easy to cultivate and transfect and allow high yields of recombinant protein expression.

7.2.2 Cell culture

7.2.2.1 Culture conditions

Human and mouse fibroblasts, as well as HEK-293T cells, were grown in Dulbecco's modified Eagle's medium (DMEM) containing GlutaMAX, sodium pyruvate, and 4.5 g/l D-glucose and supplemented with 10% (v/v) fetal calf serum (FCS), 100 U/ml penicillin, and 100 µg/ml streptomycin (all reagents from Gibco Invitrogen). Cells were manipulated under a sterile vertical laminar flow hood (Herasafe KS, Thermo Fisher Scientific) and were kept at 37°C in a humidified chamber (Binder 9040-0038) at a CO₂ level of 5% (v/v).

7.2.2.2 Passaging

After one wash with PBS, cells were detached with 0.25% (w/v) trypsin/ethylenediaminetetraacetic acid (EDTA; Gibco Invitrogen) and seeded in a new flask containing fresh medium at a cell dilution ranging from 1:3 to 1:20, depending on the cell proliferation rate. The volumes of reagents used for cell culture are listed in Table 7.1.

When required, detached cells were counted in a Neubauer chamber. Cell concentration was calculated as follows: number of cells/ml = number of cells in the chamber/9 x 10,000.

7.2.2.3 Freezing/Thawing

Freezing. Complete medium was added to detached cells (see above) to neutralize the effect of trypsin and EDTA. Cells were centrifuged at 400 x g for 10 min, resuspended in FCS supplemented with 10% (v/v) dimethylsulfoxide (DMSO; Sigma-Aldrich), and transferred into cryotubes (2 cryotubes per T80 flask). Tubes were placed in a cryobox filled with isopropanol and transferred from 4°C to -80°C to ensure a slow decrease of the temperature. After one day, cells were transferred to liquid nitrogen for long-term storage.

Thawing. Cell suspensions were transferred from -196° to 37°C. After thawing, cells were seeded in T80 culture flasks containing fresh culture medium. After one night, the medium was renewed to remove traces of DMSO.

	P48 well (0.84 cm ²)	P24 well (2 cm ²)	P6 well (9.5 cm ²)	T25 flask (25 cm ²)	T80 flask (80 cm ²)
PBS	0.5 ml	0.5–1 ml	1–2 ml	2–5 ml	5–10 ml
Trypsin		-	-	1 ml	2 ml
Culture medium	0.5 ml	0.5 ml	1 ml	5 ml	10 ml
OptiMEM		50 µl	100 µl	-	-
Lipofectamine 2000	-	0.75 µl	1.5 µl	-	-
Plasmid DNA	-	250 ng	1 µg	-	-
RIPA buffer	-	100 µl	100–150 µl	0.5 ml	1 ml
RLT buffer		100 µl	100 µl	350 µl	1 ml

Table 7.1: Volume or quantity of reagents used for cell culture and treatment.

7.2.3 Cell treatment

The volumes of reagents used for cell-based experiments are depicted in Table 7.1.

7.2.3.1 Serum starvation

For all experiments involving FCS starvation, cells were seeded in culture flasks or plates coated with poly-L-lysine (0.01%, Sigma-Aldrich) to prevent cell detachment. After one wash with PBS, adherent cells were maintained in FCS-free culture medium for up to 3 days.

7.2.3.2 Transient transfection

Cloning of a vector encoding the expression of the pathogenic $\Delta 5$ HTRA1 is described below. pcDNA₄/TO/Myc-His expression vectors (Thermo Fisher Scientific) encoding the cDNA of human wild-type (wt) HTRA1 or HTRA1 bearing an active site mutation (S328A) as well a pcDNA₆/V5-His expression vector encoding the cDNA of a carboxyterminally truncated form of human LTBP-1s have previously been described (Beaufort, Scharrer et al. 2014).

Cells were seeded in 6- or 24-well plates and transfected at a density of 50%–80%. Lipofectamine 2000 (Invitrogen) and plasmid DNA (quantities reported in Table 7.1) were mixed in OptiMEM (Gibco Invitrogen) at a ratio of 1.5 μ l Lipofectamine/1 μ g DNA for 15 min at room temperature. Cells were washed with PBS and treated with complete (for inhibition of protein translation) or FCS-free medium (for HTRA1 secretion and protease activity assays). The transfection mix was added dropwise to the cells and cells were cultured for a further 24–72 h.

7.2.3.3 Inhibition of protein translation

Cells were exposed to culture medium containing 0.05 mg/ml cycloheximide (Sigma-Aldrich) for 0.5 h, 1.5 h, 5 h, or 24 h. Since cycloheximide is solubilized in DMSO, cells exposed to medium with an equivalent concentration of DMSO (0.05%; Sigma-Aldrich) were used as the control.

7.2.4 Collection of cell extracts

The composition of the buffers used to collect cell extracts is reported in Table 7.2.

7.2.4.1 Cell culture media

Culture medium was collected and centrifuged for 10 min at 400 x g to discard debris. Culture medium of human skin fibroblasts was concentrated by centrifugation at 3000 x g in a 10 kDa cut-off Amicon filter (Millipore). Three to five 5 min centrifugation runs at 300 x g were performed until the expected concentration factor (20x) was obtained. Samples were aliquoted and stored at -80°C until further analysis.

7.2.4.2 Cell lysates

Genomic DNA analysis. Cells were detached with trypsin/EDTA (as described above), resuspended in complete medium and centrifuged at 400 x g for 10 min. After one rinse with PBS, cell pellets were resuspended in 100 µl of 50 mM NaOH and incubated 30 min at 97°C, followed by neutralization with 30 µl of 1 M Tris(hydroxymethyl)aminomethane (Tris)-HCl (pH 7).

RNA analysis. Cells were rinsed with PBS, then lysed with RLT buffer (Qiagen) containing 1% (v/v) β-mercaptoethanol (Gibco Invitrogen) for 5 min on ice. Lysates were stored at -80°C.

Protein analysis. Cells were rinsed with PBS, then lysed with RIPA buffer (see Table 7.2) containing EDTA-free protease inhibitor and phosphatase inhibitor cocktails (Roche) for 20 minutes at 4°C. Samples were centrifuged for 10 min at 11,000 x g to remove RIPA-insoluble material, and lysates were stored at -20°C.

RIPA buffer (1x)	50 mM Tris 150 mM NaCl 1% (w/v) sodium deoxycholate 1% (v/v) Triton X-100 0.5% (w/v) SDS pH 7.4
Tris lower gel buffer	25 mM Tris-base 0.08% SDS (w/v)

	4% acrylamide (acrylamide stock: 30% (w/v) acrylamide and 0.8% (w/v) N,N'-Methylenebisacrylamide acrylamide stock (National Diagnostics) pH 6.8
Tris upper gel buffer	375 mM Tris-base 0.08% (w/v) SDS 7.5%–12.5% acrylamide (see above) pH 8.8
Laemmli buffer (final concentration)	75 mM Tris-base 6% (v/v) Glycerol 1.2% (w/v) SDS 100 mM DTT 0.006% (w/v) bromophenol blue pH 6.8
Protein electrophoresis buffer	25 mM Tris-base 192 mM glycine 0.1% (w/v) SDS dH ₂ O pH 8.3
Protein transfer buffer	25 mM Tris-base 192 mM glycine 20% (v/v) methanol dH ₂ O pH 8.3
Colloidal Coomassie solution	0.02% (w/v) Coomassie Brilliant Blue R (Sigma-Aldrich) 5% (w/v) aluminum sulfate hydrate 2% (v/v) o-phosphoric acid 10% (v/v) ethanol
TBS-T (Tris-buffered saline-Tween)	10 mM Tris-base 150 mM NaCl 0.05% Tween 20 (v/v) dH ₂ O pH 8
Agarose gel	1% agarose, 0.013% SYBR Safe (Invitrogen) prepared in 1x TAE buffer (Invitrogen)
LB (Luria broth)-agar	5 g/l yeast extract 10 g/l peptone 5 g/l NaCl 1.5% Agar-Agar pH 7.0
LB solution	5 g/l yeast extract 10 g/l peptone 5 g/l NaCl pH 7.0

Table 7.2: Buffer composition

7.3 GENOMIC DNA ANALYSIS

7.3.1 DNA amplification

Genomic DNA was amplified from 0.5 µl cell lysate in a 40 µl reaction mixture containing KCl Buffer (Fermentas), 2 mM MgCl₂ (Fermentas), 0.2 mM deoxyribonucleoside triphosphates (dNTPs; GE Healthcare), 5U Taq-Polymerase (Fermentas), and 0.2 µM primers (Metabion) targeting the 5' and 3' of *HTRA1* exon 5:

Exon 5-forward: 5'-CGGCACCTCTAAAAC TTT-3'

Exon 5-reverse: 5'-CCTGCCTCAAAAACAAAC-3'.

Amplification was performed in a Peqlab Gradient Cyclor using the following protocol:

Cycle(s)	Time	Temperature
1	10 min	95°C
30	2 min 1 min 30 sec	95°C 67°C 72°C
1	10 min	72°C
1	Infinite	4°C

7.3.2 DNA electrophoresis

To confirm the amplification of a PCR product at the expected size (i.e., 325 bp), loading buffer (New England Biolabs) was added to 10 µl of PCR product, which was then run on a 1% SYBR Safe agarose gel in TAE buffer (Carl Roth) at 80 V for 1 h. PeqGold DNA ladder (100–10,000 bp) was used as standard (Peqlab). DNA was visualized with a UV table (Vilber Lourmat).

7.3.3 DNA sequencing

DNA was purified using a PCR Purification Kit (Roche) according to the manufacturer's instructions, which included DNA binding to a silica membrane, washings, and elution. After elution in 30 µl H₂O, DNA concentration was determined on a Nanodrop ND-1000 spectrophotometer (Thermo Fisher Scientific).

For sequencing, 500 µg DNA were sent to GATC Biotech (Supreme Sequencing) together with 20 µl of exon 5 reverse primer diluted to 10 pmol/µl in H₂O (see sequences above). Sequences were compared to that of human *HTR41* using the CLC Workbench (Qiagen).

7.4 MRNA ANALYSIS

7.4.1 RNA isolation

RNA was extracted using the RNeasy Mini Kit (Qiagen) according to the manufacturer's instructions. Briefly, RNA was bound to a silica membrane in a small column. After centrifugation and washing, DNA was discarded by incubation with 0.39 U/µl RNase-free DNase (Qiagen) for 20 min at room temperature. Following serial washings, RNA was eluted in 30 µl RNase-free H₂O. RNA concentration was determined on a Nanodrop ND-1000 spectrophotometer and samples were stored at -80°C.

7.4.2 cDNA synthesis

Reverse transcription was performed using the Omniscript RT kit (Qiagen) according to the manufacturer's instructions. Up to 1 µg RNA was mixed with 2.86 µM oligo(dT)₁₅ primers (Metabion), 20 mM dNTP (Invitrogen), 4 units reverse transcriptase and compatible buffer in a final volume of 20 µl H₂O. mRNA-free and reverse transcriptase-free samples were prepared as controls. The mix was incubated for 1 h at 37°C, then stored at -20°C.

7.4.3 Analysis of splicing variants

150 ng cDNA were amplified using *HTR41* primers targeting exons 1 and 7:

Forward primer: 5'-CAACACCTACGCCAACCT-3'

Reverse primer: 5'-GCTGGACGTGAGTGACAT-3'

and the AccuPrime DNA polymerase (Qiagen, buffer A) according to the manufacturer's instruction in a Peqlab Cycler using the protocol shown below.

Cycle(s)	Time	Temperature
1	5 min	95°C
35	30 sec	95°C
	30 sec	50°C
	90 sec	72°C
1	10 min	72°C
1	Infinite	4°C

Gel electrophoresis and sequencing were conducted as described above.

7.4.4 Quantitative real-time PCR

Primers. Exon-spanning primers were designed using the Universal Probe Library Probe Finder (Roche). A primer list is provided in Table 7.3.

Sample preparation. 2 μ l 1:10 (v/v) cDNA was added to 6 μ l Brilliant II SYBR Green MasterMix (Agilent Technologies) and 200 nM each of forward and reverse primers (all diluted in DNase- and RNase-free water). mRNA-free and reverse transcriptase-free samples, prepared as described above, were included as negative controls. Samples were loaded in technical triplicate on a 384-well plate sealed with adhesive foil.

PCR program. PCR was run on a Roche Light Cycler using the following steps:

Step/Cycle(s)	Time	Temperature
Denaturation/1	10 min	95°C
Amplification/40	30 sec	95°C
	1 min	60°C
Melting curve/1	10 sec	95°C
	10 sec	60°C
	Continuous (5 acquisitions per °C)	95°C
Cooling/1	Infinite	4°C

Data analysis. Samples displaying multi-peak dissociation curves, crossing point (CP) values over 35, or high variability among triplicates (i.e., SD over 0.2) were excluded and the cDNA quantity

was derived using the following formula: absolute cDNA quantity = $2^{-(C_p)}$. *Gapdh* was used as normalizer.

Gene/Protein	Sequence
human	
<i>Gapdh</i> /GAPDH	Forward primer: 5'-GCCTCAAGATCATCAGC-3' Reverse primer: 5'-ACCACTGACACGTTGGC-3'
<i>HTRA1</i> /HTRA1	Forward primer: 5'-GGAGTCCCATGACCGACA-3' Reverse primer: 5'-GAGTGACATCATTCGGATACCA-3'
mouse	
<i>cnn1</i> /calponin 1	Forward primer: 5'-CGGCTTGTCTGCTGAAGTAA-3' Reverse primer: 5'-ACCCCTCAATCCACTCTCT-3'
<i>gapdh</i> /Gapdh	Forward primer: 5'-ATTGTCAGCAATGCATCCTG-3' Reverse primer: 5'-ATGGACTGTGGTCATGAGCC-3'
<i>htra1</i> /HtraA1	Forward primer: 5'-GGCGAGGTGATTGGGATTAA-3' Reverse primer: 5'-TCCGTTGATGCTGATGATG-3'
<i>klf4</i> /Klf4	Forward primer: 5'-CGGGAAGGGAGAAGACACT-3' Reverse primer: 5'-GAGTTCCTCACGCCAACG-3'
<i>klf5</i> /Klf5	Forward primer: 5'-CCGGAGACGATCTGAAACAC-3' Reverse primer: 5'-CAGATACTTCTCCATTTCACATCTTG-3'
<i>tagln</i> /SM22	Forward primer: 5'-CCTTCCAGTCCACAAACGAC-3' Reverse primer: 5'-GTAGGATGGACCCTTGTTGG-3'

Table 7.3: List of RT-qPCR primers (all from Metabion)

7.5 PROTEIN ANALYSIS

The composition of the buffers is provided in Table 7.2.

7.5.1 Determination of total protein concentration

For protein concentration measurements, the bicinchoninic acid (BCA) assay (Pierce BCA Protein Assay Kit, Thermo Fisher Scientific) was used. Bovine serum albumin (BSA, Bio-Rad) at a range of 0.0125 to 2 mg/ml was used as a standard. Ten μ l of BSA or sample diluted in RIPA buffer were placed in wells of a 96-well plate. After addition of 75 μ l of BCA solution (50:1 ratio of Buffer A:B), plates were incubated for 20 min at 37°C. The absorbance at 595 nm was measured in a spectrophotometer (iMark microplate reader, Bio-Rad). Sample concentration was extrapolated from the BSA standard curve.

7.5.2 Sodium dodecyl sulfate polyacrylamide gel electrophoresis (SDS-PAGE)

Gel preparation. Gels were prepared following the description in Table 7.2. Polymerization was induced by the addition of ammonium persulfate and tetramethylethylenediamine (Temed) and gel solutions were poured in a Bio-Rad casting system.

Sample preparation. Samples (20 μ l of culture medium; 5–25 μ g total protein for cell or tissue lysates) were mixed with Laemmli buffer. Samples were incubated at 95°C for 5 min. The Precision Plus Protein All Blue Standard (5 μ l, Bio-Rad) was included in each run to evaluate the apparent protein molecular mass (M_r range: 10,000–250,000).

Electrophoresis. Protein electrophoresis was performed in a Mini-Protean 3 device (Bio-Rad) filled with electrophoresis buffer for 1 h at 150 V.

7.5.3 Immunoblot

Proteins were transferred onto a polyvinylidene fluoride (PVDF) membrane (Immobilon-P, 0.45 μ m; Millipore) for 1 h at 100 V in a Mini-Protean Tetra Cell wet transfer system (Bio-Rad) filled

with protein transfer buffer. Membranes were incubated on a shaker for 15 min in TBS-T with 4% (w/v) skim milk to prevent non-specific Ab binding. Subsequently, membranes were incubated in a solution of primary Ab prepared in TBS-T/milk for 1 or 2 h at room temperature up to overnight at 4°C (primary and secondary antibodies are listed in Table 7.4). Following 3 washings in TBS-T for 10 min, membranes were incubated 1–2 h at room temperature in a solution of horseradish peroxidase (HRP)-coupled secondary antibody prepared in TBS-T/milk. After washings in TBS-T, HRP activity was revealed using the Immobilon Western Chemiluminescent HRP Substrate (Millipore). Luminescence was detected with a Fusion FX7 cooled camera (Fusion, Vilber Lourmat) and images were prepared using the Fusion software (Vilber Lourmat). Signal quantification was performed using ImageJ software (Fiji). B-actin or tubulin were used as normalizers.

Antigen	Host	Company	Working dilution
Primary Antibodies			
α -SMA	mouse	Sigma-Aldrich	1/1000
β -actin	rabbit	Sigma-Aldrich	1/1000
Calponin-1	rabbit	Millipore	1/1000
c-Myc	mouse	Santa Cruz Biotechnology	1/5000
Fibronectin	goat	Sigma-Aldrich	1/1000
Galectin 3	rat	Biozol Systems	1/1000
HTRA1	rabbit	kindly provided by S. Fauser (Univ. Cologne) (Vierkotten et al. 2011)	1/1000
Phospho-Smad2/3	rabbit	Cell Signaling Technologies	1/1000
SM22	goat	Abcam	1/1000
Smad2	mouse	Abcam	1/1000
Tubulin	mouse	Sigma-Aldrich	1/1000
V5	mouse	Gibco Invitrogen	1/5000
HRP-coupled Secondary Antibodies			
Mouse Immunoglobulins	goat	Dako	1/10,000
Rabbit Immunoglobulins	goat	Dako	1/10,000

Goat Immunoglobulins	rabbit	Dako	1/10,000
Rat Immunoglobulins	rabbit	Dako	1/10,000

Table 7.4: List of primary and secondary antibodies

7.6 CLONING OF A $\Delta 5$ HTRA1 EXPRESSION VECTOR

7.6.1 Preparation of the insert

150 ng cDNA derived from fibroblasts were amplified using *HTRA1* primers targeting exons 1 and 9:

Forward primer: 5'-CTCTTCTCCCGCTGCTC-3'

Reverse primer: 5'-TTCITTCGGGAATCACTGT-3'

and the AccuPrime DNA polymerase (Qiagen, buffer A) according to the manufacturer's instructions in a Peqlab Cycler using the protocol shown below.

Cycle(s)	Time	Temperature
1	5 min	95°C
35	30 sec	95°C
	30 sec	50°C
	90 sec	72°C
1	10 min	72°C
1	Infinite	4°C

Gel electrophoresis was performed as described above to confirm the amplification of the expected 1379 bp product.

After PCR purification, the insert was prepared, taking advantage of restriction sites for BstEII and EcoRV naturally present within *HTRA1* cDNA. 1 μ g DNA was diluted in Cutsmart buffer and treated with 10 units BstEII and 20 units EcoRV for 1 h 30 min at 37°C (all reagents from New England Biolabs). After agarose gel electrophoresis, a gel piece containing the expected 741 bp DNA fragment was excised.

7.6.2 Preparation of the vector

1 µg pcDNA₄/TO/Myc-His encoding human HTRA1 wild-type (6560 bp) was digested with BstEII and EcoRV as described above. DNA was dephosphorylated for 1 h at 37°C using 5 units Antarctic Phosphatase (New England Biolabs) prepared in alkaline phosphatase buffer. The expected 5819 and 741 bp fragments were separated by gel electrophoresis and a piece of gel containing the 5819 bp fragment was excised.

7.6.3 DNA ligation

Insert and vector were extracted from the gel using the GeneJET DNA Extraction Kit (Thermo Fisher Scientific). Briefly, the gel was melted by heating in binding buffer, then DNA was trapped on a silica membrane and washed and eluted. DNA concentration was measured using a Nanodrop spectrophotometer.

Insert and vector were mixed in a molecular ratio of 3:1 and mixed with 4 units T4 DNA Ligase (New England Biolabs) and DNA ligase buffer. The mixture was incubated 1 h at room temperature.

7.6.4 Bacterial transformation and amplification

Competent *E. coli* DH5α cells (50 µl of in-house prepared suspension) were thawed on ice and incubated with 2 µl ligation mix for 30 min at 4°C. After heat shock for 90 s at 42°C, 300 µl LB medium was added to the bacteria, which was then incubated for 30 min at 37°C. The bacterial suspension was then spread on an LB-agar plate containing 0.1 mg/ml ampicillin (Sigma-Aldrich).

After overnight growth at 37°C, single colonies were transferred to 2 ml liquid LB medium containing 0.1 mg/ml ampicillin in a 5 ml round bottom tube (Miniculture). Bacteria were cultivated for at least 8 h at 37°C at 225 orbital rotations per min. For maxicultures, 1 ml of bacterial suspension was seeded in 100 ml LB medium with ampicillin in a 250 ml Erlenmeyer flask. Cultures were grown overnight as described above.

7.6.5 DNA mini- and midipreps

Plasmid DNA was extracted from bacterial cultures using the NucleoSpin Plasmid kit (small cultures) or the NucleoBond Xtra Midi kit (large cultures) from Macherey-Nagel according to the manufacturer's instructions. DNA concentration was determined on a Nanodrop spectrophotometer. The HTRA1-Δ5 sequence was verified by Supreme Sequencing (GATC Biotech) using GATC primer pcDNA3.1-RP1.

7.7 PROTEASE ACTIVITY ASSAYS

7.7.1 Processing of LTBP-1

5 μl medium from cells transfected to overexpress LTBP-1 were added to 20 μl culture medium derived from cells expressing endogenous (i.e., skin fibroblasts) or recombinant (i.e., transfected HEK-293T cells) HTRA1 in a protein LoBind Eppendorf tube. Samples were incubated for up to 72 h at 37°C and LTBP-1 proteolysis was examined by SDS-PAGE and immunoblot using an antibody detecting the carboxyterminal V5 tag of LTBP-1 (see above).

7.8 STATISTICS

Statistical analysis was performed in GraphPad. Normality was assessed using the Kolmogorov-Smirnov test. To compare two groups, analysis used the unpaired Student's t-test (normal distribution) or the Mann-Whitney U-test (non-normal distribution) as appropriate and indicated in the Figure Legends. p-values ≤ 0.05 were considered statistically significant.

8 RESULTS

8.1 CONSEQUENCES OF HTRA1 DEFICIENCY ON CONTRACTILE CELL DIFFERENTIATION

8.1.1 Consequences of HtrA1 deficiency on the contractile differentiation of mouse embryonic fibroblasts

To evaluate the consequences of HTRA1 deficiency on the differentiation status of contractile cells, I initially used immortalized fibroblasts derived from *htra1*^{+/+} or *htra1*^{-/-} embryos (n = 7–8/genotype). Note that similar to VSMCs, embryonic fibroblasts (as well as human skin fibroblasts, see section 8.2.4) express a panel of contraction markers and can contract (Liu, Wen et al. 2003). Moreover, previous analyses of the very same cultures had revealed reduced TGF- β signaling – one of the main signaling pathways promoting contractile differentiation – in *htra1*^{-/-} compared to *htra1*^{+/+} fibroblasts (Beaufort, Scharrer et al. 2014, Scharrer 2015).

8.1.1.1 HtrA1 deficiency reduces the abundance of contractile markers in mouse embryonic fibroblasts

In a first step, I determined the abundance of three well-described and widely used contractile differentiation markers (i.e., calponin, SM22, and α -SMA) by immunoblot analysis in *htra1*^{+/+} and *htra1*^{-/-} cell lysates (Figure 8.1). Actin served as a normalizer.

I found calponin and SM22 protein levels to be markedly reduced (i.e., by > 80% and > 40%, respectively) in *htra1*^{-/-} compared to *htra1*^{+/+} fibroblasts. Overall, the abundance of α -SMA was neither markedly (by < 25%) nor significantly down-regulated. Nonetheless, with the exception of two outlier cultures exhibiting high α -SMA levels, the abundance of α -SMA was reduced in *htra1*^{-/-} compared to *htra1*^{+/+} fibroblasts (by > 75%; p < 0.05, graph not depicted).

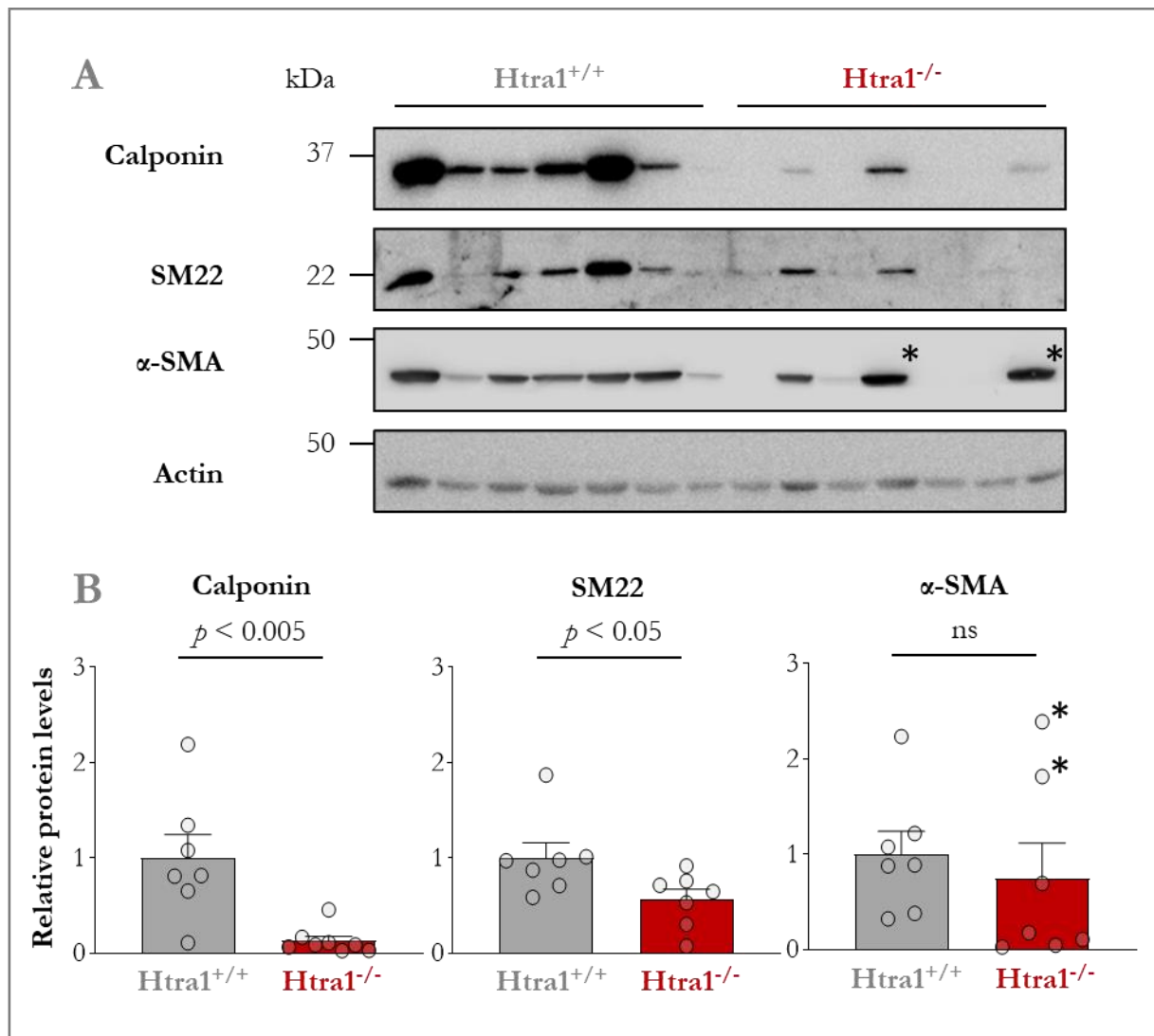


Figure 8.1: Calponin, SM22, and α -SMA protein levels in mouse embryonic fibroblasts. Fibroblasts from *htra1*^{+/+} or *htra1*^{-/-} embryos (n = 7/genotype) were lysed followed by detection of calponin, SM22, and α -SMA by immunoblot. Actin served as normalizer. (A) Representative images. (B) Histograms depict the mean normalized protein level +SEM. Circles represent single data points. The mean protein level measured in *htra1*^{+/+} fibroblasts was set to 1. p was calculated with a Mann–Whitney U test (calponin, SM22) or an unpaired Student’s t-test (α -SMA). Asterisks mark two outlier *htra1*^{-/-} cultures exhibiting high α -SMA protein levels. ns: not significant; SEM: standard error of the mean; α -SMA: α -smooth muscle actin; SM22: smooth muscle protein 22-a.

8.1.1.2 The transcription of contractile markers is reduced in Htra1-deficient mouse embryonic fibroblasts

Reduced TGF- β signaling is expected to attenuate the expression of contractile markers at the transcriptional level (Guo and Chen 2012). Hence, I used RT-qPCR to determine calponin (*cnn1*) and SM22 (*tagln*) mRNA levels in *htra1*^{+/+} and *htra1*^{-/-} fibroblasts. *Gapdh* served as a housekeeping gene.

As shown in Figure 8.2, calponin and SM22 mRNA levels were reduced by > 95% and > 85%, respectively, in *htra1*^{-/-} compared to *htra1*^{+/+} cultures. Note that exclusion of two *htra1*^{+/+} cultures exhibiting high calponin and SM22 levels did not invalidate this trend, with both calponin and SM22 still being reduced by > 75% ($p = 0.1$ and $p < 0.01$, respectively; graphs not illustrated).

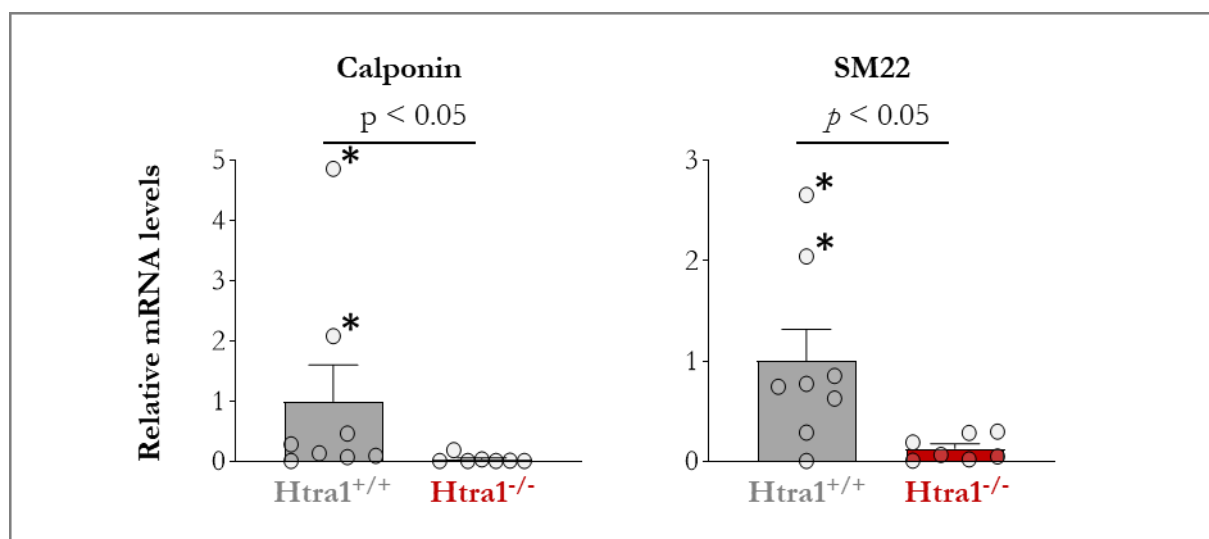


Figure 8.2: Calponin and SM22 mRNA levels in mouse embryonic fibroblasts. cDNA derived from *htra1*^{+/+} or *htra1*^{-/-} fibroblasts ($n = 7-8$ /genotype) was analyzed by RT-qPCR. Histograms depict the mean +SEM mRNA level normalized to *Gapdh*. Circles represent single data points. The mean mRNA level measured in *htra1*^{-/-} fibroblasts was set to 1. p was calculated with a Mann–Whitney U test. Asterisks mark two outlier *htra1*^{+/+} cultures exhibiting high calponin and SM22 mRNA levels. RT-qPCR: quantitative real-time polymerase chain reaction; SEM: standard error of the mean; SM22: smooth muscle protein 22-a.

8.1.1.3 Synthetic and phagocytic differentiation markers are unaffected by Htra1 deficiency in mouse embryonic fibroblasts

During phenotypic modulation, the transcriptional repression of contractile markers is typically accompanied by a transcriptional activation of synthetic or phagocytic markers (Hao, Gabbiani et al. 2003, Rong, Shapiro et al. 2003, Gomez and Owens 2012, Sandison, Dempster et al. 2016). Accordingly, previous observations from my laboratory revealed a switch from the contractile toward the phagocytic phenotype in skin fibroblasts from *HTRA1* mutation carriers (Landing 2021).

To test this possibility, I determined the abundance of fibronectin and galectin 3, which are archetypal TGF- β -regulated (Tian, Yuan et al. 2016, Varadaraj, Jenkins et al. 2017) synthetic and phagocytic markers, respectively, in *htra1*^{+/+} and *htra1*^{-/-} fibroblasts (Figure 8.3). Immunoblot

analysis revealed that, despite a trend toward upregulation, neither fibronectin nor galectin 3 was consistently deregulated in *htra1*^{+/+} compared to *htra1*^{-/-} cultures.

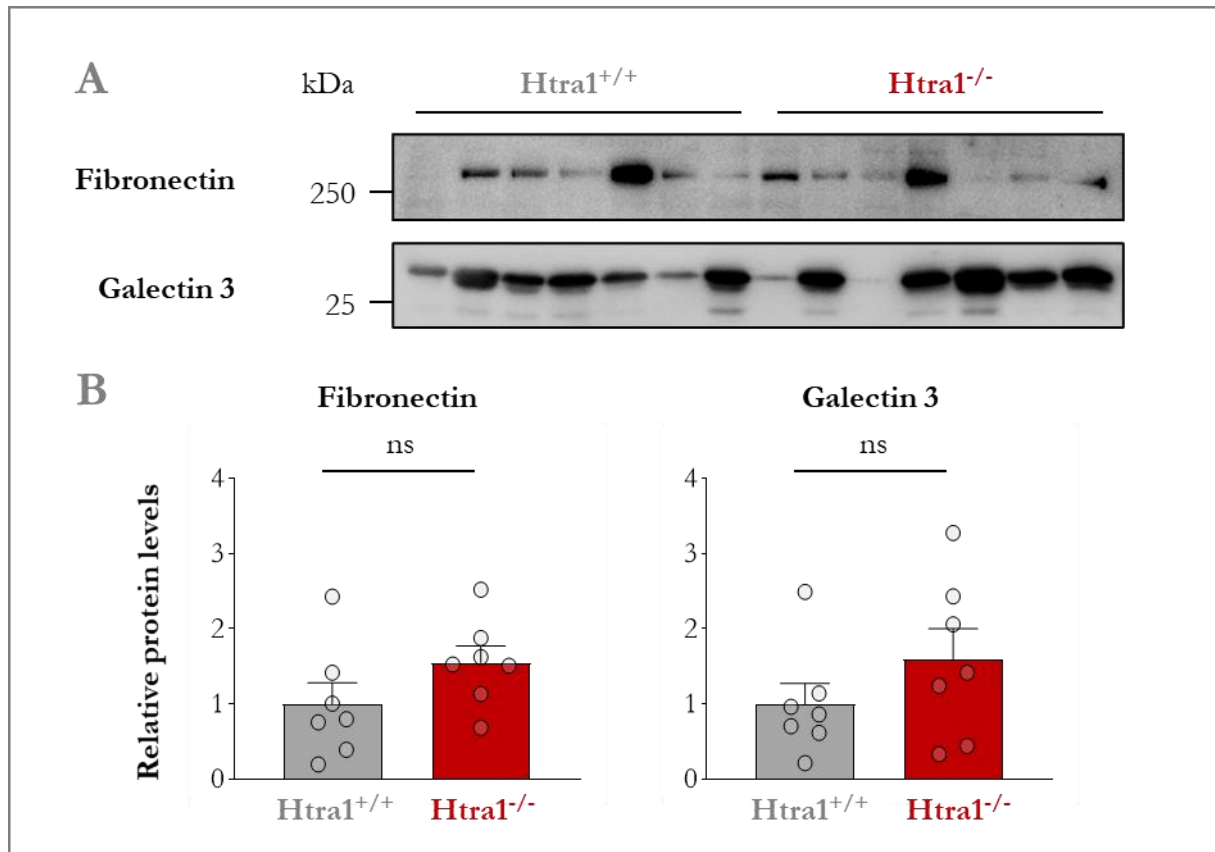


Figure 8.3: Fibronectin and galectin 3 protein levels in mouse embryonic fibroblasts. Fibroblasts from *htra1*^{+/+} or *htra1*^{-/-} embryos (n = 7/genotype) were lysed followed by detection of fibronectin and galectin 3 by immunoblot. Actin served as normalizer. (A) Representative images (actin is depicted in Figure 1A). (B) Histograms depict the mean normalized protein level +SEM. Circles represent single data points. The mean protein level measured in *htra1*^{+/+} fibroblasts was set to 1. *p* was calculated using unpaired Student's t-test. ns: not significant; SEM: standard error of the mean.

8.1.1.4 The transcriptional regulators of contractile cell differentiation *Klf4* and *Klf5* are unaffected by *Htra1* deficiency in mouse embryonic fibroblasts

KLF4 and (to a lesser extent) KLF5 are well-established key transcriptional regulators of contractile cell differentiation (Liu, Sinha et al. 2003, Salmon, Gomez et al. 2012, Shankman, Gomez et al. 2015). Moreover, a pilot study from my laboratory suggested that *KLF4* transcripts were reduced in skin fibroblasts from *HTRA1* mutation carriers compared to control fibroblasts (Landing 2021).

Thus, I analyzed *Klf4* and *Klf5* gene expression by RT-qPCR (Figure 8.4). I found comparable *Klf4* and *Klf5* mRNA levels in *htra1^{+/+}* and *htra1^{-/-}* fibroblasts, indicating that reduced contractile marker expression is not mediated by alterations in *Klf4* or *Klf5* mRNA levels.

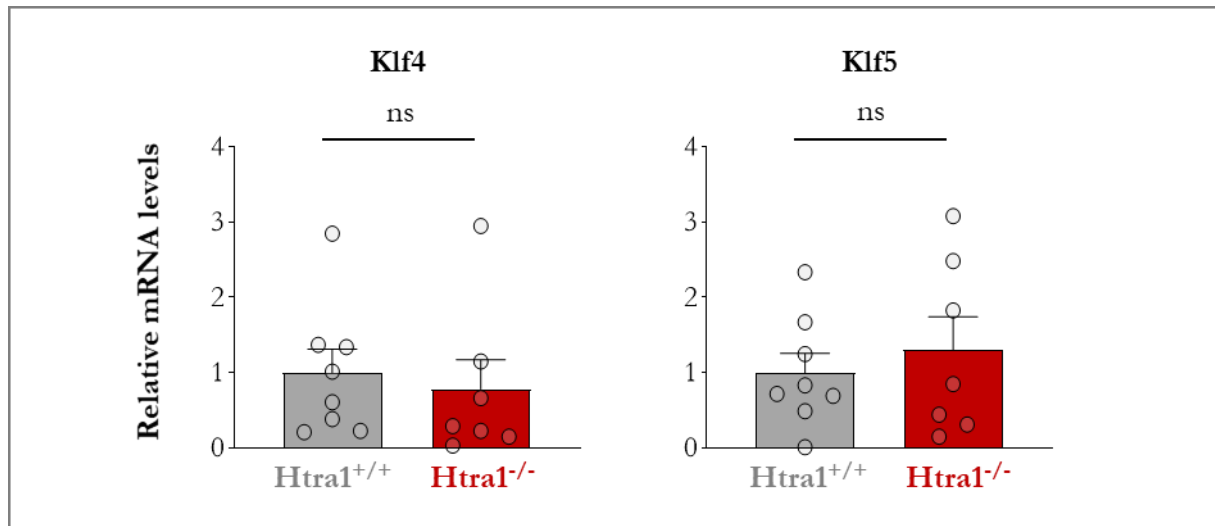


Figure 8.4: *Klf4* and *Klf5* mRNA levels in mouse embryonic fibroblasts. cDNA derived from *htra1^{+/+}* or *htra1^{-/-}* fibroblasts (n = 7–8/genotype) was analyzed by RT-qPCR. Histograms depict the mean +SEM mRNA levels normalized to *Gapdh*. Circles represent single data points. The mean mRNA level measured in *htra1^{+/+}* fibroblasts was set to 1. *p* was calculated using unpaired Student's t-test. *Klf4*: Krüppel-like factor 4; *Klf5*: Krüppel-like factor 5; ns: not significant.

8.1.2 Consequences of HtraA1 deficiency on calponin protein levels in mouse brain

To complement my *in vitro* observations, I evaluated the abundance of calponin (the contractile differentiation marker exhibiting the strongest reduction in *htra1^{-/-}* fibroblasts) in brain lysates from 12-month-old *htra1^{+/+}* and *htra1^{-/-}* mice.

As depicted in Figure 8.5, calponin levels were reduced in *htra1^{-/-}* brain extracts, in line with phenotypic modulation toward a less contractile phenotype.

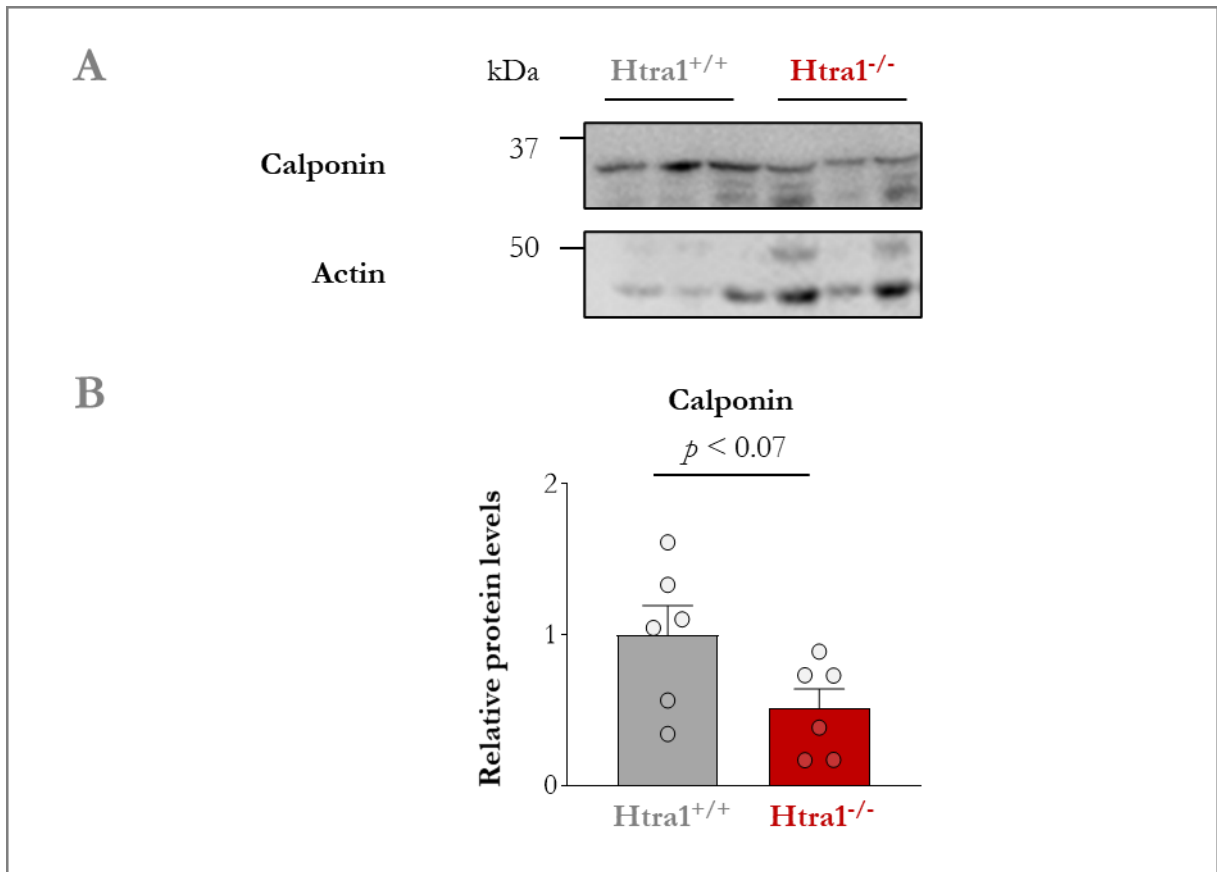


Figure 8.5: Calponin protein levels in mouse brain extracts. Brains from 12-month-old *htra1*^{+/+} or *htra1*^{-/-} mice (n = 6/genotype) were lysed and calponin was detected by immunoblot. Actin served as normalizer. (A) Representative images. (B) Histograms depict the mean normalized calponin level +SEM. Circles represent single data points. The mean calponin level measured in control brains was set to 1. *p* was calculated with unpaired Student's t-test. SEM: standard error of the mean.

8.2 ANALYSIS OF HUMAN SKIN FIBROBLASTS CARRYING THE INTRONIC *HTRA1* MUTATION c.1005+1G>T

8.2.1 Consequences of the intronic *HTRA1* mutation c.1005+1G>T on mRNA splicing

8.2.1.1 Genotyping of human skin fibroblasts carrying the splice-donor mutation c.1005+1G>T

During my laboratory work, the first German CARASIL case was identified in Tübingen (Roeben, Uhrig et al. 2016). The patient carries an *HTRA1* mutation (c.1005+1G>T) located in intron 5 that affects a canonical GT splice donor site (Figure 8.6).

Hence, I used skin fibroblasts from this proband and from his two asymptomatic heterozygous parents, as well as from three healthy individuals, to determine the impact of the c.1005+1G>T mutation on *HTRA1* protein stability and function, TGF- β signaling, and contractile cell differentiation.

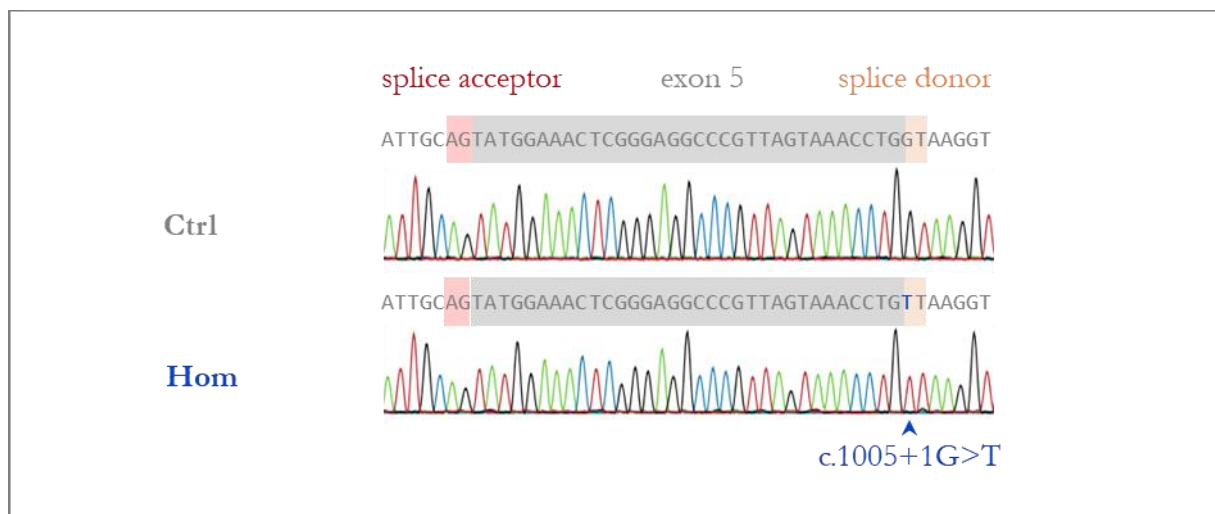


Figure 8.6: *HTRA1* genotyping in human skin fibroblasts. Genomic DNA derived from skin fibroblasts from a healthy individual (Ctrl) or from a CARASIL proband (Hom) was amplified using primers surrounding exon 5 and sequenced. The position of exon 5 as well as the intronic splice donor and splice acceptor sites are highlighted. The c.1005+1G>T mutation is marked with an arrowhead.

8.2.1.2 The c.1005+1G>T mutation induces skipping of exon 5 in human skin fibroblasts

To examine the consequences of the c.1005+1G>T mutation on *HTRA1* splicing, mRNA was isolated from control or mutation carrier fibroblasts, reverse transcribed and amplified using

primers targeting exon 1 and 7. Compared to the 811 bp amplicon derived from control fibroblasts, the amplicon derived from the homozygous mutation carrier (Hom) exhibited a slightly (< 50 bp) smaller size, suggesting altered splicing (Figure 8.7 A). Analysis of heterozygous fibroblasts (Het) yielded two amplicons comparable in size to those derived from control and homozygous mutant fibroblasts.

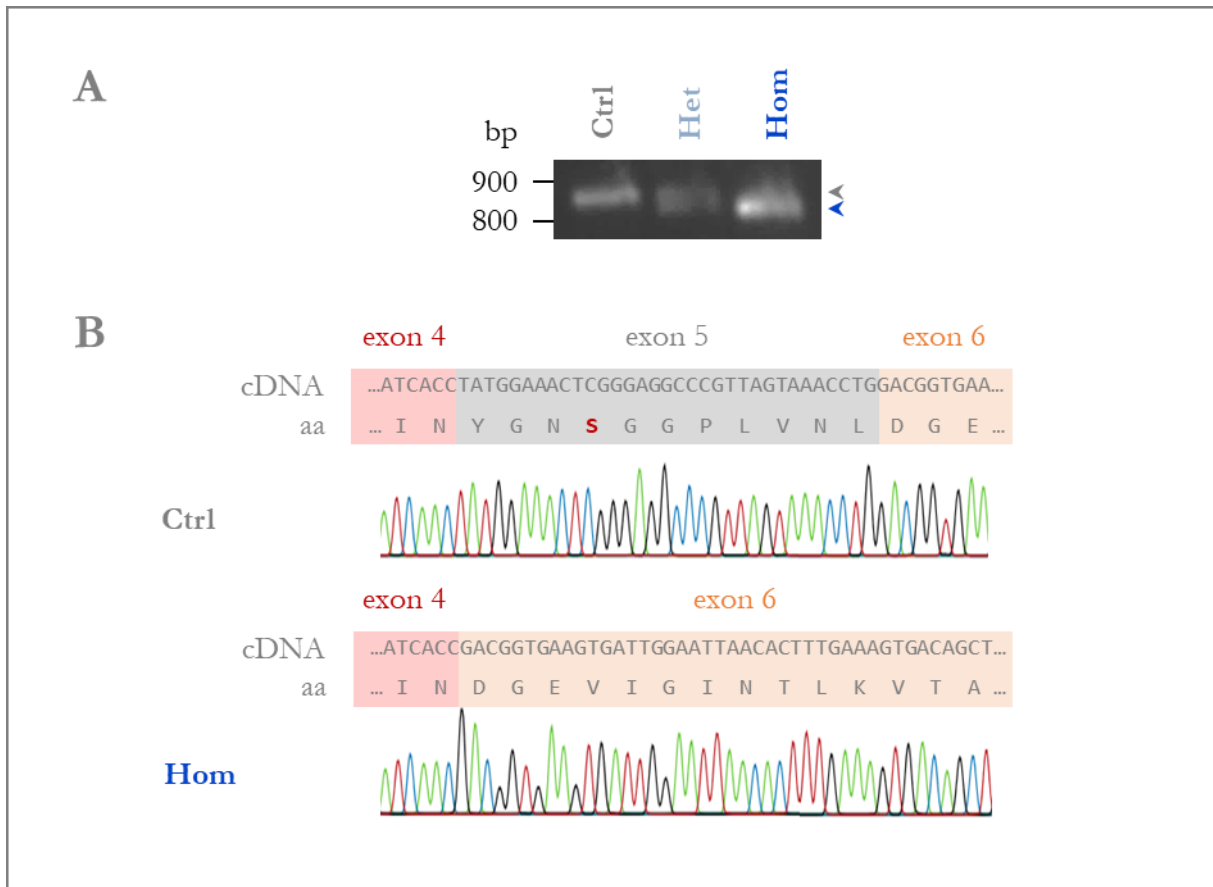


Figure 8.7: *HTRA1* splicing analysis in human skin fibroblasts. cDNA derived from skin fibroblasts from a healthy individual (Ctrl) or from heterozygous (Het) or homozygous (Hom) mutation carriers was amplified using primers targeting exon 1 and 7. Amplicons were analyzed by (A) agarose gel electrophoresis and/or (B) sequenced. In A, grey and blue arrowheads mark the position of the wild-type and mutant amplicons, respectively. In B, *HTRA1* exons are highlighted in red, grey, and orange; the nucleotide and amino acid (aa) sequences are provided; and the catalytic serine (S328) is marked in red.

Sequencing of the amplicons derived from a healthy individual and from the homozygous mutation carrier indicated that the mutant amplicon lacked a 33 bp region corresponding to skipping of the entire exon 5 (hereafter referred to as $\Delta 5$, Figure 8.7 B). Importantly, this exon encodes the catalytic serine (S328) of *HTRA1*.

Amplicons derived from heterozygous fibroblasts displayed mixed wt/ $\Delta 5$ sequences (data not illustrated).

8.2.2 Consequences of the c.1005+1G>T mutation on HTRA1 protein and protease function in overexpressing HEK-293T cells

8.2.2.1 HTRA1 is sequestered intracellularly in overexpressing HEK-293T cells

To evaluate the impact of exon 5 skipping on HTRA1 protein, I initially overexpressed recombinant $\Delta 5$ HTRA1 in human cells. Specifically, I cloned the cDNA derived from homozygous mutation carrier fibroblasts into a eukaryotic cell expression vector encoding a carboxyterminal Myc tag, followed by a transfection into human HEK-293T cells. Non-transfected cells (-) and cells transfected to overexpress wt HTRA1 or an inactive variant generated by replacing the catalytic serine with an alanine (S328A) were used as controls.

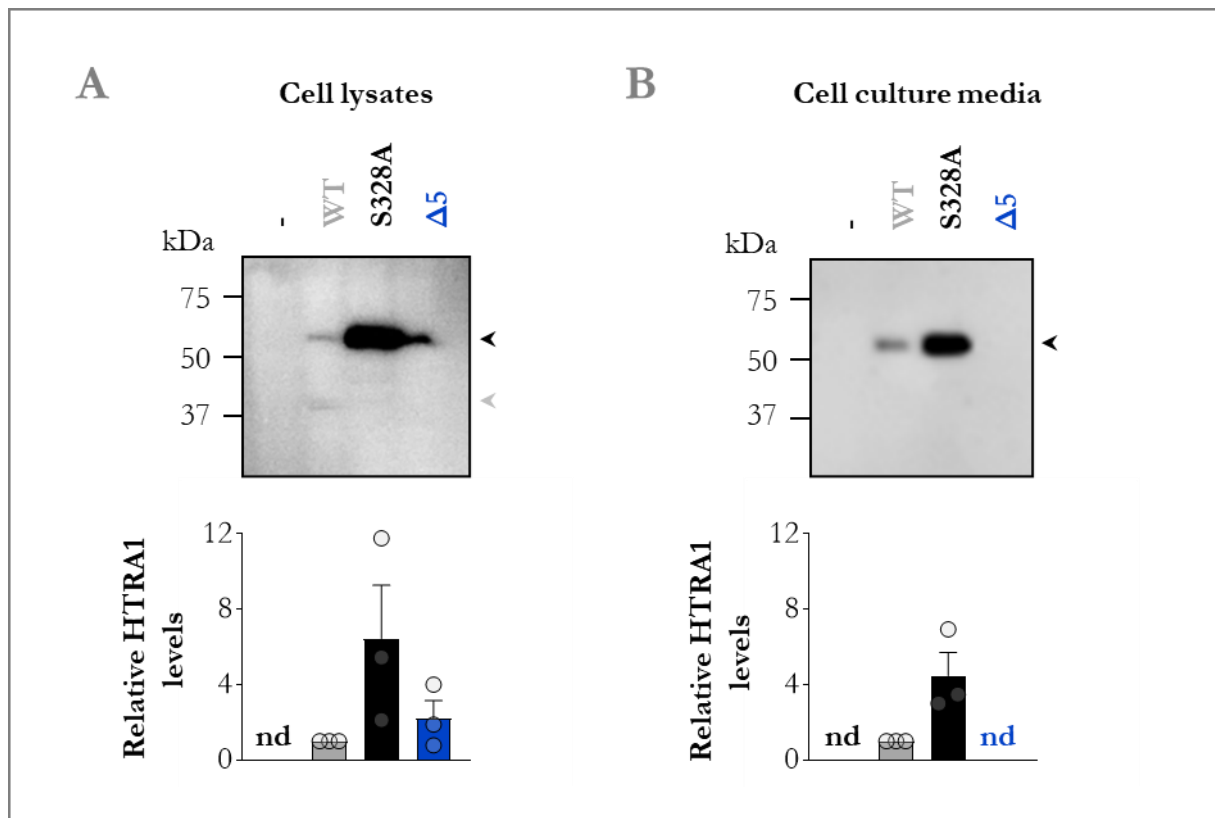


Figure 8.8: Intra- and extracellular protein levels of $\Delta 5$ HTRA1 in overexpressing HEK-293T cells. HEK-293T cells were transfected to overexpress HTRA1 wt, S328A, or $\Delta 5$. Non-transfected cells (-) served as a control. (A) Cells were lysed and (B) culture media were collected, followed by detection of recombinant HTRA1 by anti-Myc immunoblot. Upper panels: representative images. Black arrowheads: full-length HTRA1; grey arrowheads: auto-degradation products. Lower panels: histograms depict the mean signal intensity +SEM measured in three independent experiments. The signal measured for wt HTRA1 was set to 1. nd: not detected; SEM: standard error of the mean; wt: wild type.

The steady-state levels of intracellular and secreted HTRA1 were evaluated by immunoblot analysis of cell lysates (Figure 8.8 A) and culture media (Figure 8.8 B), respectively, using antibodies against the Myc tag.

As previously described (Risor, Poulsen et al. 2014), wt HTRA1 was detected as a mixture of a full-length (ca. 52 kDa) species and a truncated (ca. 37 kDa) species (see cell lysates) due to auto-degradation. The proteolytically inactive S328A mutant was exclusively detected as full-length HTRA1 and was present at higher levels both intra- and extracellularly.

Within the cells, the abundance of $\Delta 5$ HTRA1 tended to be higher than that of wt HTRA1 but lower than that of HTRA1 S328A. Moreover, $\Delta 5$ HTRA1 was solely detected as the full-length species, suggesting that – in accord with the loss of Ser³²⁸ (see Figure 8.8 B and previous paragraph) – the enzyme is proteolytically inactive (analysis of the protease activity of $\Delta 5$ HTRA1 is described in section 12.2.3.5).

Most importantly, in contrast to HTRA1 wt and S328A, the $\Delta 5$ variant was absent from cell culture media, pointing to secretion defects.

8.2.2.2 $\Delta 5$ HTRA1 exhibits reduced intracellular protein stability in overexpressing HEK-293T cells

To expand upon the previous observations, I evaluated the intracellular turnover of $\Delta 5$ HTRA1 in overexpressing HEK-293T cells. Following transfection, I exposed cells to the protein translation inhibitor cycloheximide (CHX) for 1 to 5 h. Cells were lysed and HTRA1 abundance was determined by anti-Myc immunoblot (Figure 8.9). Cells transfected to overexpress HTRA1 wt or S328A served as controls and CHX-free samples (-) were prepared as baseline samples.

Compared to wt HTRA1, the inactive variant S328A exhibited a longer half-life ($t_{1/2} > 5$ h vs. < 0.5 h). This observation reflects the fact that auto-proteolytic degradation of HTRA1 is a main promoter of HTRA1 protein turnover in overexpressing HEK-293T cells.

Although it is devoid of protease activity (see Figures 8.8 and 8.10), $\Delta 5$ HTRA1 exhibited a short half-life ($t_{1/2} < 1.5$ h), indicating protein stability defects.

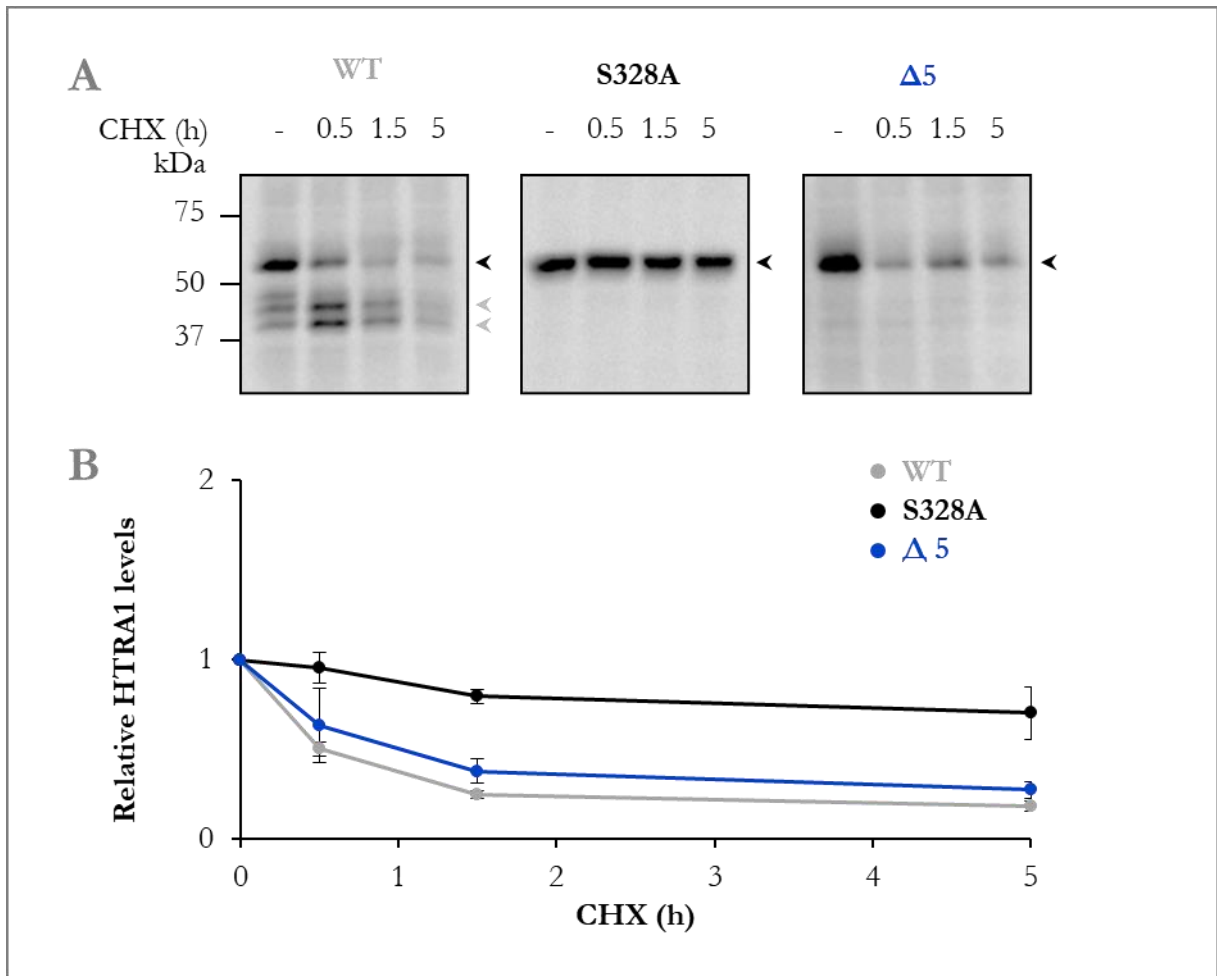


Figure 8.9: Stability of $\Delta 5$ HTRA1 in overexpressing HEK-293T cells. Following transfection as described in Figure 8.8, cells were treated with the protein translation inhibitor cycloheximide (CHX) for increasing time periods. CHX-free cells (-) were prepared as baseline samples. Cells were lysed and HTRA1 protein levels were examined by anti-Myc immunoblot. (A) Representative images. Black arrowheads: full-length HTRA1; grey arrowheads: auto-degradation products. (B) The graph depicts the mean signal intensity +SEM measured in 3–4 independent experiments. The HTRA1 signal in CHX-free cells was set to 1. SEM: standard error of the mean.

8.2.2.3 $\Delta 5$ HTRA1 is proteolytically inactive in overexpressing HEK-293T cells

To investigate the protease activity of $\Delta 5$ HTRA1, I co-transfected HEK-293T cells (*i*) with a plasmid encoding the known HTRA1 substrate LTBP-1 (Beaufort, Scharrer et al. 2014) fused to a carboxyterminal V5 tag and (*ii*) with a plasmid encoding HTRA1 wt, S328A, or $\Delta 5$. Subsequently, cells were lysed, and intracellular LTBP-1 content was examined by anti-V5 immunoblot (Figure 8.10 A). Alternatively, I co-incubated culture media of LTBP-1- and HTRA1-overexpressing cells (Figure 8.10 B).

Compared to cells transfected to overexpress LTBP-1 alone (-), co-expression of wt HTRA1 resulted in a marked reduction in LTBP-1 signal intensity. This was accompanied by conversion of some of the intact (ca. 140 kDa) into cleaved (ca. 90 kDa) LTBP-1 (Figure 8.10 A).

Conversely, co-expression of LTBP-1 with HTRA1 S328A left LTBP-1 unaffected, as also did co-expression of LTBP-1 and $\Delta 5$ HTRA1 (Figure 8.10 A), indicating loss of HTRA1 protease activity.

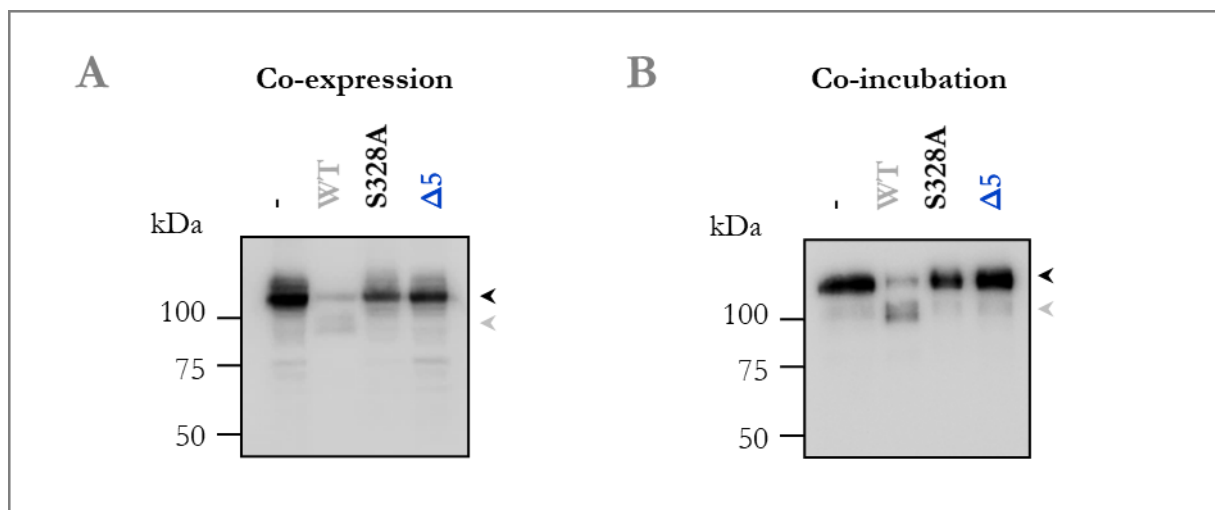


Figure 8.10: Protease activity of $\Delta 5$ HTRA1 in overexpressing HEK-293T cells. (A) HEK-293T cells were transfected to overexpress HTRA1 wt, S328A, or $\Delta 5$, followed by cell lysis. (B) Culture medium from cells transfected to overexpressed LTBP-1 was exposed to culture medium from non-transfected cells (-) or from cells transfected to overexpress HTRA1 wt, S328A, or $\Delta 5$. (A, B) LTBP-1 was analyzed by anti-V5 immunoblot. Black and grey arrowheads mark intact and cleaved LTBP-1, respectively.

As expected, co-incubation of culture medium from cells transfected to overexpress LTBP-1 with culture medium from cells transfected to overexpress $\Delta 5$ HTRA1 – which is devoid of $\Delta 5$ HTRA1 protein (Figure 8.8B) – left LTBP-1 unaffected (Figure 8.10 B).

8.2.3 Consequences of the c.1005+1G>T mutation on HTRA1 mRNA levels, protein levels and protease function in human skin fibroblasts

8.2.3.1 *HTRA1* mRNA levels are unaffected by the c.1005+1G>T mutation in human skin fibroblasts

To determine the consequences of the c.1005+1G>T mutation on *HTRA1* mRNA levels, I conducted RT-qPCR on cDNA derived from control or mutation carrier human skin fibroblasts. Specifically, I designed primers located 3' of exon 5 that would hybridize to both wt and $\Delta 5$ *HTRA1*. Samples derived from two independent passages were analyzed and *GAPDH* was used as a housekeeping gene.

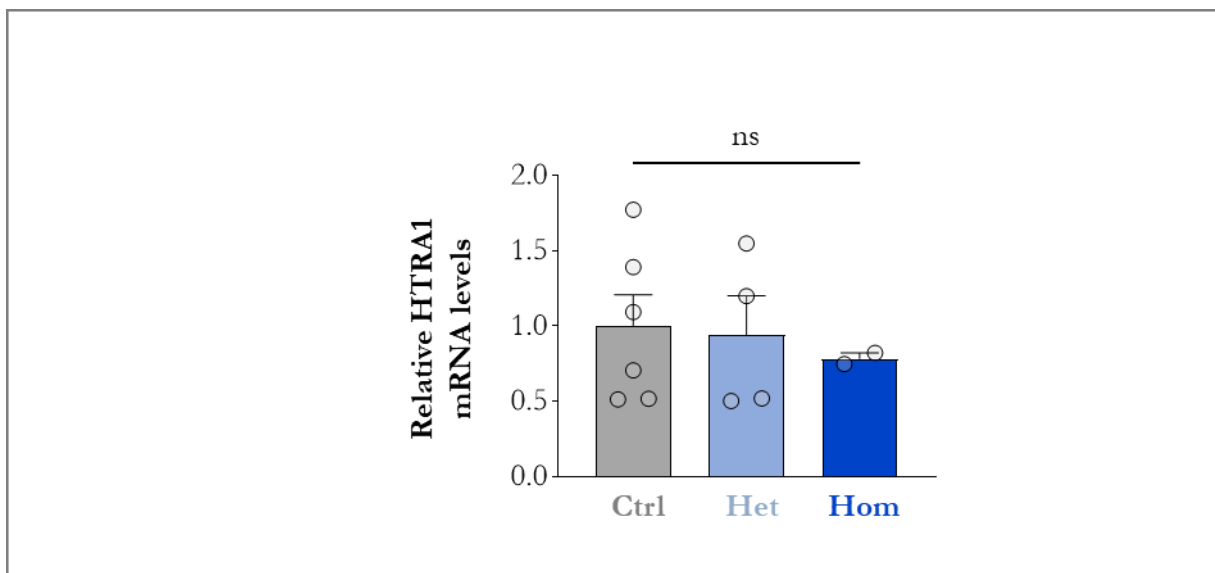


Figure 8.11: *HTRA1* mRNA levels in human skin fibroblasts. cDNA derived from control or mutation carrier fibroblasts was analyzed by RT-qPCR. Samples derived from two independent passages were analyzed. Histograms depict the mean +SEM *HTRA1* mRNA level normalized to *GAPDH*. Circles represent single data points. The mean mRNA level detected in control fibroblasts was set to 1. Normality could not be assessed for Hom datapoints (n=2). *p* was calculated with unpaired Student's t-test. Ctrl: control; Het: heterozygous; Hom: homozygous; ns: not significant.

As depicted in Figure 8.11, *HTRA1* mRNA levels were similar in control and hetero- and homozygous mutant fibroblasts.

8.2.3.2 $\Delta 5$ HTRA1 exhibits reduced intracellular protein levels in human skin fibroblasts

Next, I evaluated the steady-state levels of intracellular HTRA1 by immunoblot analysis of fibroblast lysates using a HTRA1-selective antibody (Figure 8.12). Tubulin content was measured for normalization of protein levels.

Similar to recombinant $\Delta 5$ HTRA1 protein levels, the abundance of endogenous HTRA1 was markedly ($> 80\%$) reduced in cell lysates from the homozygous but not from the heterozygous mutation carriers. Together with the observation that control and mutant fibroblasts exhibit comparable mRNA levels, this points to reduced protein translation or (most likely) to protein stability defects. Note that as expected, the apparent molecular weight of $\Delta 5$ HTRA1, which lacks a 33 bp (ca. 3.5 kDa) fragment, was undistinguishable from that of the 52 kDa wt HTRA1.

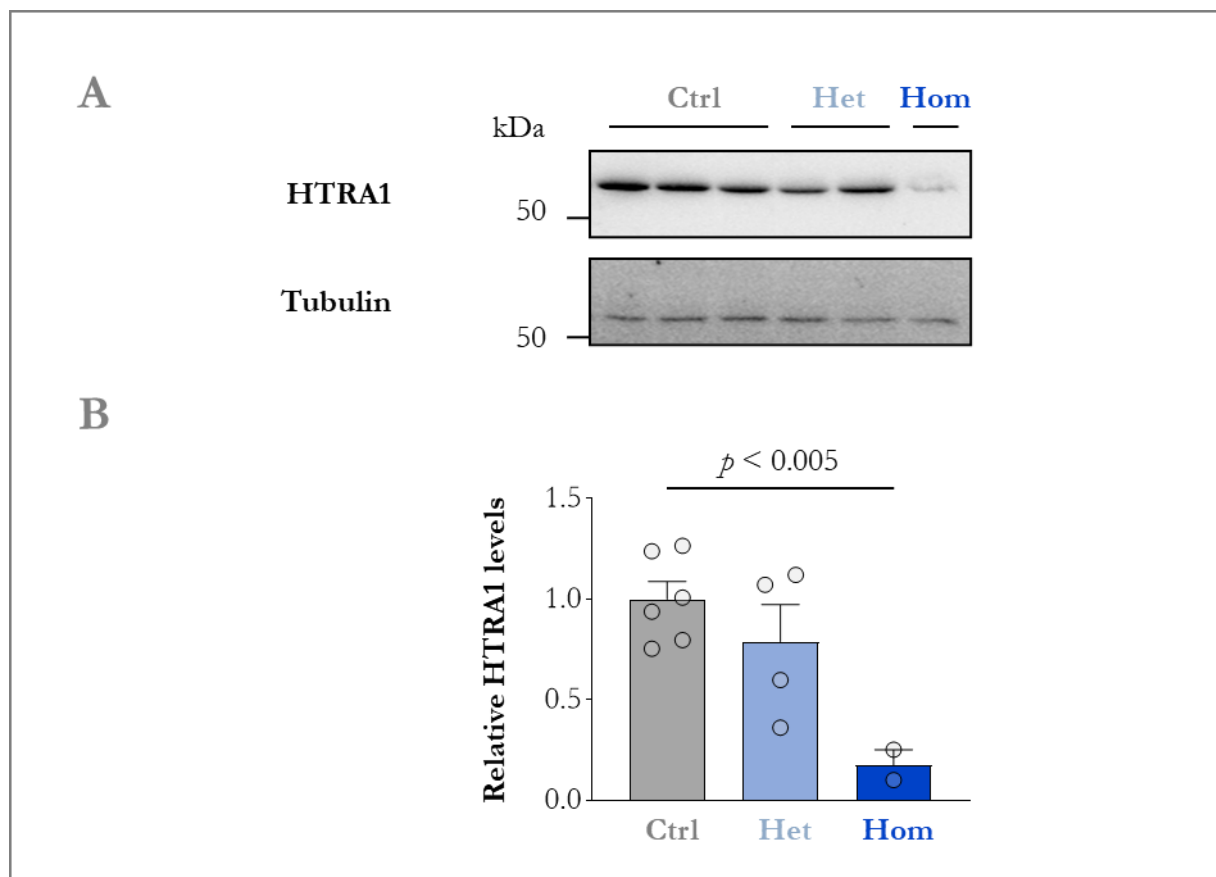


Figure 8.12: Intracellular HTRA1 protein levels in human skin fibroblasts. Lysates from control or mutation carrier fibroblasts were analyzed by immunoblot using anti-HTRA1 or anti-tubulin antibodies. Samples derived from two independent passages were analyzed. (A) Representative images. (B) Histograms depict the mean normalized HTRA1 levels +SEM. Circles represent single data points. The mean protein level detected in control fibroblasts was set to 1. Normality could not be assessed for Hom datapoints ($n=2$). p was calculated with unpaired Student's t-test. Ctrl: control; Het: heterozygous; Hom: homozygous; ns: not significant; SEM, standard error of the mean.

8.2.3.3 $\Delta 5$ HTRA1 exhibits reduced intracellular protein stability in human skin fibroblasts

In a pilot experiment, I exposed control or mutant fibroblasts to CHX for 1–24 h, followed by cell lysis and HTRA1 detection by immunoblot (Figure 8.13).

Compared to control fibroblasts, the half-life of HTRA1 in homozygous fibroblasts was markedly reduced. In accord with my observations on recombinant and endogenous HTRA1, this suggests that endogenous $\Delta 5$ HTRA1 exhibits protein stability defects.

Note that HTRA1 turnover was comparable in control and heterozygous fibroblasts.

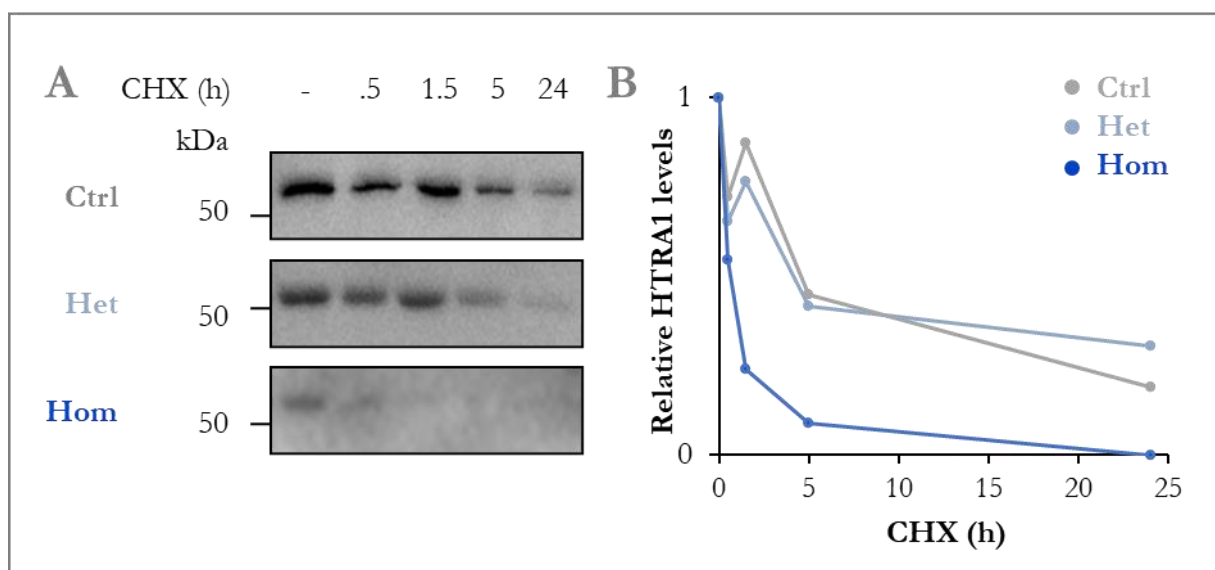


Figure 8.13: HTRA1 protein stability in human skin fibroblasts. Control or mutation carrier fibroblasts were treated with cycloheximide (CHX) for increasing time periods. Cells were lysed and HTRA1 protein levels were examined by anti-HTRA1 immunoblot. CHX-free cells (-) were prepared as baseline samples. (A) Representative images. (B) The graph depicts HTRA1 signal intensity. The signal measured in CHX-free cells was set to 1. Ctrl: control; Het: heterozygous; Hom: homozygous.

8.2.3.4 Secreted $\Delta 5$ HTRA1 displays an abnormal pattern in human skin fibroblasts

To investigate the secretion of endogenous $\Delta 5$ HTRA1, I analyzed culture media from control and mutation carrier fibroblasts by anti-HTRA1 immunoblot (Figure 8.14).

In contrast to recombinant $\Delta 5$ HTRA1, the endogenous $\Delta 5$ HTRA1 variant was detected in culture media from both hetero- and homozygous mutant fibroblasts. Moreover, HTRA1 protein abundance was comparable to that detected in control fibroblasts; it was even elevated in heterozygous compared to control fibroblasts.

However, in addition to the expected 52 kDa HTRA1 species, a distinct species exhibiting a reduced electrophoretic mobility was present in the secretome of mutation carrier fibroblasts. The identity of this species is unknown. Notably, the apparent < 3 kDa shift toward a higher molecular mass does not match with the expected 8.5 kDa shift that would result from protein ubiquitination.

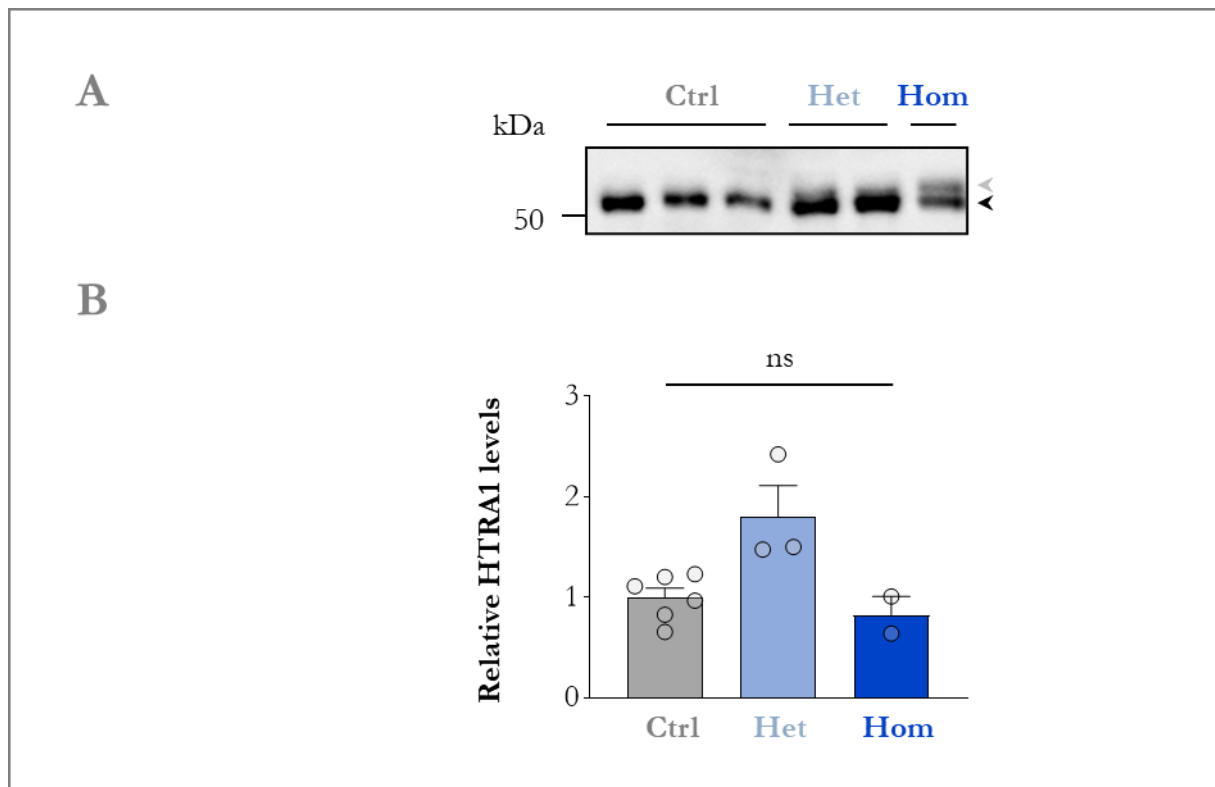


Figure 8.14: HTRA1 secretion in human skin fibroblasts. Culture media from control or mutation carrier fibroblasts were analyzed by immunoblot using anti-HTRA1 antibodies. With the exception of one heterozygous culture that was analyzed once, samples derived from two independent passages were analyzed. (A) Representative images. A black arrow marks the position of HTRA1 in control fibroblast medium; a grey arrowhead marks the position of a higher molecular mass HTRA1 species. (B) Histograms depict the mean HTRA1 protein level +SEM. Circles represent single data points. The mean protein level detected in control fibroblasts was set to 1. Normality could not be assessed for Hom datapoints (n=2). *p* was calculated with unpaired Student's t-test. Ctrl: control; Het: heterozygous; Hom: homozygous; ns: not significant; SEM: standard error of the mean.

8.2.3.5 $\Delta 5$ HTRA1 is proteolytically inactive in human skin fibroblasts

Finally, to evaluate the protease activity of endogenous $\Delta 5$ HTRA1, I exposed culture medium from cells transfected to overexpress LTBP-1 to culture medium derived from control or mutation carrier fibroblasts. LTBP-1 was detected by immunoblot, and the ratio of cleaved/intact LTBP-1 was measured as a readout of HTRA1 enzymatic activity.

As illustrated in Figure 8.15, the processing of LTBP-1 was comparable following exposure to culture medium derived from wt and heterozygous fibroblasts, but was markedly reduced following treatment with culture medium derived from homozygous mutation carrier fibroblasts.

This observation suggests that, as observed for recombinant $\Delta 5$ HTRA1, endogenous $\Delta 5$ HTRA1 lacks protease activity.

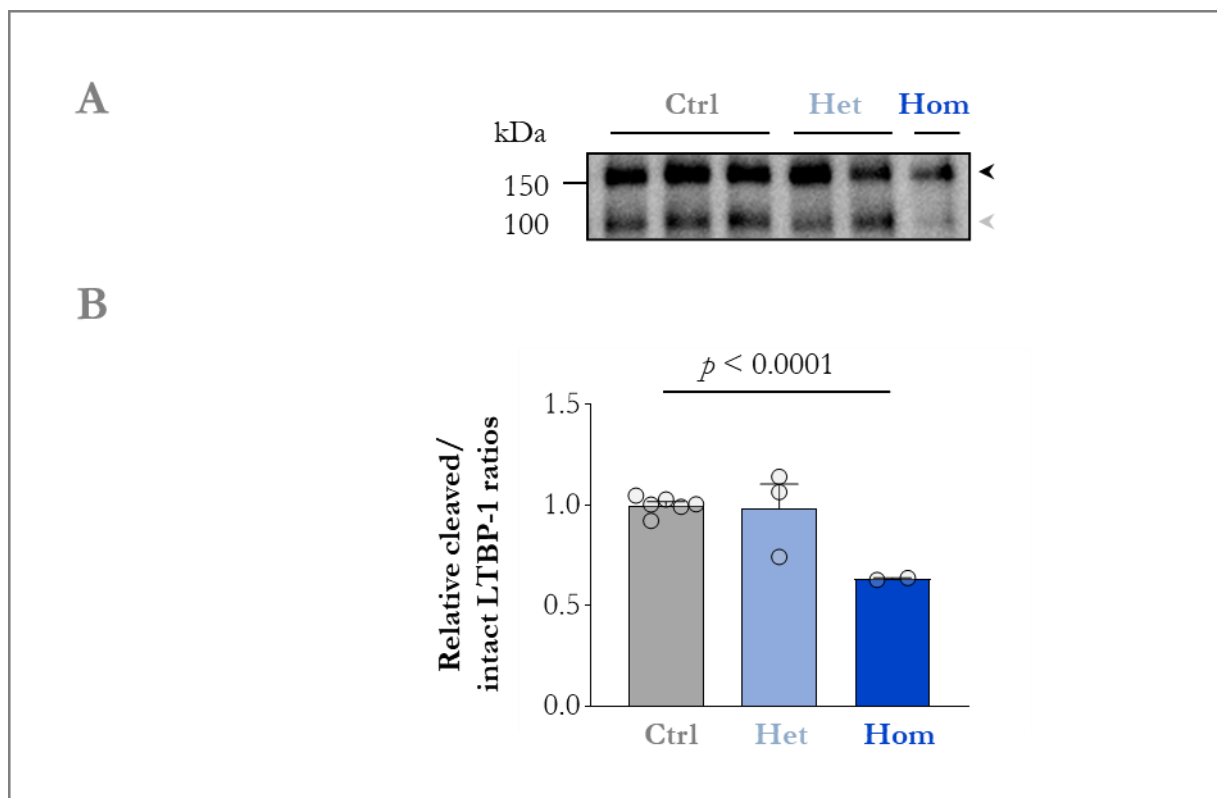


Figure 8.15: Protease activity of $\Delta 5$ HTRA1 in human skin fibroblasts. Culture medium from cells transfected to overexpressed LTBP-1 was exposed to culture medium from control or mutation carrier fibroblasts. LTBP-1 was detected by anti-V5 immunoblot. With the exception of one heterozygous culture that was analyzed once, samples derived from two independent passages were analyzed. (A) Representative images. Black and grey arrowheads mark the position of intact and cleaved LTBP-1, respectively. (B) Histograms depict the mean cleaved/intact LTBP-1 ratio +SEM. Circles represent single data points. The mean LTBP-1 ratio measured in control fibroblasts was set to 1. Normality could not be assessed for Hom datapoints ($n=2$). p was calculated with unpaired Student's t -test. Ctrl: control; Het: heterozygous; Hom: homozygous; ns: not significant; SEM: standard error of the mean.

8.2.4 Consequences of the c.1005+1G>T mutation on TGF- β signaling and contractile cell differentiation in human skin fibroblasts

8.2.4.1 The c.1005+1G>T mutation promotes TGF- β signaling in human skin fibroblasts

Previous analysis of fibroblasts derived from *btra1*^{-/-} mouse embryos (Beaufort, Scharrer et al. 2014) or from individuals carrying nonsense or missense HTRA1 mutations (Beaufort, Scharrer et al. 2014, Landinger 2021) indicated that HTRA1 loss of function is linked to reduced canonical TGF- β signaling activity. Hence, I evaluated the status of this signaling pathway in skin fibroblasts from healthy controls and c.1005+1G>T mutation carriers, using the phosphorylation of Smad2 as a readout (Figure 8.16).

In contrast with previous observations, immunoblot analysis of phospho- and total Smad2 levels suggested a gene dosage-dependent increase in phospho-/total Smad2 levels in $\Delta 5$ HTRA1 fibroblasts.

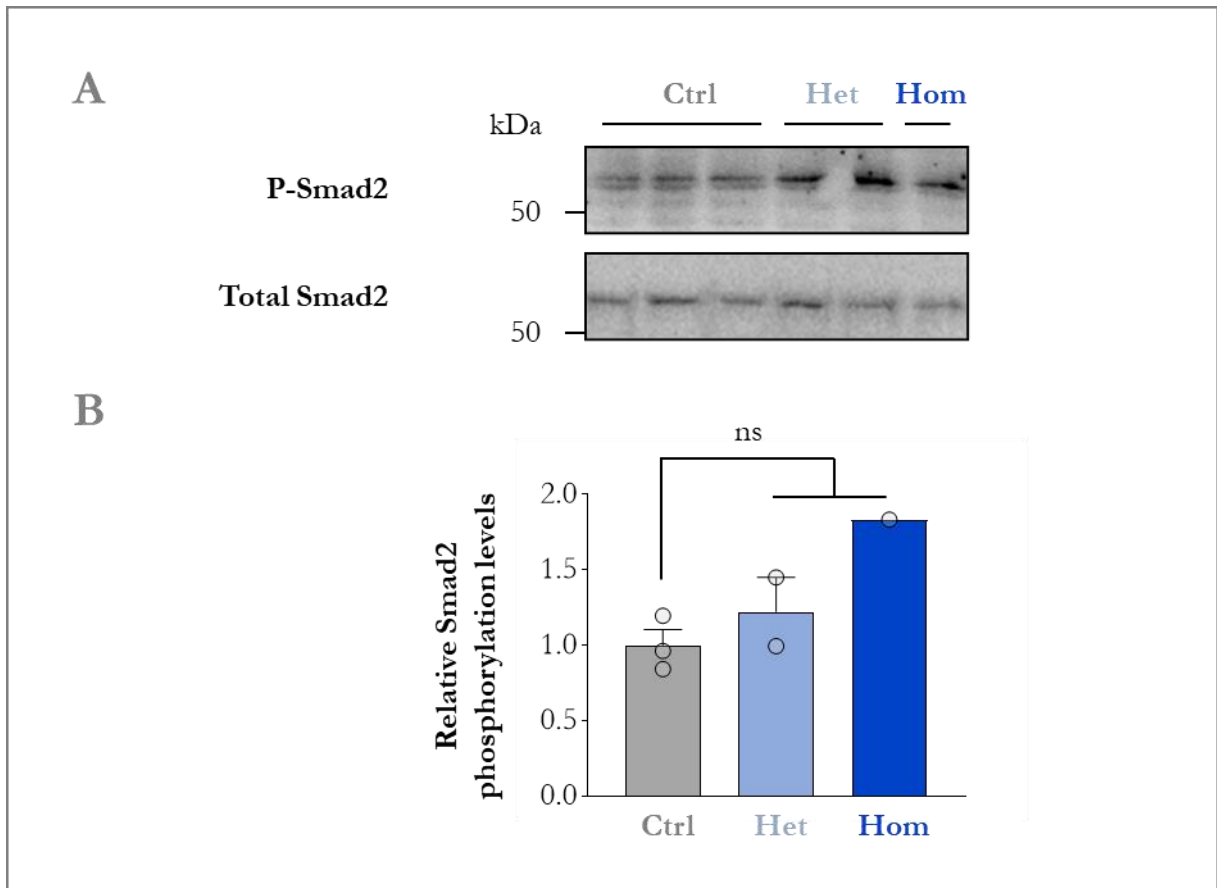


Figure 8.16: TGF- β signaling activity in human skin fibroblasts. Control or mutation carrier fibroblasts were lysed followed by immunodetection of phospho (P)- and total Smad2. (A) Representative images. (B) Histograms depict the mean P-Smad2/total Smad2 ratio +SEM. Circles represent single data points. The mean ratio measured in control fibroblasts was set to 1. p was calculated with a Mann–Whitney U test. Ctrl: control; Het: heterozygous; Hom: homozygous; ns: not significant; SEM: standard error of the mean.

8.2.4.2 The c.1005+1G>T mutation enhances the abundance of the contractile differentiation markers calponin, SM22, and α -SMA in human skin fibroblasts

I further used immunoblot to determine the abundance of the contractile differentiation markers calponin, SM22, and α -SMA in control and mutant skin fibroblasts.

As depicted in Figure 8.17, I found all three markers to be elevated in c.1005+1G>T mutation carriers' cells. Similar to the elevated TGF- β signaling (Figure 8.16), this result stands in contrast with my observations on mouse embryonic fibroblasts (Section 8.1) and on a panel of human skin fibroblasts derived from HTRA1 mutation carriers (Landinger 2021).

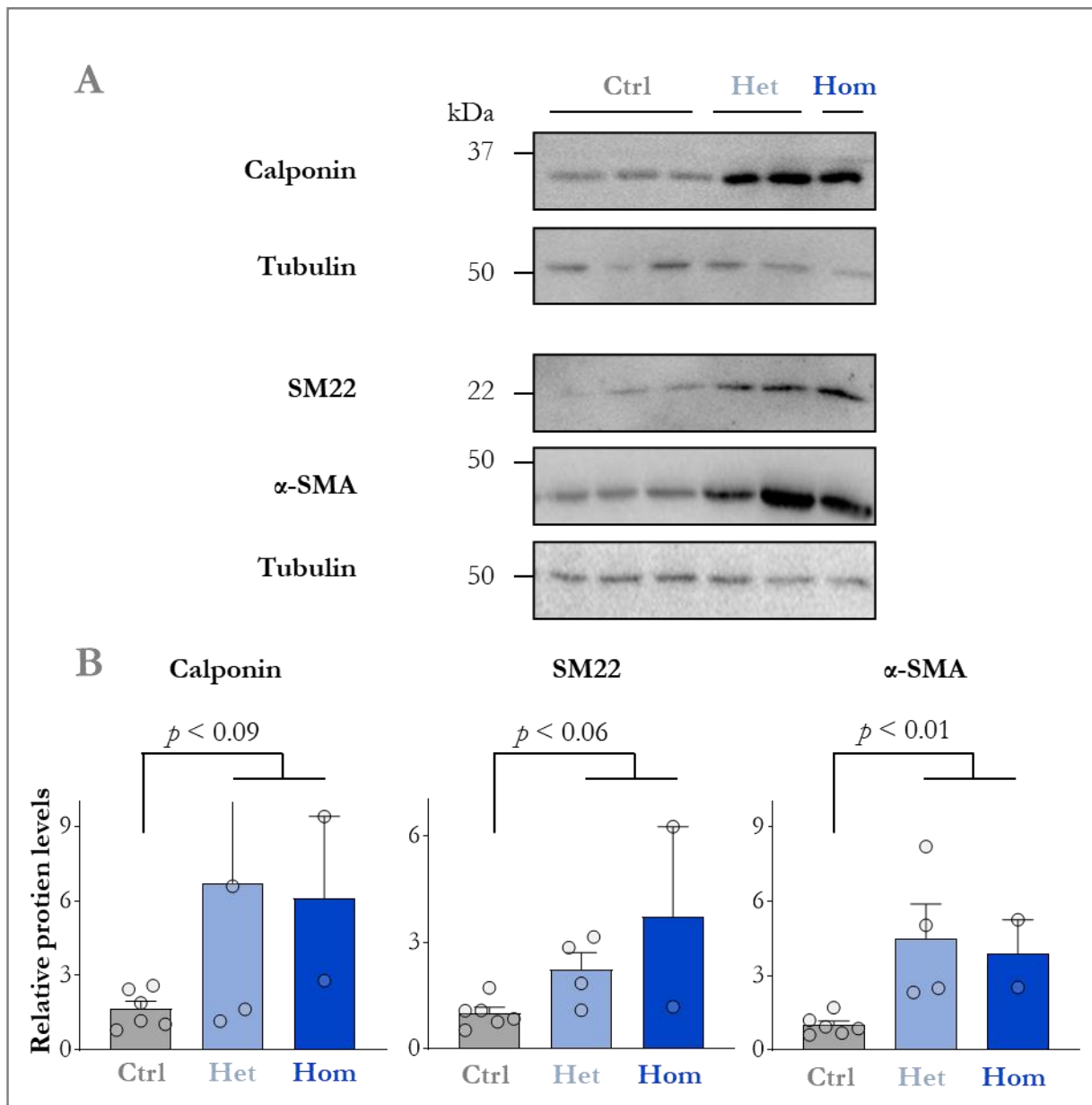


Figure 8.17: Calponin, SM22, and α -SMA protein levels in human skin fibroblasts. Control or mutation carrier fibroblasts were lysed followed by immunodetection of calponin, SM22, and α -SMA. Tubulin served as normalizer. Samples derived from two independent passages were analyzed. (A) Representative images. (B) Histograms depict the mean normalized protein level +SEM. Circles represent single data points. One outlier with a relative level > 15 is not depicted on the calponin graph. The mean protein level measured in control fibroblasts was set to 1. p was calculated with unpaired Student's t-test. Ctrl: control; Het: heterozygous; Hom: homozygous; ns: not significant; SEM: standard error of the mean.

9 DISCUSSION

Over the last decade, mutations in HTRA1 have emerged as a significant etiology for hereditary SVD. While pathogenic mutations have been shown to interfere with the protease activity of HTRA1, their consequences on the phenotype of brain vascular cells and more generally on brain vessel function remain unclear.

My work combined the analysis of embryonic fibroblasts and brain tissue derived from *htra1*^{-/-} mice and of human skin fibroblasts derived from individuals carrying an intronic HTRA1 mutation to examine the consequences of HTRA1 loss of function on contractile cell differentiation.

9.1 CONSEQUENCES OF THE PATHOGENIC HTRA1 MUTATION c.1005+1G>T ON MOLECULAR AND CELLULAR DETERMINANTS OF HTRA1 FUNCTION

Archetypal disease-causing mutations include missense mutations targeting the protease domain of HTRA1 as well as frameshift and nonsense loss-of-function mutations. They typically disrupt HTRA1 protease activity.

In my thesis, I evaluated the consequences of the c.1005+1G>T mutation, which is located in *HTRA1* intron 5 and affects a predicted splice-donor site. I established that this mutation causes skipping of exon 5 in human skin fibroblasts. Exon 5 encodes the catalytic serine Ser328, which is one of the key residues that exchanges protons during peptide bond hydrolysis. Accordingly, I demonstrated that a recombinant HTRA1 variant lacking exon 5 ($\Delta 5$ HTRA1) is devoid of enzymatic activity in overexpressing HEK-293T cells. I further documented that the c.1005+1G>T mutation interferes with the processing of the physiological HTRA1 substrate LTBP-1 in human skin fibroblasts.

In addition, I found that both recombinant and endogenous $\Delta 5$ HTRA1 exhibit a reduced intracellular protein stability and aberrant secretion. Specifically, I demonstrated that, in contrast to wt HTRA1, $\Delta 5$ HTRA1 is rapidly degraded in transfected cells and is not secreted. Moreover, despite comparable mRNA levels, $\Delta 5$ HTRA1 protein levels are reduced in mutation carrier compared to control human skin fibroblasts. In accord with this observation, I found that endogenous $\Delta 5$ HTRA1 displays a reduced intracellular half-life. $\Delta 5$ HTRA1 is secreted by human

skin fibroblasts, but unlike wt HTRA1, it is detected as two molecular species: the expected 52 kDa species and an atypical species with a slightly higher apparent molecular mass.

Of note, the impact of disease-causing mutations on the stability of HTRA1 protein has not been well characterized thus far. This aspect cannot be assessed in the animal models for HTRA1 loss of function that are currently available, as they are restricted to *htra1*^{-/-} mice (Beaufort, Scharrer et al. 2014, Scharrer 2015, Zellner, Scharrer et al. 2018, Kato, Manabe et al. 2021).

Misfolded proteins are typically detected by protein quality control systems, followed by refolding, degradation, or sequestration to ensure the integrity of the cellular proteome and avoid cytotoxicity (Chen, Retzlaff et al. 2011). In particular, misfolded proteins are classically eliminated by the unfolded protein response system, which involves ubiquitination and proteasome-dependent degradation. Alternatively, aberrant proteins can be cleared by the non-specific, lysosomal-dependent autophagy pathway. Future work should thus evaluate the contribution of these pathways to $\Delta 5$ HTRA1 turnover.

This could be achieved using selective proteasome (e.g., MG132, lactacystin) or autophagy (e.g., 3-methyladenine) inhibitors and monitoring the recovery of HTRA1 in cell lysates. In addition, following proteasome inhibition and HTRA1 pull-down, HTRA1 ubiquitination could be assessed by anti-ubiquitin immunoblot. Though ubiquitination alone is not sufficient to explain the atypical HTRA1 species detected in the secretome of mutant fibroblasts, the observed < 5 kDa shift in apparent molecular mass could be explained by an increased electrophoretic mobility of misfolded HTRA1 combined with the addition of the ca. 8.5 kDa ubiquitin. Furthermore, immunoblot analysis of LC3-I and II, a well-established approach to monitor autophagy and autophagy-related processes, could also be applied to skin fibroblast lysates. In familial SVD linked to *COL4A1* and *COL4A2* mutations, the intracellular accumulation of misfolded collagen IV, which results in endoplasmic reticulum stress and activation of the unfolded protein response, has been shown to combine with the extracellular deficiency of collagen IV to injure the brain vasculature (Kuo, Labelle-Dumais et al. 2012). In fact, treatment with a chemical chaperone targeting endoplasmic reticulum stress was sufficient to attenuate intracerebral hemorrhages in *Col4a1* mutant mice, demonstrating the contribution of this pathway to brain vessel damage (Jones, Murray et al. 2019).

Previous observations from my laboratory using mouse and human fibroblasts, as well as mouse brain tissue (Beaufort, Scharrer et al. 2014, Scharrer 2015, Landinger 2021), suggested that HTRA1 loss of function is linked to reduced TGF- β signaling. In contrast, I found that c.1005+1G>T fibroblasts exhibit elevated phospho-Smad2 and phospho-/total Smad2 levels, indicating elevated TGF- β signaling activity. I further documented a marked (> 3-fold) and significant increase in

contractile expression markers in fibroblasts carrying c.1005+1G>T, which again contradicts previous data from my laboratory and other groups (Ikawati, Kawaichi et al. 2018, Klose, Prinz et al. 2019, Landinger 2021) and with my own observations using *htra1*^{-/-} mouse fibroblasts and brain lysates (see Section 9.2). Since endoplasmic reticulum stress and the unfolded protein response are linked to TGF- β signaling and myofibroblast differentiation (Jiang, He et al. 2018), I speculate that these discrepancies might be due – at least in part – to c.1005+1G>T hijacking the cell quality control systems.

A limitation of my work is that the experiments were conducted on a low number of fibroblast cultures derived from a single pedigree and including two hetero- and one homozygous mutation carriers. Another obvious limitation is that my work is restricted to ex vivo assays using transfected cells and 2D cultures of patient-derived human skin fibroblasts. These aspects could be overcome using, for example, genome-edited induced pluripotent stem cells (iPSCs) (Weisheit, Kroeger et al. 2021). A strength of this approach is that iPSCs can be differentiated into most if not all major cerebrovascular cell types and can be used to engineer 3D co-culture models mimicking the brain vasculature (Delsing, Herland et al. 2020).

9.2 CONSEQUENCES OF HTRA1 LOSS OF FUNCTION ON THE CONTRACTILE CELL PHENOTYPE

My laboratory and other teams have shown that HTRA1 loss of function is linked to a cerebrovascular accumulation of secreted and matrisomal proteins, including numerous HTRA1 substrates (Zellner, Scharrer et al. 2018, Kato, Manabe et al. 2021). These observations are consistent with the emerging concept that alteration of the cerebrovascular matrisome is a convergent pathway in SVD (Joutel, Haddad et al. 2016). Conversely, the impact of HTRA1 loss of function on the phenotype of vascular cells remains mostly unknown. Nonetheless, several lines of evidence suggest that HTRA1 deficiency causes mural cell dysfunction, a well-described feature in SVD. For example, the brain vasculature of HTRA1 mutation carriers exhibits reduced α -SMA levels (Oide, Nakayama et al. 2008), which might reflect SMC loss and/or an aberrant mural cell phenotype. Moreover, reduced pericyte coverage has recently been reported in the capillaries of *htra1*^{-/-} mice (Kato, Manabe et al. 2021).

Previous analysis from my laboratory using mouse and human fibroblasts as well as mouse brain tissue uncovered that HTRA1 loss of function reduces TGF- β signaling (Beaufort, Scharrer et al. 2014, Scharrer 2015, Landinger 2021). Moreover, using a unique collection of skin fibroblasts from HTRA1 mutation carriers, HTRA1 loss of function was found to interfere with the expression of contractile differentiation markers as well as cell contractile function, while treatment with exogenous TGF- β , which is a key regulator of contractile differentiation (Guo and Chen 2012), was sufficient to alleviate this phenotype (Landinger 2021). My work extends these observations: I found that three well-established contractile differentiation markers (α -SMA, calponin and SM22) display reduced mRNA and/or protein levels in embryonic fibroblasts derived from *htra1*^{-/-} mice compared to those derived from *htra1*^{+/+} mice. I further validated that brain extracts from *htra1*^{-/-} mice exhibit reduced calponin protein levels compared to brain extracts from *htra1*^{+/+} mice. In accord with my observations, recent work using HTRA1-silenced human aortic SMCs or aortic SMCs derived from *htra1*^{-/-} mice also concluded that HTRA1 loss of function impairs contractile cell differentiation based on gene and protein expression analyses and/or contraction assays (Ikawati, Kawaichi et al. 2018, Klose, Prinz et al. 2019). Both studies further suggested that loss of contractile marker expression is combined with excessive ECM production, increased cell proliferation and elevated cell migration, indicating a switch from the contractile to the synthetic phenotype. Of note, whether and how TGF- β signaling affects the phenotype of HTRA1-deficient contractile cells remains controversial, as TGF- β signaling activity was found to be unchanged, elevated or impaired in the context of HTRA1 deficiency, depending on the working group (Beaufort, Scharrer et al. 2014, Ikawati, Kawaichi et al. 2018, Klose, Prinz et al. 2019).

As stated in the introduction, immunohistological analysis of cerebral vessels from HTRA1 mutation carriers revealed a loss of α -SMA along with intimal hyperplasia with ECM protein accumulation, two features that might result from VSMC phenotypic switching (Oide, Nakayama et al. 2008). Notably, loss of the highly differentiated, contractile state of VSMCs is expected to impact vessel tone and blood flow. Moreover, uncontrolled ECM production might increase vessel stiffness and/or drive inward vessel remodeling with narrowing of the lumen resulting in reduced blood flow.

In conclusion, my work sheds light on novel aspects underlying HTRA1-related vasculopathy. Specifically, I characterized how an intronic disease-causing mutation interferes with HTRA1 proteostasis and function. I further provide further evidence that HTRA1 loss of function alters the phenotype of contractile cells.

10 COPYRIGHT DECLARATION

Figure	Authors/Year	Title	Publisher	License number
Figure 1.1	Joanna M Wardlaw, Colin Smith, Martin Dichgans (2019)	Small vessel disease: mechanisms and clinical implications.	Elsevier, Inc.	4671891042727
Figure 1.2 and Figure 1.3	Joanna M Wardlaw, Colin Smith, Martin Dichgans (2013a)	Mechanisms of sporadic cerebral small vessel disease: insights from neuroimaging.	Elsevier, Inc.	4672520547911
Figure 1.4	Inês Menezes Cordeiro, Hipólito Nzwalo, Francisca Sá, et al. (2015)	Shifting the CARASIL paradigm.	Wolters Kluwer Health, Inc.	4672570922452
Figure 1.5	Takashi Oide, Hiroshi Nakayama, Sohei Yanagawa, Nobuo Ito, Shuichi Ikeda, Kunimasa Arima (2008)	Extensive loss of arterial medial smooth muscle cells and mural extracellular matrix in cerebral autosomal recessive arteriopathy with subcortical infarcts and leukoencephalopathy (CARASIL).	John Wiley and Sons, Inc.	4672520167440

Table 11.1: License numbers and copyright holders for Figures 1.1–1.5

All figures without a source provided have been created by the author. The permission has been obtained through RightsLink (<https://www.copyright.com/publishers/rightslink-permissions/>).

11 REFERENCES

- Arima, K., S. Yanagawa, N. Ito and S. Ikeda (2003). "Cerebral arterial pathology of CADASIL and CARASIL (Maeda syndrome)." Neuropathology **23**(4): 327-334.
- Beaufort, N., E. Scharrer, E. Kremmer, V. Lux, M. Ehrmann, R. Huber, H. Houlden, D. Werring, C. Haffner and M. Dichgans (2014). "Cerebral small vessel disease-related protease HtrA1 processes latent TGF-beta binding protein 1 and facilitates TGF-beta signaling." Proc Natl Acad Sci U S A **111**(46): 16496-16501.
- Bianchi, S., C. Di Palma, G. N. Gallus, I. Taglia, A. Poggiani, F. Rosini, A. Rufa, D. F. Muresanu, A. Cerase, M. T. Dotti and A. Federico (2014). "Two novel HTRA1 mutations in a European CARASIL patient." Neurology **82**(10): 898-900.
- Bos, D., F. J. Wolters, S. K. L. Darweesh, M. W. Vernooij, F. de Wolf, M. A. Ikram and A. Hofman (2018). "Cerebral small vessel disease and the risk of dementia: A systematic review and meta-analysis of population-based evidence." Alzheimers Dement **14**(11): 1482-1492.
- Bugiani, M., S. H. Kevelam, H. S. Bakels, Q. Waisfisz, C. Ceuterick-de Groote, H. W. Niessen, T. E. Abbink, S. A. Lesnik Oberstein and M. S. van der Knaap (2016). "Cathepsin A-related arteriopathy with strokes and leukoencephalopathy (CARASAL)." Neurology **87**(17): 1777-1786.
- Chabriat, H., A. Joutel, M. Dichgans, E. Tournier-Lasserre and M. G. Bousser (2009). "Cadasil." Lancet Neurol **8**(7): 643-653.
- Chamley-Campbell, J., G. R. Campbell and R. Ross (1979). "The smooth muscle cell in culture." Physiol Rev **59**(1): 1-61.
- Chen, B., M. Retzlaff, T. Roos and J. Frydman (2011). "Cellular strategies of protein quality control." Cold Spring Harb Perspect Biol **3**(8): a004374.
- Chen, J., C. M. Kitchen, J. W. Streb and J. M. Miano (2002). "Myocardin: a component of a molecular switch for smooth muscle differentiation." J Mol Cell Cardiol **34**(10): 1345-1356.
- Craggs, L. J., Y. Yamamoto, V. Deramecourt and R. N. Kalaria (2014). "Microvascular pathology and morphometrics of sporadic and hereditary small vessel diseases of the brain." Brain Pathol **24**(5): 495-509.
- de Laat, K. F., A. M. Tuladhar, A. G. van Norden, D. G. Norris, M. P. Zwiers and F. E. de Leeuw (2011). "Loss of white matter integrity is associated with gait disorders in cerebral small vessel disease." Brain **134**(Pt 1): 73-83.
- Debette, S., S. Schilling, M. G. Duperron, S. C. Larsson and H. S. Markus (2019). "Clinical Significance of Magnetic Resonance Imaging Markers of Vascular Brain Injury: A Systematic Review and Meta-analysis." JAMA Neurol **76**(1): 81-94.

Deguchi, J., T. Namba, H. Hamada, T. Nakaoka, J. Abe, O. Sato, T. Miyata, M. Makuuchi, K. Kurokawa and Y. Takuwa (1999). "Targeting endogenous platelet-derived growth factor B-chain by adenovirus-mediated gene transfer potently inhibits in vivo smooth muscle proliferation after arterial injury." Gene Ther **6**(6): 956-965.

Delsing, L., A. Herland, A. Falk, R. Hicks, J. Synnergren and H. Zetterberg (2020). "Models of the blood-brain barrier using iPSC-derived cells." Mol Cell Neurosci **107**: 103533.

Dennler, S., S. Itoh, D. Vivien, P. ten Dijke, S. Huet and J. M. Gauthier (1998). "Direct binding of Smad3 and Smad4 to critical TGF beta-inducible elements in the promoter of human plasminogen activator inhibitor-type 1 gene." EMBO J **17**(11): 3091-3100.

Derynck, R. and Y. E. Zhang (2003). "Smad-dependent and Smad-independent pathways in TGF-beta family signalling." Nature **425**(6958): 577-584.

Dichgans, M., S. L. Pulit and J. Rosand (2019). "Stroke genetics: discovery, biology, and clinical applications." Lancet Neurol **18**(6): 587-599.

Duering, M., B. Gesierich, S. Seiler, L. Pirpamer, M. Gonik, E. Hofer, E. Jouvent, E. Duchesnay, H. Chabriat, S. Ropele, R. Schmidt and M. Dichgans (2014). "Strategic white matter tracts for processing speed deficits in age-related small vessel disease." Neurology **82**(22): 1946-1950.

Etherton, M. R., O. Wu, P. Cougo, A. K. Giese, L. Cloonan, K. M. Fitzpatrick, A. S. Kanakis, G. Boulouis, H. H. Karadeli, A. Lauer, J. Rosand, K. L. Furie and N. S. Rost (2017). "Integrity of normal-appearing white matter and functional outcomes after acute ischemic stroke." Neurology **88**(18): 1701-1708.

Feil, S., B. Fehrenbacher, R. Lukowski, F. Essmann, K. Schulze-Osthoff, M. Schaller and R. Feil (2014). "Transdifferentiation of vascular smooth muscle cells to macrophage-like cells during atherogenesis." Circ Res **115**(7): 662-667.

Feng, X. H. and R. Derynck (1997). "A kinase subdomain of transforming growth factor-beta (TGF-beta) type I receptor determines the TGF-beta intracellular signaling specificity." EMBO J **16**(13): 3912-3923.

Fukutake, T. (2011). "Cerebral autosomal recessive arteriopathy with subcortical infarcts and leukoencephalopathy (CARASIL): from discovery to gene identification." J Stroke Cerebrovasc Dis **20**(2): 85-93.

Fukutake, T. and K. Hirayama (1995). "Familial young-adult-onset arteriosclerotic leukoencephalopathy with alopecia and lumbago without arterial hypertension." Eur Neurol **35**(2): 69-79.

Gabbiani, G., E. Schmid, S. Winter, C. Chaponnier, C. de Ckhas-tonay, J. Vandekerckhove, K. Weber and W. W. Franke (1981). "Vascular smooth muscle cells differ from other smooth muscle

cells: predominance of vimentin filaments and a specific alpha-type actin." Proc Natl Acad Sci U S A **78**(1): 298-302.

Gomez, D. and G. K. Owens (2012). "Smooth muscle cell phenotypic switching in atherosclerosis." Cardiovasc Res **95**(2): 156-164.

Graham, B. B., J. Chabon, L. Gebreab, J. Poole, E. Debella, L. Davis, T. Tanaka, L. Sanders, N. Dropcho, A. Bandeira, R. W. Vandivier, H. C. Champion, G. Butrous, X. J. Wang, T. A. Wynn and R. M. Tuder (2013). "Transforming growth factor-beta signaling promotes pulmonary hypertension caused by *Schistosoma mansoni*." Circulation **128**(12): 1354-1364.

Grau, S., P. J. Richards, B. Kerr, C. Hughes, B. Caterson, A. S. Williams, U. Junker, S. A. Jones, T. Clausen and M. Ehrmann (2006). "The role of human HtrA1 in arthritic disease." J Biol Chem **281**(10): 6124-6129.

Guo, X. and S. Y. Chen (2012). "Transforming growth factor-beta and smooth muscle differentiation." World J Biol Chem **3**(3): 41-52.

Haffner, C., R. Malik and M. Dichgans (2016). "Genetic factors in cerebral small vessel disease and their impact on stroke and dementia." J Cereb Blood Flow Metab **36**(1): 158-171.

Hansen, G. and R. Hilgenfeld (2013). "Architecture and regulation of HtrA-family proteins involved in protein quality control and stress response." Cell Mol Life Sci **70**(5): 761-775.

Hao, H., G. Gabbiani and M. L. Bochaton-Piallat (2003). "Arterial smooth muscle cell heterogeneity: implications for atherosclerosis and restenosis development." Arterioscler Thromb Vasc Biol **23**(9): 1510-1520.

Hara, K., A. Shiga, T. Fukutake, H. Nozaki, A. Miyashita, A. Yokoseki, H. Kawata, A. Koyama, K. Arima, T. Takahashi, M. Ikeda, H. Shiota, M. Tamura, Y. Shimoe, M. Hirayama, T. Arisato, S. Yanagawa, A. Tanaka, I. Nakano, S. Ikeda, Y. Yoshida, T. Yamamoto, T. Ikeuchi, R. Kuwano, M. Nishizawa, S. Tsuji and O. Onodera (2009). "Association of HTRA1 mutations and familial ischemic cerebral small-vessel disease." N Engl J Med **360**(17): 1729-1739.

Herrmann, L. L., M. Le Masurier and K. P. Ebmeier (2008). "White matter hyperintensities in late life depression: a systematic review." J Neurol Neurosurg Psychiatry **79**(6): 619-624.

Hilal, S., V. Mok, Y. C. Youn, A. Wong, M. K. Ikram and C. L. Chen (2017). "Prevalence, risk factors and consequences of cerebral small vessel diseases: data from three Asian countries." J Neurol Neurosurg Psychiatry **88**(8): 669-674.

Iadecola, C. (2017). "The Neurovascular Unit Coming of Age: A Journey through Neurovascular Coupling in Health and Disease." Neuron **96**(1): 17-42.

Ikawati, M., M. Kawaichi and C. Oka (2018). "Loss of HtrA1 serine protease induces synthetic modulation of aortic vascular smooth muscle cells." PLoS One **13**(5): e0196628.

Inzitari, D., G. Pracucci, A. Poggesi, G. Carlucci, F. Barkhof, H. Chabriat, T. Erkinjuntti, F. Fazekas, J. M. Ferro, M. Hennerici, P. Langhorne, J. O'Brien, P. Scheltens, M. C. Visser, L. O. Wahlund, G. Waldemar, A. Wallin, L. Pantoni and L. S. Group (2009). "Changes in white matter as determinant of global functional decline in older independent outpatients: three year follow-up of LADIS (leukoaraiosis and disability) study cohort." *BMJ* **339**: b2477.

Ito, J., H. Nozaki, Y. Toyoshima, T. Abe, A. Sato, H. Hashidate, S. Igarashi, O. Onodera, H. Takahashi and A. Kakita (2018). "Histopathologic features of an autopsied patient with cerebral small vessel disease and a heterozygous HTRA1 mutation." *Neuropathology*.

Iyemere, V. P., D. Proudfoot, P. L. Weissberg and C. M. Shanahan (2006). "Vascular smooth muscle cell phenotypic plasticity and the regulation of vascular calcification." *J Intern Med* **260**(3): 192-210.

Jiang, S., R. He, L. Zhu, T. Liang, Z. Wang, Y. Lu, J. Ren, X. Yi, D. Xiao and K. Wang (2018). "Endoplasmic reticulum stress-dependent ROS production mediates synovial myofibroblastic differentiation in the immobilization-induced rat knee joint contracture model." *Exp Cell Res* **369**(2): 325-334.

Jones, F. E., L. S. Murray, S. McNeilly, A. Dean, A. Aman, Y. Lu, N. Nikolova, R. Malomgre, K. Horsburgh, W. M. Holmes, K. E. Kadler and T. Van Agtmael (2019). "4-Sodium phenyl butyric acid has both efficacy and counter-indicative effects in the treatment of Col4a1 disease." *Hum Mol Genet* **28**(4): 628-638.

Joutel, A., I. Haddad, J. Ratelade and M. T. Nelson (2016). "Perturbations of the cerebrovascular matrisome: A convergent mechanism in small vessel disease of the brain?" *J Cereb Blood Flow Metab* **36**(1): 143-157.

Kato, T., R. I. Manabe, H. Igarashi, F. Kametani, S. Hirokawa, Y. Sekine, N. Fujita, S. Saito, Y. Kawashima, Y. Hatano, S. Ando, H. Nozaki, A. Sugai, M. Uemura, M. Fukunaga, T. Sato, A. Koyama, R. Saito, A. Sugie, Y. Toyoshima, H. Kawata, S. Murayama, M. Matsumoto, A. Kakita, M. Hasegawa, M. Ihara, M. Kanazawa, M. Nishizawa, S. Tsuji and O. Onodera (2021). "Candesartan prevents arteriopathy progression in cerebral autosomal recessive arteriopathy with subcortical infarcts and leukoencephalopathy model." *J Clin Invest* **131**(22).

Khan, U., L. Porteous, A. Hassan and H. S. Markus (2007). "Risk factor profile of cerebral small vessel disease and its subtypes." *J Neurol Neurosurg Psychiatry* **78**(7): 702-706.

Klose, R., A. Prinz, F. Tetzlaff, E. M. Weis, I. Moll, J. Rodriguez-Vita, C. Oka, T. Korff and A. Fischer (2019). "Loss of the serine protease HTRA1 impairs smooth muscle cells maturation." *Sci Rep* **9**(1): 18224.

Kuo, D. S., C. Labelle-Dumais and D. B. Gould (2012). "COL4A1 and COL4A2 mutations and disease: insights into pathogenic mechanisms and potential therapeutic targets." Hum Mol Genet **21**(R1): R97-110.

Landinger, T. (2021). Contractile Cell Plasticity in Inherited Cerebral Small Vessel Disease. MD, LMU München.

Lee, Y. C., C. P. Chung, N. C. Chao, J. L. Fuh, F. C. Chang, B. W. Soong and Y. C. Liao (2018). "Characterization of Heterozygous HTRA1 Mutations in Taiwanese Patients With Cerebral Small Vessel Disease." Stroke **49**(7): 1593-1601.

Li, D. Y., B. Brooke, E. C. Davis, R. P. Mecham, L. K. Sorensen, B. B. Boak, E. Eichwald and M. T. Keating (1998). "Elastin is an essential determinant of arterial morphogenesis." Nature **393**(6682): 276-280.

Liu, X., F. Q. Wen, T. Kobayashi, S. Abe, Q. Fang, E. Piek, E. P. Bottinger, A. B. Roberts and S. I. Rennard (2003). "Smad3 mediates the TGF-beta-induced contraction of type I collagen gels by mouse embryo fibroblasts." Cell Motil Cytoskeleton **54**(3): 248-253.

Liu, Y., S. Sinha and G. Owens (2003). "A transforming growth factor-beta control element required for SM alpha-actin expression in vivo also partially mediates GSKF-dependent transcriptional repression." J Biol Chem **278**(48): 48004-48011.

Lopez-Casillas, F., J. L. Wrana and J. Massague (1993). "Betaglycan presents ligand to the TGF beta signaling receptor." Cell **73**(7): 1435-1444.

Maeda, S., H. Nakayama, K. Isaka, Y. Aihara and S. Nemoto (1976). "Familial unusual encephalopathy of Binswanger's type without hypertension." Folia Psychiatr Neurol Jpn **30**(2): 165-177.

Majesky, M. W., X. R. Dong, J. N. Regan and V. J. Hoglund (2011). "Vascular smooth muscle progenitor cells: building and repairing blood vessels." Circ Res **108**(3): 365-377.

Malik, R. and M. Dichgans (2018). "Challenges and opportunities in stroke genetics." Cardiovasc Res **114**(9): 1226-1240.

Massague, J. (2012). "TGF-beta signaling in development and disease." FEBS Lett **586**(14): 1833.

Massague, J., J. Seoane and D. Wotton (2005). "Smad transcription factors." Genes Dev **19**(23): 2783-2810.

Menezes Cordeiro, I., H. Nzwalo, F. Sa, R. B. Ferreira, I. Alonso, L. Afonso and C. Basilio (2015). "Shifting the CARASIL paradigm: report of a non-Asian family and literature review." Stroke **46**(4): 1110-1112.

Miano, J. M. (2015). "Myocardin in biology and disease." J Biomed Res **29**(1): 3-19.

Mishra, A., G. Chauhan, M. H. Violleau, D. Vojinovic, X. Jian, J. C. Bis, S. Li, Y. Saba, B. Grenier-Boley, Q. Yang, T. M. Bartz, E. Hofer, A. Soumare, F. Peng, M. G. Duperron, M. Foglio, T. H.

Mosley, R. Schmidt, B. M. Psaty, L. J. Launer, E. Boerwinkle, Y. Zhu, B. Mazoyer, M. Lathrop, C. Bellenguez, C. M. Van Duijn, M. A. Ikram, H. Schmidt, W. T. Longstreth, M. Fornage, S. Seshadri, A. Joutel, C. Tzourio and S. Debette (2019). "Association of variants in HTRA1 and NOTCH3 with MRI-defined extremes of cerebral small vessel disease in older subjects." Brain **142**(4): 1009-1023.

Mok, V. and J. S. Kim (2015). "Prevention and Management of Cerebral Small Vessel Disease." J Stroke **17**(2): 111-122.

Muller, K., G. Courtois, M. V. Ursini and M. Schwaninger (2017). "New Insight Into the Pathogenesis of Cerebral Small-Vessel Diseases." Stroke **48**(2): 520-527.

Munoz Maniega, S., F. M. Chappell, M. C. Valdes Hernandez, P. A. Armitage, S. D. Makin, A. K. Heye, M. J. Thrippleton, E. Sakka, K. Shuler, M. S. Dennis and J. M. Wardlaw (2017). "Integrity of normal-appearing white matter: Influence of age, visible lesion burden and hypertension in patients with small-vessel disease." J Cereb Blood Flow Metab **37**(2): 644-656.

Murwantoko, M. Yano, Y. Ueta, A. Murasaki, H. Kanda, C. Oka and M. Kawaichi (2004). "Binding of proteins to the PDZ domain regulates proteolytic activity of HtrA1 serine protease." Biochem J **381**(Pt 3): 895-904.

Nishimoto, Y., M. Shibata, M. Nihonmatsu, H. Nozaki, A. Shiga, A. Shirata, K. Yamane, A. Kosakai, K. Takahashi, M. Nishizawa, O. Onodera and N. Suzuki (2011). "A novel mutation in the HTRA1 gene causes CARASIL without alopecia." Neurology **76**(15): 1353-1355.

Nozaki, H., T. Kato, M. Nihonmatsu, Y. Saito, I. Mizuta, T. Noda, R. Koike, K. Miyazaki, M. Kaito, S. Ito, M. Makino, A. Koyama, A. Shiga, M. Uemura, Y. Sekine, A. Murakami, S. Moritani, K. Hara, A. Yokoseki, R. Kuwano, N. Endo, T. Momotsu, M. Yoshida, M. Nishizawa, T. Mizuno and O. Onodera (2016). "Distinct molecular mechanisms of HTRA1 mutants in manifesting heterozygotes with CARASIL." Neurology **86**(21): 1964-1974.

Nozaki, H., M. Nishizawa and O. Onodera (2014). "Features of cerebral autosomal recessive arteriopathy with subcortical infarcts and leukoencephalopathy." Stroke **45**(11): 3447-3453.

Ochieng, J., V. Furtak and P. Lukyanov (2002). "Extracellular functions of galectin-3." Glycoconj J **19**(7-9): 527-535.

Oide, T., H. Nakayama, S. Yanagawa, N. Ito, S. Ikeda and K. Arima (2008). "Extensive loss of arterial medial smooth muscle cells and mural extracellular matrix in cerebral autosomal recessive arteriopathy with subcortical infarcts and leukoencephalopathy (CARASIL)." Neuropathology **28**(2): 132-142.

Oka, C., R. Tsujimoto, M. Kajikawa, K. Koshiba-Takeuchi, J. Ina, M. Yano, A. Tsuchiya, Y. Ueta, A. Soma, H. Kanda, M. Matsumoto and M. Kawaichi (2004). "HtrA1 serine protease inhibits signaling mediated by Tgfbeta family proteins." Development **131**(5): 1041-1053.

Owens, G. K., M. S. Kumar and B. R. Wamhoff (2004). "Molecular regulation of vascular smooth muscle cell differentiation in development and disease." Physiol Rev **84**(3): 767-801.

Pantoni, L. (2010). "Cerebral small vessel disease: from pathogenesis and clinical characteristics to therapeutic challenges." Lancet Neurol **9**(7): 689-701.

Papaspyridonos, M., E. McNeill, J. P. de Bono, A. Smith, K. G. Burnand, K. M. Channon and D. R. Greaves (2008). "Galectin-3 is an amplifier of inflammation in atherosclerotic plaque progression through macrophage activation and monocyte chemoattraction." Arterioscler Thromb Vasc Biol **28**(3): 433-440.

Rensen, S. S., P. A. Doevendans and G. J. van Eys (2007). "Regulation and characteristics of vascular smooth muscle cell phenotypic diversity." Neth Heart J **15**(3): 100-108.

Rincon, F. and C. B. Wright (2014). "Current pathophysiological concepts in cerebral small vessel disease." Front Aging Neurosci **6**: 24.

Risor, M. W., E. T. Poulsen, L. R. Thomsen, T. F. Dyrland, T. A. Nielsen, N. C. Nielsen, K. W. Sanggaard and J. J. Enghild (2014). "The autolysis of human HtrA1 is governed by the redox state of its N-terminal domain." Biochemistry **53**(23): 3851-3857.

Roeben, B., S. Uhrig, B. Bender and M. Synofzik (2016). "Teaching NeuroImages: When alopecia and disk herniations meet vascular leukoencephalopathy: CARASIL." Neurology **86**(15): e166-e167.

Rong, J. X., M. Shapiro, E. Trogan and E. A. Fisher (2003). "Transdifferentiation of mouse aortic smooth muscle cells to a macrophage-like state after cholesterol loading." Proc Natl Acad Sci U S A **100**(23): 13531-13536.

Rutten-Jacobs, L. C. A. and N. S. Rost (2020). "Emerging insights from the genetics of cerebral small-vessel disease." Ann N Y Acad Sci **1471**(1): 5-17.

Rutten, J. W., J. Haan, G. M. Terwindt, S. G. van Duinen, E. M. Boon and S. A. Lesnik Oberstein (2014). "Interpretation of NOTCH3 mutations in the diagnosis of CADASIL." Expert Rev Mol Diagn **14**(5): 593-603.

Salmon, M., D. Gomez, E. Greene, L. Shankman and G. K. Owens (2012). "Cooperative binding of KLF4, pELK-1, and HDAC2 to a G/C repressor element in the SM22alpha promoter mediates transcriptional silencing during SMC phenotypic switching in vivo." Circ Res **111**(6): 685-696.

Sandison, M. E., J. Dempster and J. G. McCarron (2016). "The transition of smooth muscle cells from a contractile to a migratory, phagocytic phenotype: direct demonstration of phenotypic modulation." J Physiol **594**(21): 6189-6209.

Scharrer, E. (2015). Consequences of HtrA1 deficiency on TGF-Beta signaling. PhD, LMU München.

Schmierer, B. and C. S. Hill (2007). "TGFbeta-SMAD signal transduction: molecular specificity and functional flexibility." Nat Rev Mol Cell Biol **8**(12): 970-982.

Shankman, L. S., D. Gomez, O. A. Cherepanova, M. Salmon, G. F. Alencar, R. M. Haskins, P. Swiatlowska, A. A. Newman, E. S. Greene, A. C. Straub, B. Isakson, G. J. Randolph and G. K. Owens (2015). "KLF4-dependent phenotypic modulation of smooth muscle cells has a key role in atherosclerotic plaque pathogenesis." Nat Med **21**(6): 628-637.

Shiga, A., H. Nozaki, A. Yokoseki, M. Nihonmatsu, H. Kawata, T. Kato, A. Koyama, K. Arima, M. Ikeda, S. Katada, Y. Toyoshima, H. Takahashi, A. Tanaka, I. Nakano, T. Ikeuchi, M. Nishizawa and O. Onodera (2011). "Cerebral small-vessel disease protein HTRA1 controls the amount of TGF-beta1 via cleavage of proTGF-beta1." Hum Mol Genet **20**(9): 1800-1810.

Ter Telgte, A., E. M. C. van Leijsen, K. Wiegertjes, C. J. M. Klijn, A. M. Tuladhar and F. E. de Leeuw (2018). "Cerebral small vessel disease: from a focal to a global perspective." Nat Rev Neurol **14**(7): 387-398.

Thompson, C. S. and A. M. Hakim (2009). "Living beyond our physiological means: small vessel disease of the brain is an expression of a systemic failure in arteriolar function: a unifying hypothesis." Stroke **40**(5): e322-330.

Tian, Y., W. Yuan, J. Li, H. Wang, M. G. Hunt, C. Liu, I. M. Shapiro and M. V. Risbud (2016). "TGFbeta regulates Galectin-3 expression through canonical Smad3 signaling pathway in nucleus pulposus cells: implications in intervertebral disc degeneration." Matrix Biol **50**: 39-52.

Tikka, S., M. Baumann, M. Siitonen, P. Pasanen, M. Poyhonen, L. Myllykangas, M. Viitanen, T. Fukutake, E. Cognat, A. Joutel and H. Kalimo (2014). "CADASIL and CARASIL." Brain Pathol **24**(5): 525-544.

Truebestein, L., A. Tennstaedt, T. Monig, T. Krojer, F. Canellas, M. Kaiser, T. Clausen and M. Ehrmann (2011). "Substrate-induced remodeling of the active site regulates human HTRA1 activity." Nat Struct Mol Biol **18**(3): 386-388.

Uemura, M., H. Nozaki, A. Koyama, N. Sakai, S. Ando, M. Kanazawa, T. Kato and O. Onodera (2019). "HTRA1 Mutations Identified in Symptomatic Carriers Have the Property of Interfering the Trimer-Dependent Activation Cascade." Front Neurol **10**: 693.

van der Flier, W. M., E. C. van Straaten, F. Barkhof, A. Verdelho, S. Madureira, L. Pantoni, D. Inzitari, T. Erkinjuntti, M. Crisby, G. Waldemar, R. Schmidt, F. Fazekas and P. Scheltens (2005). "Small vessel disease and general cognitive function in nondisabled elderly: the LADIS study." Stroke **36**(10): 2116-2120.

van Veluw, S. J., A. Y. Shih, E. E. Smith, C. Chen, J. A. Schneider, J. M. Wardlaw, S. M. Greenberg and G. J. Biessels (2017). "Detection, risk factors, and functional consequences of cerebral microinfarcts." Lancet Neurol **16**(9): 730-740.

Varadaraj, A., L. M. Jenkins, P. Singh, A. Chanda, J. Snider, N. Y. Lee, A. R. Amsalem-Zafran, M. Ehrlich, Y. I. Henis and K. Myhre (2017). "TGF-beta triggers rapid fibrillogenesis via a novel TbetaRII-dependent fibronectin-trafficking mechanism." Mol Biol Cell **28**(9): 1195-1207.

Verdura, E., D. Herve, F. Bergametti, C. Jacquet, T. Morvan, C. Prieto-Morin, A. Mackowiak, E. Manchon, H. Hosseini, C. Cordonnier, I. Girard-Buttaz, S. Rosenstingl, C. Hagel, G. Kuhlenbaumer, E. Leca-Radu, D. Goux, L. Fleming, T. Van Agtmael, H. Chabriat, F. Chapon and E. Tournier-Lasserre (2016). "Disruption of a miR-29 binding site leading to COL4A1 upregulation causes pontine autosomal dominant microangiopathy with leukoencephalopathy." Ann Neurol **80**(5): 741-753.

Verdura, E., D. Herve, E. Scharrer, M. Amador Mdel, L. Guyant-Marechal, A. Philippi, A. Corlobe, F. Bergametti, S. Gazal, C. Prieto-Morin, N. Beaufort, B. Le Bail, I. Viakhireva, M. Dichgans, H. Chabriat, C. Haffner and E. Tournier-Lasserre (2015). "Heterozygous HTRA1 mutations are associated with autosomal dominant cerebral small vessel disease." Brain **138**(Pt 8): 2347-2358.

Vinters, H. V., C. Zarow, E. Borys, J. D. Whitman, S. Tung, W. G. Ellis, L. Zheng and H. C. Chui (2018). "Review: Vascular dementia: clinicopathologic and genetic considerations." Neuropathol Appl Neurobiol **44**(3): 247-266.

Wagenseil, J. E. and R. P. Mecham (2009). "Vascular extracellular matrix and arterial mechanics." Physiol Rev **89**(3): 957-989.

Wang, G., L. Jacquet, E. Karamariti and Q. Xu (2015). "Origin and differentiation of vascular smooth muscle cells." J Physiol **593**(14): 3013-3030.

Wardlaw, J. M., C. Smith and M. Dichgans (2013a). "Mechanisms of sporadic cerebral small vessel disease: insights from neuroimaging." Lancet Neurol **12**(5): 483-497.

Wardlaw, J. M., C. Smith and M. Dichgans (2019). "Small vessel disease: mechanisms and clinical implications." Lancet Neurol **18**(7): 684-696.

Wardlaw, J. M., E. E. Smith, G. J. Biessels, C. Cordonnier, F. Fazekas, R. Frayne, R. I. Lindley, J. T. O'Brien, F. Barkhof, O. R. Benavente, S. E. Black, C. Brayne, M. Breteler, H. Chabriat, C. Decarli, F. E. de Leeuw, F. Doubal, M. Duering, N. C. Fox, S. Greenberg, V. Hachinski, I. Kilimann, V. Mok, R. Oostenbrugge, L. Pantoni, O. Speck, B. C. Stephan, S. Teipel, A. Viswanathan, D. Werring, C. Chen, C. Smith, M. van Buchem, B. Norrving, P. B. Gorelick, M. Dichgans and S. T. f. R. V. c. o. nEuroimaging (2013b). "Neuroimaging standards for research into small vessel disease and its contribution to ageing and neurodegeneration." Lancet Neurol **12**(8): 822-838.

Weisheit, I., J. A. Kroeger, R. Malik, B. Wefers, P. Lichtner, W. Wurst, M. Dichgans and D. Paquet (2021). "Simple and reliable detection of CRISPR-induced on-target effects by qPCR and SNP genotyping." Nat Protoc **16**(3): 1714-1739.

Wolinsky, H. and S. Glagov (1964). "Structural Basis for the Static Mechanical Properties of the Aortic Media." Circ Res **14**: 400-413.

Yanagawa, S., N. Ito, K. Arima and S. Ikeda (2002). "Cerebral autosomal recessive arteriopathy with subcortical infarcts and leukoencephalopathy." Neurology **58**(5): 817-820.

Zellner, A., E. Scharrer, T. Arzberger, C. Oka, V. Domenga-Denier, A. Joutel, S. F. Lichtenthaler, S. A. Muller, M. Dichgans and C. Haffner (2018). "CADASIL brain vessels show a HTRA1 loss-of-function profile." Acta Neuropathol **136**(1): 111-125.

12 ACKNOWLEDGEMENTS

The presented work was carried out between February 2016 and March 2017 under the supervision of Prof. Dr. med. Martin Dichgans and Dr. rer. nat. Nathalie Beaufort at the Institute for Stroke and Dementia Research, Ludwig-Maximilians University Munich within “Förderung für Forschung und Lehre” (FöFoLe) program of the medical faculty of Ludwig-Maximilians-University Munich.

I would first like to express my gratitude to Prof. Dr. med. Martin Dichgans for granting me the opportunity to work on this topic within his group and laboratory, for the regular and constructive advice and input concerning the progress of the project as well as for the impressive vigor and work ethic that he displays, which inspires one to yield more. In addition, I would like to thank the 2nd rapporteur (Berichterstatter) for the effort of assessing my thesis as part of the examination board.

To Dr. rer. nat. Nathalie Beaufort: I am most grateful for your dedication and support over the period of my dissertation. She has chaperoned the project in a very thorough manner, from its initiation, through all the developments and adjustments that come with work in research, to the final written thesis.

I would like to thank the entire Dichgans Lab for the collaborative work and constructive exchanges, as well as the technical support in conducting experiments. I want to acknowledge the opportunity Dr. rer. nat. Dr. med. Steffen Tiedt has given me by co-setting up the initial project and supporting it through the modifications along the way. In particular, I would like to thank Timon Landinger, my predecessor as an MD student, whose work laid the foundation for my thesis. Furthermore, I would like to thank Dr. rer. nat. Eva Scharrer for leaving her mouse cell lines to me.

I would like to credit my fellow MD students in the laboratory, especially Jonathan Gernert, Nicola Schieferdecker, and Luya Lydia Lu, for the productive discussions and their companionship.

Finally, to my parents, three sisters, grandmother and dear friends – words cannot express my gratitude.

13 AFFIDAVIT

Eidesstattliche Versicherung

Ich erkläre hiermit an Eides statt,
dass ich die vorliegende Dissertation mit dem Thema

„Phenotypic switching of contractile cells in HTRA1-related cerebral small vessel disease“

selbständig verfasst, mich außer der angegebenen keiner weiteren Hilfsmittel bedient und alle Erkenntnisse, die aus dem Schrifttum ganz oder annähernd übernommen sind, als solche kenntlich gemacht und nach ihrer Herkunft unter Bezeichnung der Fundstelle einzeln nachgewiesen habe. Ich erkläre des Weiteren, dass die hier vorgelegte Dissertation nicht in gleicher oder in ähnlicher Form bei einer anderen Stelle zur Erlangung eines akademischen Grades eingereicht wurde.

München, 30.08.2023

Sophie von Brauchitsch

14 CURRICULUM VITAE

Sophie von Brauchitsch

Nationality: German and Austrian

Professional Career

10/2019–present: Neurological resident at the Center of Epilepsy Frankfurt Rhein-Main
Department of Neurology, University Hospital of the Goethe University,
Frankfurt am Main, Germany

Academic Studies

02/2016–03/2017: Experimental research for medical dissertation at the Institute for Stroke
and Dementia Research (ISD), Munich, Germany
*Title: “The phenotype of contractile cells in HTRA1-related cerebral small vessel
disease.”*
Supervisor: Prof. Dr. med. Martin Dichgans

04/2013–03/2018: Studies of Philosophy at Hochschule für Philosophie, Munich, Germany
Bachelor of Arts (BA)

10/2012–06/2019: Studies of human medicine (preclinical and clinical) at Ludwig-Maximilians-
University (LMU), Munich, Germany
08/2014 Preliminary (first) medical state examination
04/2018 Second (theoretical) medical state examination
05/2019 Third (practical) medical state examination

Clinical Electives (selection)

01/2019–04/2019: Clinical elective within the practical (final) year in Neurology, Queen Square
Institute of Neurology, University College London, London, United
Kingdom

09/2018–12/2018: Clinical elective within the practical (final) year in Surgery, Klinikum Dritter
Orden (attached to Ludwig-Maximilians-University), Munich, Germany

05/2018–09/2018: Clinical elective within the practical (final) year in Medical Specialties,
University of Queensland, Brisbane, Australia

Scholarships and Prizes (selection)

05/2018–09/2018: Scholarship of the “Students Excellency Program” (MeCuM-StEP) of the
medical faculty of the Ludwig-Maximilians-University, Munich, Germany

05/2016–11/2017: Scholarship at the doctoral study course “Förderung für Forschung und
Lehre” (FöFoLe) of the medical faculty of Ludwig-Maximilians-University,
Munich, Germany

School Education

09/2009–06/2011: St. Columba’s College, Dublin, Ireland
Graduation: Irish Leaving Certificate

08/2003–07/2009: Erzbischöfliches St. Joseph-Gymnasium, Rheinbach, Germany

08/1999–07/2003: Primary School, Rheinbach-Merzbach, Germany

15 PUBLICATIONS

Poster

Sophie von Brauchitsch, Timon Landinger, Nathalie Beaufort, Eva Scharrer, Martin Dichgans. Pathogenic HTRA1 Mutations Alter TGF- β Signaling and Cell Differentiation in Familial Cerebral Small Vessel Disease. 90. Jahrestagung der Deutsche Gesellschaft für Neurologie. Leipzig, 2017.

Sophie von Brauchitsch, Adam Strzelczyk, Felix Rosenow, Elisabeth Neuhaus, Joachim P. Steinbach, Martin Voss. Hohe Prävalenz von epileptischen Anfällen in Patienten mit primären und sekundären Hirntumoren am Ende des Lebens. 60. Jahrestagung der Deutschen Gesellschaft für Epileptologie (DGfE) e. V. Leipzig, 2022.

Presentation

Daniela Beer, Sophie von Brauchitsch, Julia Grill, Julian Leberzammer, Veronika Loiko, Caroline Plett, Jonas Schaller, Sebastian Sigl, Sebastian Stolz, Johannes Tossounidis, Katharina Wach, Pawel Wróbel, Martin R. Fischer. IPC-KompAKT – InterProfessional Collaboration – Kompetent als Klinisches Team – Ein Kurs zur interprofessionellen Ausbildung an der Ludwig-Maximilians-Universität München. Jahrestagung der Gesellschaft für Medizinische Ausbildung (GMA), Frankfurt am Main, 2017.

Publications

Hochbaum M, Kienitz R, Rosenow F, Schulz J, Habermehl L, Langenbruch L, Kovac S, Knake S, von Podewils F, von Brauchitsch S, Hamacher M, Strzelczyk A, Willems LM. Trends in antiseizure medication prescription patterns among all adults, women, and older adults with epilepsy: A German longitudinal analysis from 2008 to 2020. *Epilepsy Behav.* 2022 May;130:108666. doi: 10.1016/j.yebeh.2022. Epub 2022 Mar 25. PMID: 35339390.

Friedauer L, Foerch C, Steinbach J, Hattingen E, Harter PN, Armbrust M, Urban H, Steidl E, Neuhaus E, von Brauchitsch S. The Acute Superficial Siderosis Syndrome - Clinical Entity, Imaging Findings, and Histopathology. *Cerebellum.* 2022 Mar 22. doi: 10.1007/s12311-022-01387-3. Epub ahead of print. PMID: 35316464.